FutureWings Project

(www.futurewings.eu)

7th Framework Programme
AERONAUTICS and AIR TRANSPORT (AAT)
Call identifier: FP7-AAT-2012-RTD-L0

"Wings of the future"

Work Package 1: Feasibility of the integration of MFC into the primary structures of aircrafts and definition of control system requirements

Deliverable D.1.1

"Feasibility analysis on the use of piezo-electric materials as actuators of thin walled active structures"

Issued by: Dept. of Civil and Industrial Engineering, Aerospace Unit, University of Pisa, Italy
Resarch Team of Prof. Mario Rosario Chiarelli

Piaggio Aero Industries SPA, Italy
Dr. Aniello Cozzolino

Smart Material GmbH, Germany
Dr. Jan Kunzmann

iChrome Ltd
Dr. Luca Lanzi

Date: 22 October 2013

Release: 1.0

FutureWings is a Collaborative International Project.
It has received funding from the EU 7th Framework Programme under G.A. N. 335042

Index

1 State-of-the-art on embedded piezo-electric elements in composite structures

The idea of active controllable aircraft structures is going along with the development of novel actuator materials allowing either a bonding onto or an embedding into typical aircraft materials like carbon fiber reinforced composites.

For this background the major requirements for such actuator materials can be defined as follows:

- Conformity to composite materials
- Good surface adhesion to structural epoxy systems
- Temperature stability in accordance to composite curing cycles
- Anisotropic strain generation
- Usage of the bigger d_{33} effect in-plane
- Reliability in accordance to aircraft component requirements
- Suitable electrical wiring and easy to control

With respect to this especially thin piezoelectric actuators have been identified for the use in controllable aircraft structures. Based on the general need the development of novel types of piezo actuators started more than 20 years ago as shown in Figure 1.

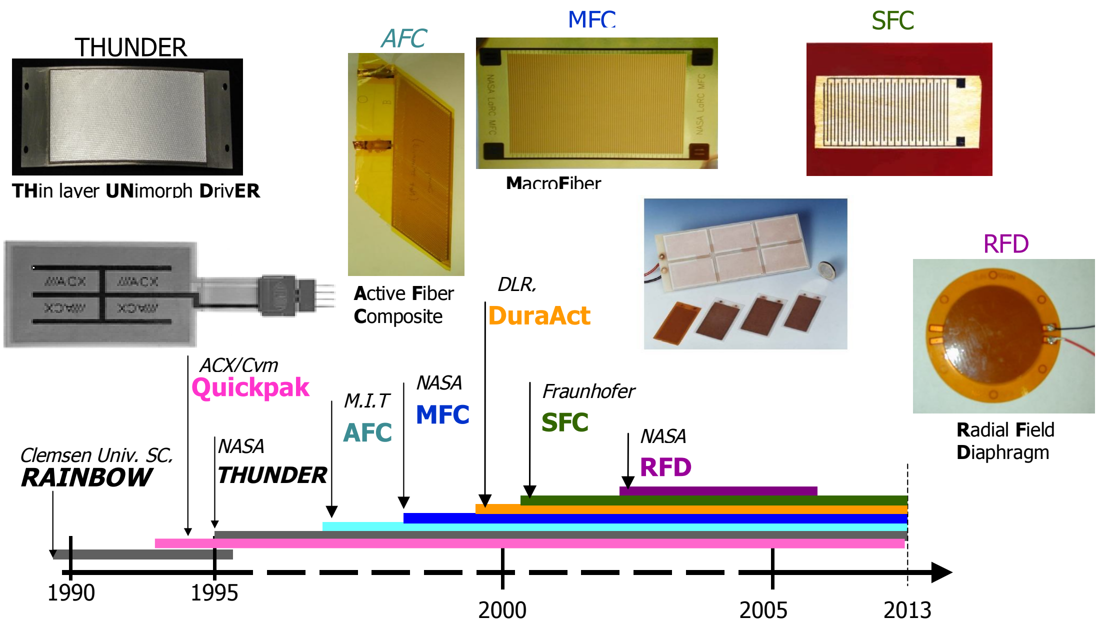

Figure 1: History of thin piezo-actuators

Due to their thin structure the most of them are generally useable in thin walled composite aircraft components. Nowadays are only the QuickPack (Midé), the Active Fiber Composites-AFC or Piezofiber Composites-PFC (ACI), the Macro Fiber Composite-MFC (Smart Material) and the DuraAct (PI) commercially available on the market.

To compare their specific properties a benchmark test has been done in a way that their behavior has been reflected on the major requirement as defined above. Table 1 gives a general overview regarding the advantages and drawback of the different available actuator systems based on an intensive study of all available information in papers, datasheets and on the web. A collection of references is given at the end of this report.

Table 1: *Benchmark test for commercial thin walled actuator materials*

Requirement	**QuickPack**	**AFC/PFC**	**MFC**	**DuraAct**
Composite conformity	0	++	++	0
Adhesion to structural epoxy	-	+	+	+
Stability vs. curing cycle	0	++	++	0
Anisotropic behavior	-	+	++	0
d_{33} usage	-	++	++	0
Reliability	0 (n/s)	0 (n/s)	++ (10^{10})	++ (10^{10})
Wiring & control voltages	++	+	+	++

The ***QuickPack*** is one of the earliest developed thin piezo actuators and consists of a thin pre-electroded piezo wafer. The encapsulation between two polymer foils with a coarse electrode pattern increases the reliability of the actuator compared with a single piezoceramic plate. This design leads to an isotropic in-plane strain generation only using the smaller d_{31} effect (new d_{33} actuators just started). Normally the polyester surface (for earlier types) has to be seen as critical for any bonding process as only a few potentially good glues on the market for this type of material, that's why the manufacturer switched to a Kapton foil material now.

With the development of a suitable technology for the manufacturing of piezoceramic fibers the basis for the ***AFC/PFC*** was given. Due to its fibrous design the actuator element becomes flexible and is therefore also more tolerant against the requirements coming from the composite curing cycle. The combination of the unidirectional piezofiber layer with the so-called interdigitated electrodes leads to an improved actuator behavior with a possible anisotropic strain generation using the d_{33} effect for the first time.

The ***MFC*** has to be seen as an alternative actuator material but with a much better profile of properties compared to the AFC. In difference to the AFC the MFC is using a diced piezo wafer inside instead of the monolayer of round ceramic fibers. Due to this the coupling of the electric field into the ceramic material is much better and based on the rectangular shape of the fibers the fill factor in the active cross-section is much higher compared with the AFC. This leads finally to a better actuator strain and due to a special electrode pattern the MFC can be modified for an anisotropic generation of a torsional deformation of a structure.

The latest development is the ***DuraAct*** which is more or less comparable to the Quickpak. It also consists of an un-diced piezoelectric wafer but due to a different production technology the reliability has been rated to be little bit better. Latest information material shows that first actuators with d_{33} effect and anisotropic behavior are available now but their sizes are currently limited to about $2cm^2$ max.

The following Figure 2 gives an more detailed overview regarding the structural design for all the 4 analyzed actuator types.

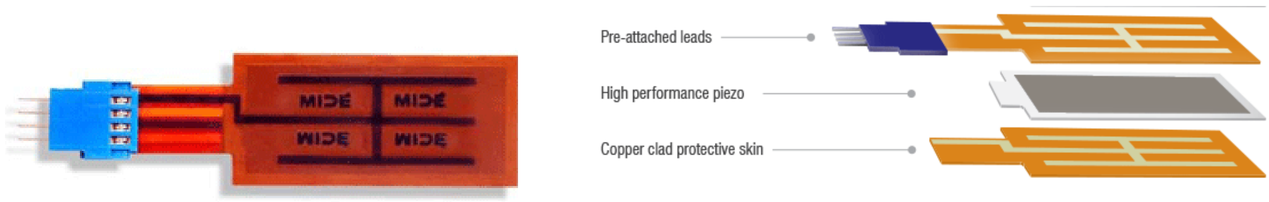

a) QuickPack – actuator and design

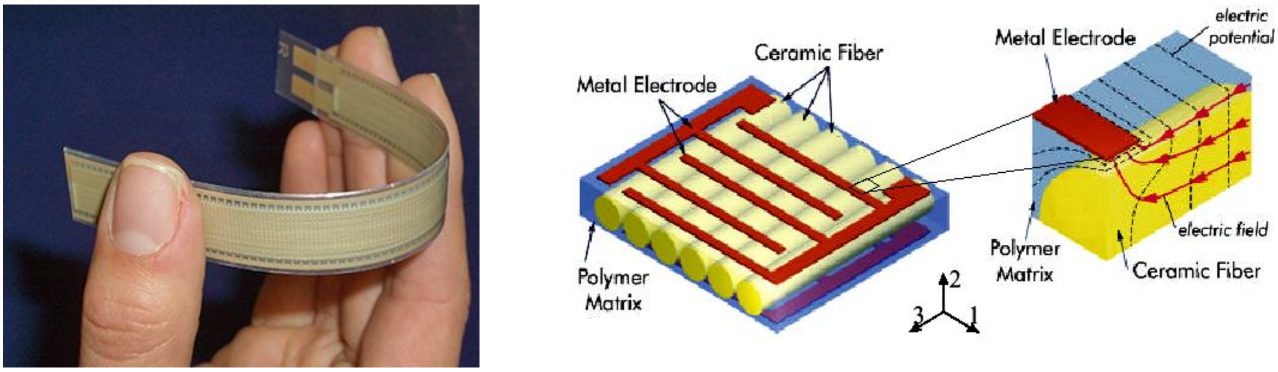

b) AFC (PFC) – actuator and design

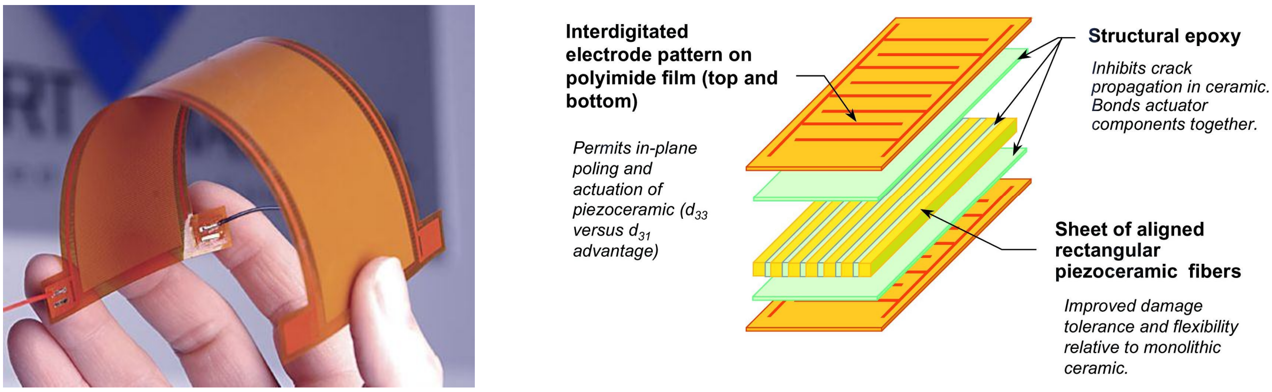

c) MFC – actuator and design

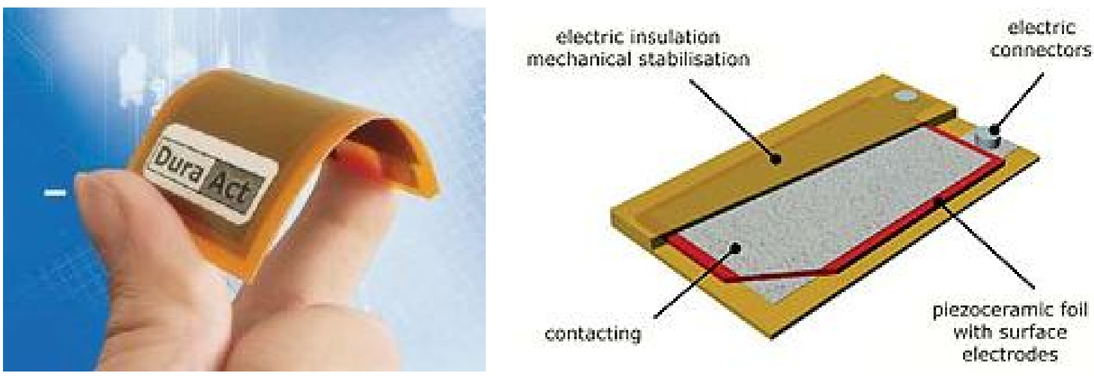

d) DuraAct – actuator and design

Figure 2: Structural design of the analyzed actuators

In summary, it can be stated that currently 4 actuator systems are available on the market. While the QuickPack and the DuraAct are comparable and started with d_{31} actuators first the AFC/PFC and the MFC are typical high performance d_{33} actuators from the beginning. Due to the rectangular cross-section of the fibers the MFC is typically showing a little bit better strain and blocking force data compared with the AFC. Therefore the MFC is being selected at this point and shall be used for all further investigations and tests within this project.

Based on the availability of such Advanced Low Profile Actuators (ALPA's) on the market several research projects raised during the last two decades with the aim of the development of novel controllable surfaces for aircraft structures. The following examples are giving a quick overview regarding the activities with MFC actuators especially in the field of aircraft structures.

Vibration damping on F18 tail-buffet (NASA/AFRL/Boeing)

First projects came up shortly after the MFC was developed as a new actuator material for morphing wings and the damping of structural vibrations. NASA started together with some other partners to study the reduction of vibrations on the tail-buffet of the F18 fighter. As one can see in Figure 3 the MFC has been used on a down-scaled model and at this time typically the actuators have been only attached to the structure's surface.

Figure 3: actuated tail-buffet using MFC actuators

It could be shown that due to the excellent actuator performance the vibration of the first torsional mode has been reduced by a factor of 5. This high damping rate is of course a result of working in the fundamental resonance point where the structure undergoing a minimum at its dynamic stiffness response.

Reducing eddy currents on helicopter blades (NASA/ARL/UoMichigan/Sikorsky)

In a further project the reduction of eddy currents in helicopter blades has been studied as this effect can cause blade failures and reduces dramatically the lifetime for the blades. With respect to the fact that eddy currents are mainly generated due to torsional vibrations of the blade at this time a special type of MFC with a fiber alignment under an angle of 45° was introduced for the first time. As the major stress under a torsion are running under 45° this MFC is an excellent antagonist to work against any torsional vibration.

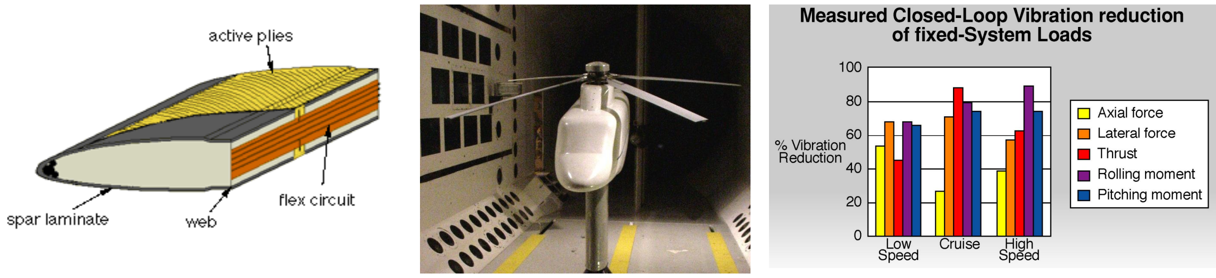

Figure 4: MFC based vibration damping on a helicopter blade

As one can see from Figure 4 at this time the actuators have been embedded into the carbon fiber skin of the blade and became therefore an integral part of the aircraft structure. The effects of the actuation could be studied on down-scaled models in a wind-tunnel and a remarkable reduction of the vibration and its effect on the blade loads could be observed. Up to now 3 different research groups are still working worldwide on this topic. Meanwhile the models became bigger and several additional dynamic effects have to be studied.

omissis

omissis

2 Collection and analysis of material properties for the used piezo materials

Based on the results of the previous chapter all available technical data on the pre-selected 4 piezo actuator systems have been collected from different sources like personal meetings, exhibition contacts and the web. For a global overview this collection is attached to this report in Appendix A (Unfortunately the DuraAct brochure is available only in German).

In a second step those data resources have been studied and analyzed deeply to prepare an objective comparison of the actuator potential of the different piezo material systems. Typically the actuator behavior for all piezoelectric actuators can be described within the work diagram as shown in Figure 8.

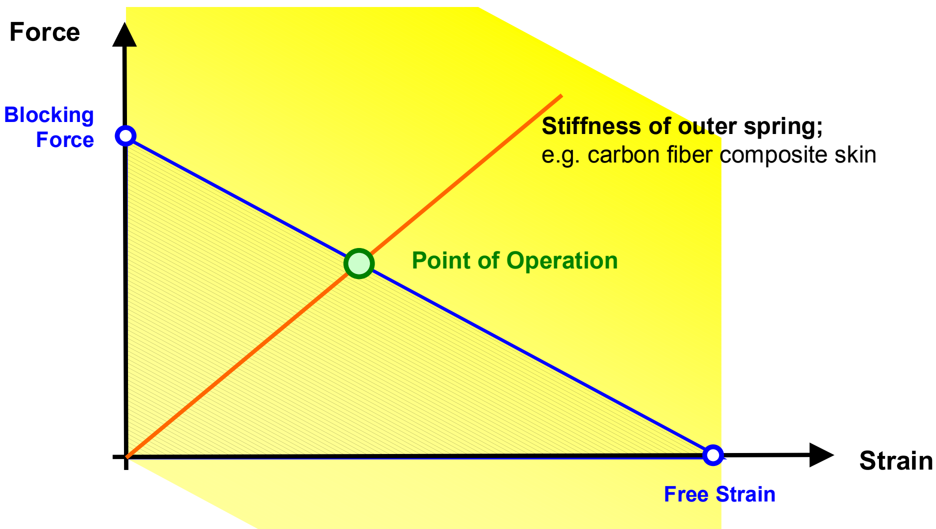

Figure 8: Work diagram for piezoelectric actuators

Every piezo element has two typical parameters, the free strain where the max deformation without any outer load can be observed and the blocking force where the actuator system is completely clamped so that now deformation is possible and the force is getting maximal. These 2 points defining the line of operation and the area below this curve is an expression for the energy potential of this actuator. Once the actuator is connected to any mechanical system with a certain stiffness the max strain and force values for the actuator are now defined with the point of operation where the stiffness curve of the structure and the line of operation for the actuator (actuator stiffness) intersect. At this point the actuator force and the spring force of the outer attached system are balanced.

For this background the free strain and the blocking force values for the selected actuator types have been compared together with some other important values like Young's modulus and min and max operational Voltages. The results are given in a clear manner in the following Figure 9 a) … d).

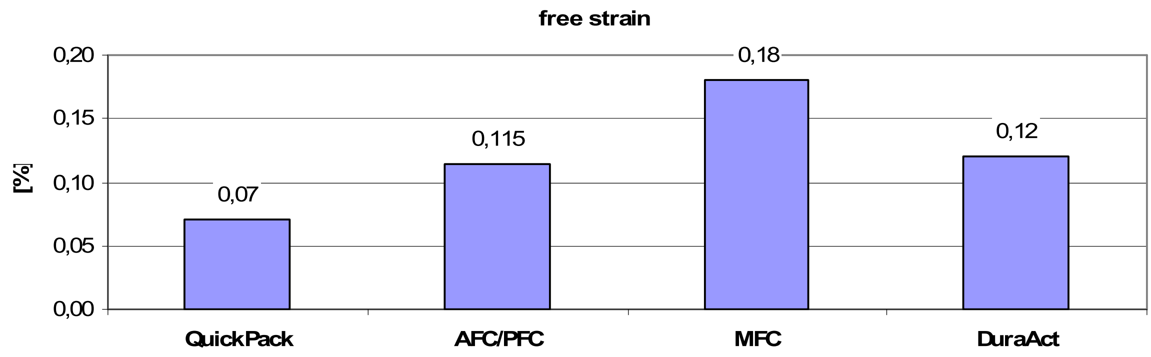

a) maximal free strain at maximal positive voltage

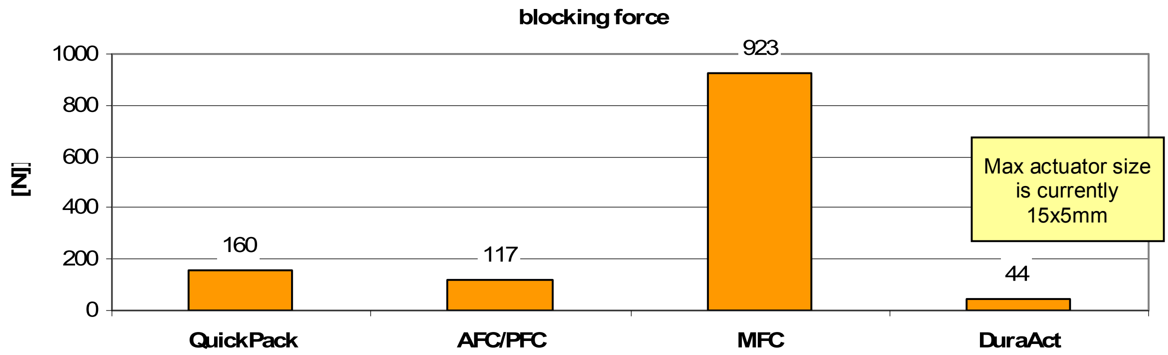

b) maximal blocking force at maximal positive voltage

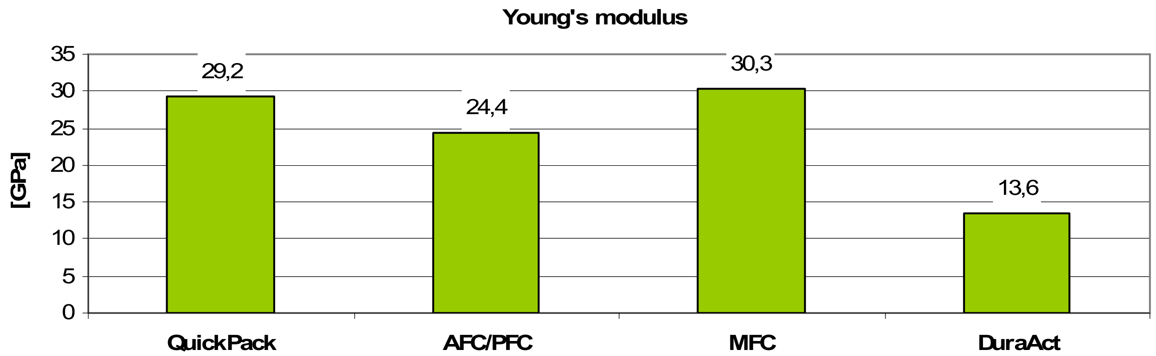

c) Young's modulus

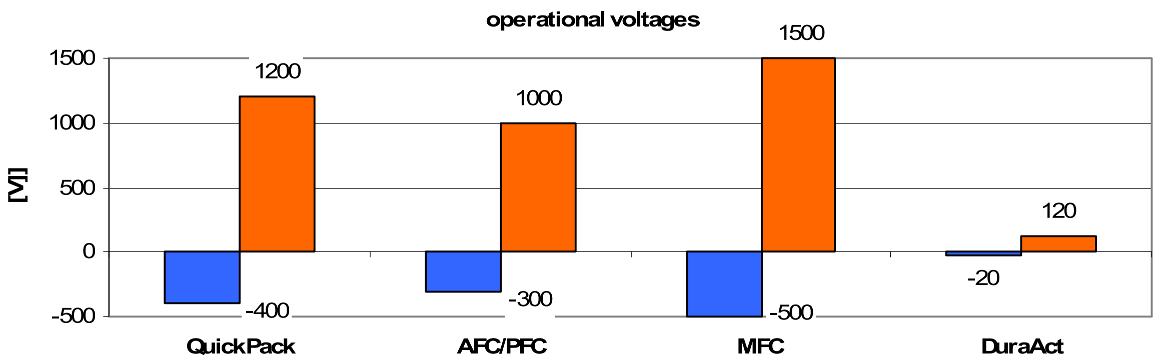

d) maximal positive and negative operational voltage

Figure 9: Piezo actuator comparison

In conclusion it can be stated that especially with respect to the important piezo-mechanical properties the MFC offers the best figure of merit for the use in high power applications. Furthermore with its Young's modulus, which is the highest within this group, it makes the gap to the high modulus carbon fiber composites as narrow as possible so that structural impacts can probably be minimized.

On the other hand the MFC requires currently the highest operational voltages as due to a bigger pitch of the electrode fingers the efficiency of actively driven piezo material can be increased. Possible approaches for a voltage reduction shall be developed and tested within this project.

3 Preliminary requirements for a suitable production strategy

Depending on the simulation results for a best active behavior the piezoelectric actuator needs either be bond onto the aircraft structure's surface or embedded into this host structure. For this background two different manufacturing strategies are necessary.

A) Preliminary bonding technology

Assuming that the piezo actuator is doing the best job on top of the basic mechanical structure or can't be embedded for any reason like the possible risk of initiating a delamination inside the composite structure the actuator has to be glued onto the aircraft structure's surface. The following requirements have to be met with a suitable bonding technology:

- applicable on flat and curved surfaces
- no autoclave needed with respect to costs
- ensures constant and uniform pressures during cure
- in accordance with warm and cold (RT) curing cycles
- ensures only minimal content of air bubbles in the glue layer
- high reproducibility

For this background a first draft of a possible procedure for bonding MFC actuators on different substrate materials has been developed. This technological approach is shown in Figure 10.

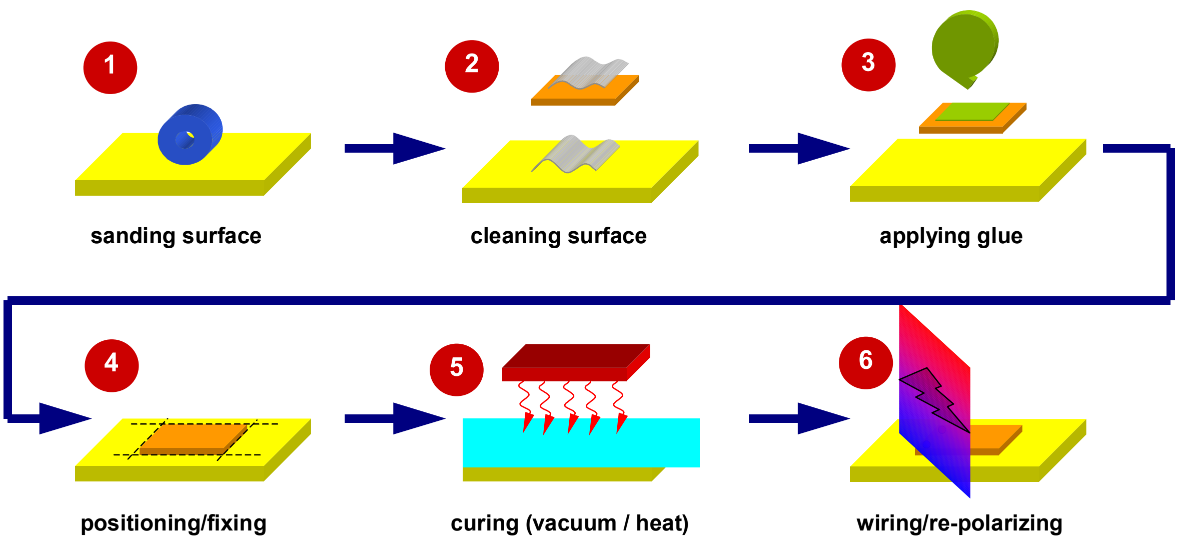

Figure 10: preliminary technology for bonding MFCs

The different steps can be described as follows:

1. Sanding substrate surface for higher roughness and better adhesion
2. Cleaning both surfaces to degrease them
3. Applying and spreading the glue thin and uniform on the actuator
4. place the actuator in the right position and fix it with removable tape
5. curing process under vacuum to degas + heat if necessary
6. wiring and re-polarization (only if actuator was warmed up to 0.5 T_{curie})

B) Preliminary embedding technology

In difference to the bonding technology where an additional glue layer is needed to attach the actuator to the structure the embedding technology offers the advantage of a direct combination of the actuator with the structural epoxy coming from the used composite material. Due to this the efficiency of strain coupling can be increased. The typical requirements for an embedding technology are:

- applicable on flat and curved surfaces
- good surface conformity to structural epoxy (adhesion)
- constant & uniform pressures during cure (vacuum bag or autoclave)
- curing temperature as low as possible (depolarization effect)
- structural solution for wiring and contact pad insulation
- process integrated re-polarization procedure
- high accuracy and reproducibility

Based on this preliminary requirements the following possible procedure for an in-situ embedding of piezoelectric actuators has been developed as shown in Figure 11.

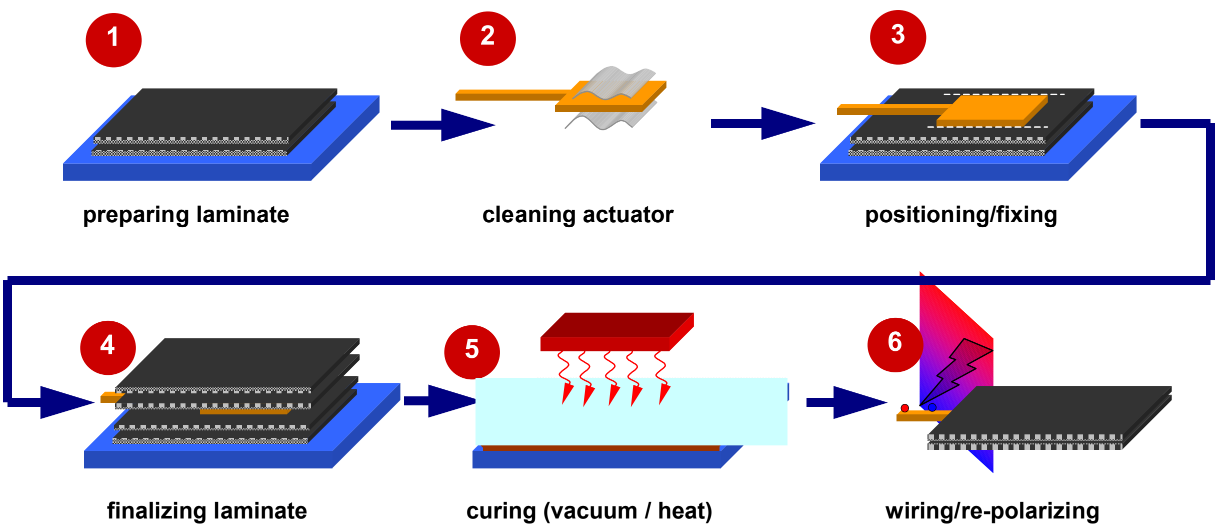

Figure 11: preliminary technology for a composite embedding of MFCs

The different steps can be described as follows:

1. preparing the basic component laminate
2. cleaning all actuator's surfaces to degrease them
3. place the actuator on the tacky laminate in the correct position
4. finalizing the lay-up for the laminate as calculated
5. applying pressure and heat to cure the laminate; depolarization can occur
6. final wiring and re-polarization of the embedded actuator

4 Preliminary cost analysis for active piezoelectric/composite components

In general it has to be noted that a cost analysis at this very early stage of the project can't really match the any real cost structure as the most of the necessary parameters are unknown at this point. Independently on this the overall costs can be divided in 3 bigger parts – material costs; manufacturing costs and certification costs.

A) Material costs

Due to the combination of the standard aircraft structure material with an advanced low profile actuator a certain amount of a high performance material will be added. For the background that all the new materials (smart materials) are currently still expensive the overall material costs will be much higher depending on the ratio of active area related to the passive structure area. This ratio can't be estimated yet as this is a result of the ongoing project work.

At this point the only rough cost analysis can be done for the MFC actuator itself. As Figure 12 shows the most expensive part of the actuator depends on the volume of needed or manufactured MFCs. While for standard MFCs with higher volumes the piezoelectric material is the biggest cost driver is the electrode foil for small series (up to 100 pcs) the most expensive part due to the high NRE costs of the flex PCB suppliers.

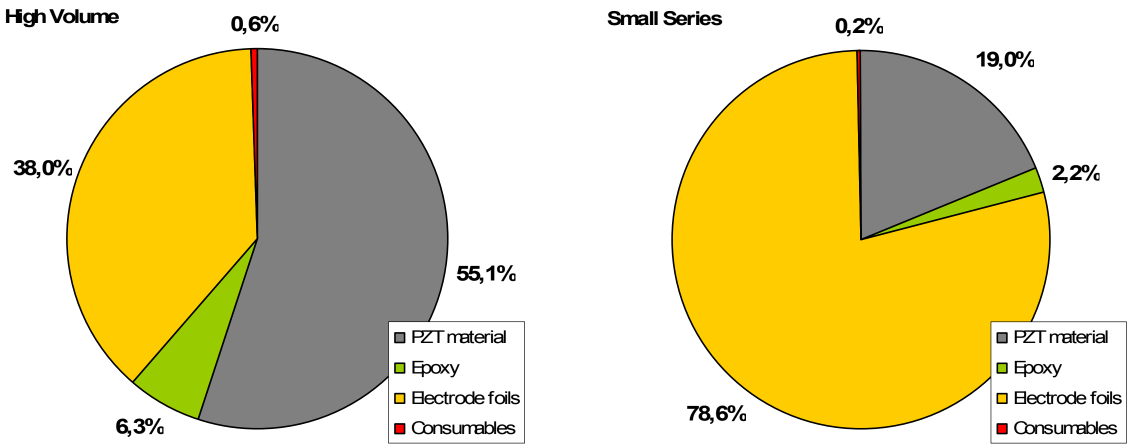

Figure 12: material cost analysis for the MFC

B) Manufacturing costs

As there isn't any well defined production technology available yet the cost analysis can only be done based on the technological drafts under topic 3 and known manufacturing times for each step based on the own long-term experiences. As an example a square flat composite plate (4 layers;

250mm x 250mm) was manufactured and the cost distribution for both a MFC bonding and a MFC embedding process as well is being shown in Figure 13.

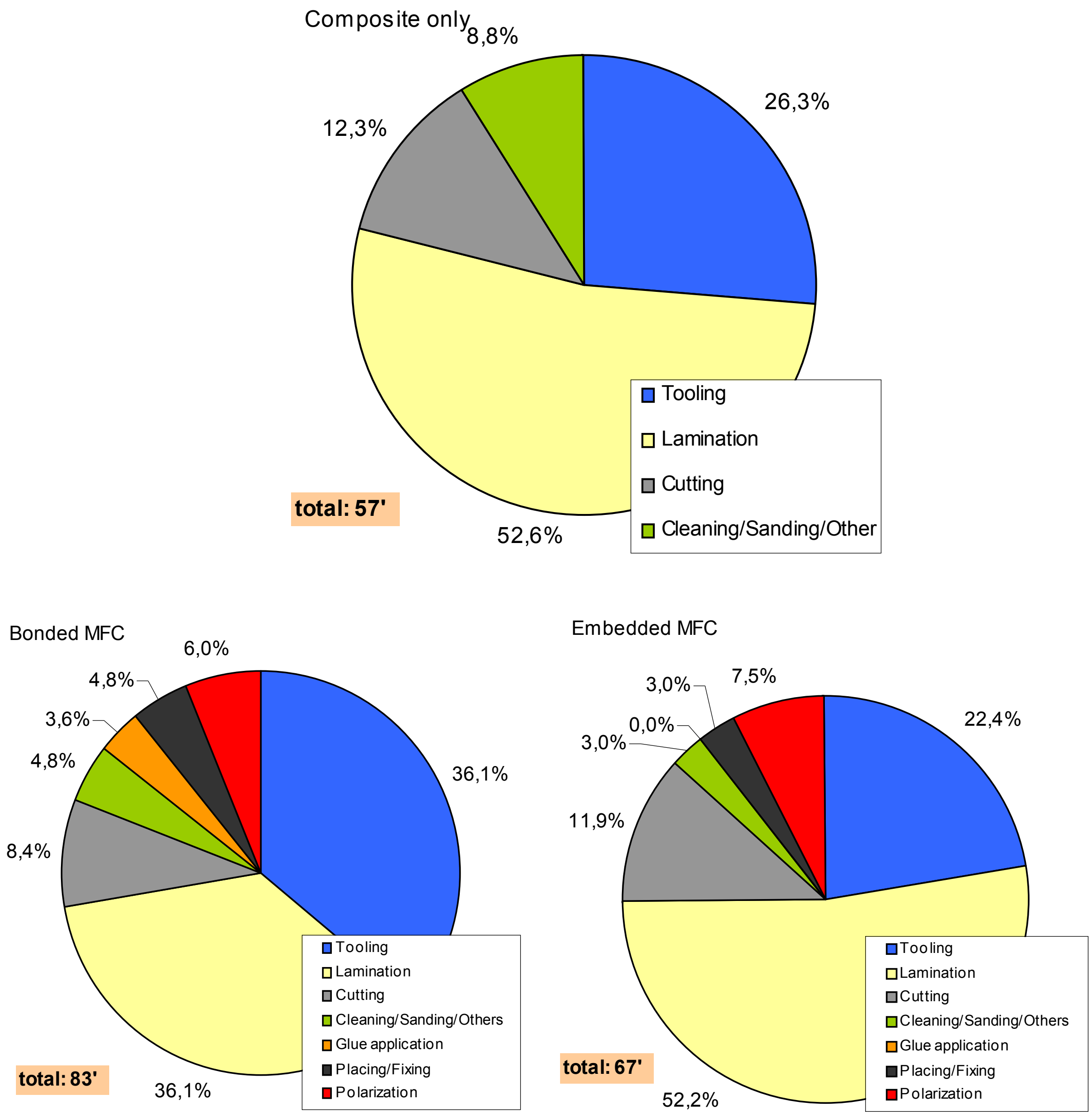

Figure 13: Manufacturing cost analysis

It can be shown that based on the production time for the passive plate without any actuators that an bonding process onto the surface of the plate needs about 46% more time for this exemplary made component. In difference to this the embedding process saves a significant amount of time as no surface preparation and additional glue application is necessary so that finally only about 18% more time and costs will be needed to manufacture the part with integrated actuators. For this background the embedding process can be considered as the more cost efficient solution.

C) Certification costs

As generally known parts, structures and systems for aircraft vehicles have to be certified before their use in a series production. Based on several personal interviews with partners from the aircraft manufactures branch it can be expected that the costs for an active wingbox will increase due to the active parts by a factor of 5 up to 10 compared with the ones for a passive carbon fiber structure. While the passive structure needs to pass a component and structural test the active wingbox is considered as a system as per definition and therefore several additional tests have to be done to finally get a system qualification and certificate.

5 Hybrid structures simulation results

In the technical literature exists a number of preliminary application of MFC to control the deformability of aerospace structures. As an example, interesting applications are reported in the works [5.1] and [5.2]. The MFC are used in these cases to control the dynamic behavior of rotor blade models. Experimental and numerical simulation are carried out to define the mechanical and electro-mechanical characteristics of such active structures. More in particular the problem of the optimized distribution of MFC in these structures has been accounted for. The effects on mass and stiffness distributions on the aeroelastic response of an innovative rotor blade configuration are examined in these preliminary works. From an overall point of view, these works provide in an explicit way a demonstrative application of the MFC as elements that can be used to control the deformed shape of a thin walled structure (Figure 14, Figure 15).

As explained in [5.3] MFC elements can reduce noise and vibration, determined by blade vortex interactions, during helicopter descent flight. This result can be achieved embedding MFC actuators into the blade skin and modeling their fiber directions in order to twist the blades when required.

To deform shape, before using MFC actuators, PZT actuators and their behavior have been studied. PZT actuators are composed by layers that can be mounted in various ways, constituting different kinds of actuators. As described in [5.4], bender, unimorph and building-block actuators are used to change wing curvature. In bender actuators PZT structure is related to flap hinge and it exploits his strain to move flap (Figure 16).

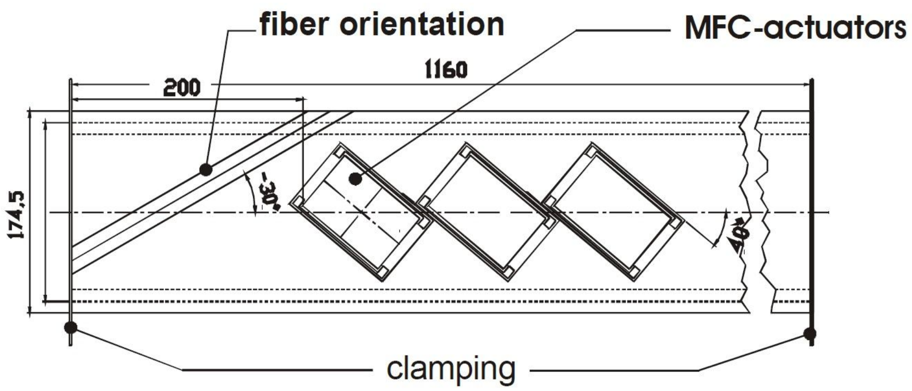

Figure 14: Geometry of the ATBx and Position of the Actuators [5.1]

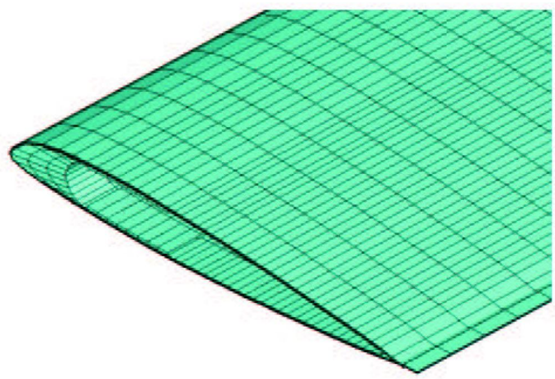

Figure 15: Active Twist Blade FEM model [5.2]

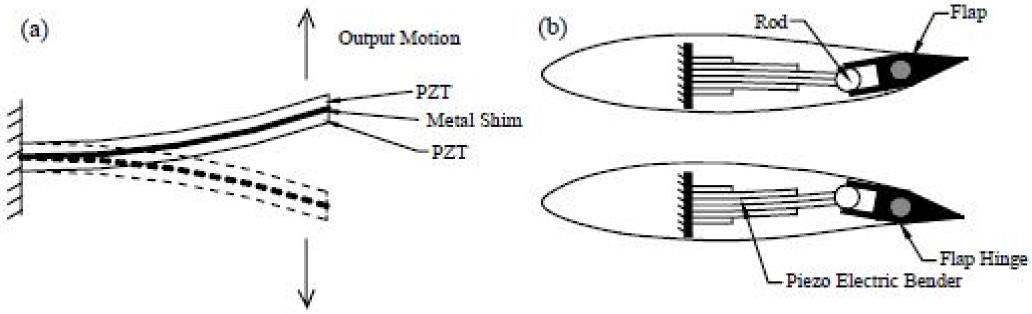

Figure 16: (a) Typical Bimorph Actuator in a Cantilevered Configuration, (b) Piezoelectric Tapered Bender Used to Control Flap [5.4].

In unimorph and building-block actuators the PZT displacement are used to deform the thickness of the wing and accordingly his curvature (Figure 17, Figure 18).

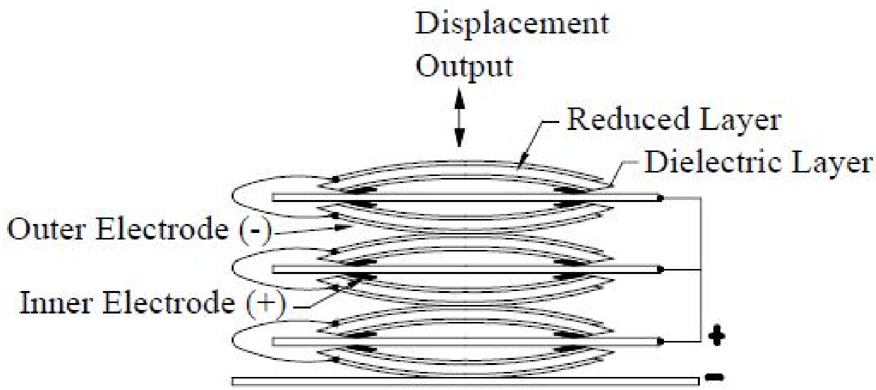

Figure 17: Three Unimorph Actuators Stacked in Series [5.4]

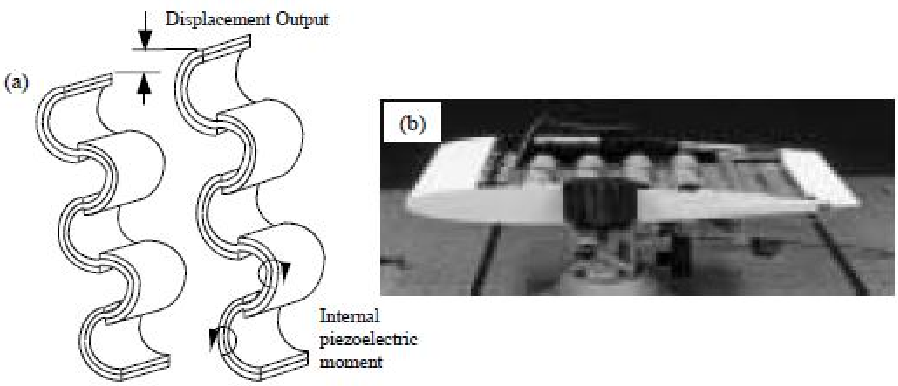

Figure 18: (a) Diagram of C-Block Actuator Showing Displacement Output, (b) Fabricated C-Blocks Shown Actuating A Flap [5.4].

If a closed loop control is added to these structures the deformation can be exploit to damp vibrations.
In [5.5] an example of trailing edge moved by MFC is shown. The actuators are attached on the upper surface of the wing and they curve themselves by a voltage application (Figura 19).

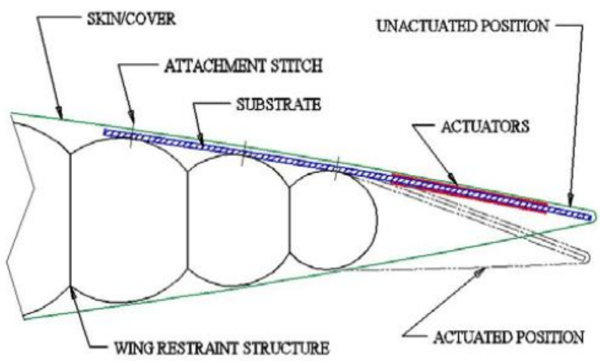

Figure 19: Trailing Edge Configuration [5.5].

Properties of PZT and MFC can be, also, exploit to move whole parts of robotic mechanism as explained in [5.6]. In this instance an unimorph actuator composed by a piezoelectric layer glued on an elastic layer is used. The whole structure is related to the root of the wing. The deformation of actuator allows the flapping of the wings. Changing MFC fiber orientations feathering can be matched to flapping, as described in [5.7] (Figure 20).

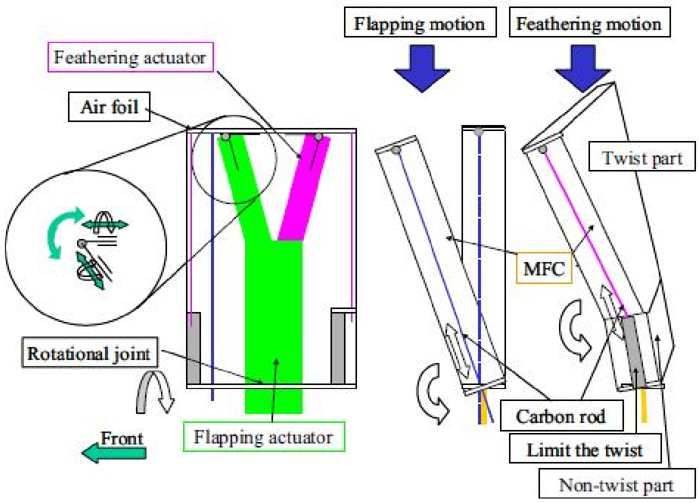

Figure 20: Configuration of Mechanism [5.7].

One of the principal objectives of the FutureWings project concerns the design and the testing of a set of specimen made of hybrid composite material. By means of these numerical and experimental campaigns the fundamental technical issues relevant to the design, the manufacturing and controlling of the FutureWings model (made of a number of FutureWings Units) will be addressed.

To define the technical specification for the manufacturing and testing of the specimens a campaign of numerical analyses has been carried out: in this section are shown the results of this activity carried out within the FutureWings project.

As reference geometry, a rectangular thin panel having 90 mm width and 150 mm length has been used. The overall thickness of the panel is equal to 3.6 mm. For the panel has been modeled two type of substrates: (1) aluminum and (2) carbon fibers (**T300-934**). In a first hybrid configuration the active layers (made of MFC) are "glued" on the outer surfaces of the panel. It is assumed to use 18 MFC components (**M5628-P1)** (9 patches for each outer surface of the panel). The thickness of the layers of MFC is assumed equal to 0.3 mm. The thickness of the carbon-fiber lamina is assumed equal to 0.125 mm. Three-dimensional Finite Element models have been set up using 20 nodes brick elements.

The Material Dielectric Properties of the active layers (made of MFC patches) are:

D11 = D22 = D33 = 1.63802x10^{-8} F/m (isotropic model is assumed for the dielectric behavior)

The Material Piezo-Elastic Strain Coefficient used in the analyses to simulate the active layers is:

d33 = 4.6x10^{10} m/V (this coefficient couples mechanical and electrical responses of the patch)

The Material Elastic Properties of the Piezo active lamina are (orthotropic behavior):

E11 = 30.336 GPa

E22 = 15.87 GPa

ν12 = 0.31

ν21 = 0.16

G12 = 5.515 GPa

In the Finite Element analyses the voltage loads have been applied on the upper and lower surfaces of the volumes that model the piezo-electric layers (Figure 21). For this reason the 3-3 effect has been formally assumed as a 3-1 effect. In other words in the matrix of the Piezo-Electric Strain Coefficient in the position 3-1 has been introduced the **d33** coefficient of the MFC patches as shown in the equation (5.1).

$$[d]=\begin{bmatrix} 0 & 0 & 0 & 0 & 0 & 0 \\ 0 & 0 & 0 & 0 & 0 & 0 \\ 4.6\cdot 10^{10} & 0 & 0 & 0 & 0 & 0 \end{bmatrix}\frac{m}{V} \quad . \tag{5.1}$$

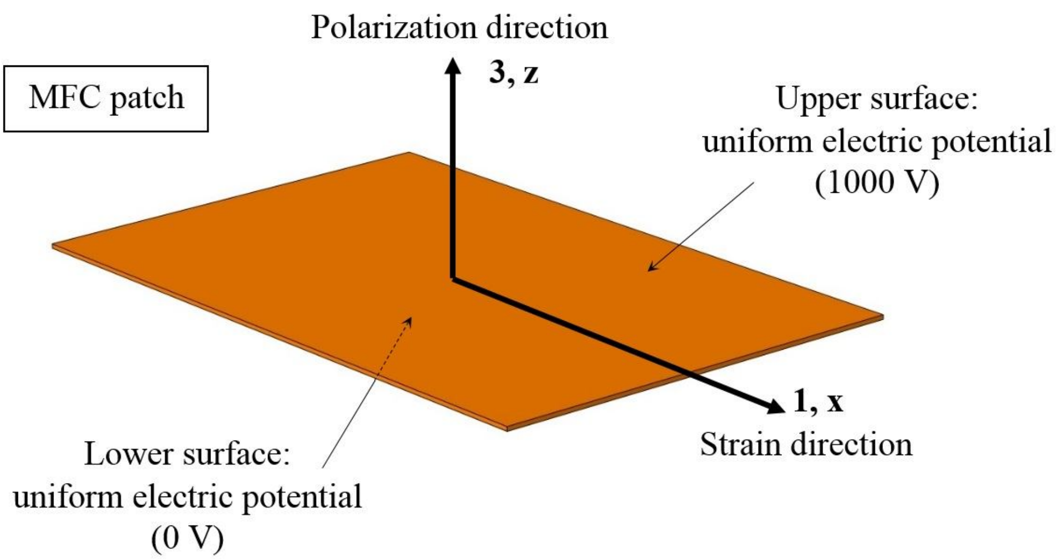

Figure 21: Method used to apply the voltage loading conditions to the active layers

5.1 Hybrid specimens with aluminum substrate: Specimen Type 1

The first group of specimens analyzed are composed with a substrate of isotropic aluminum sheet together with piezo-electric active layers.

The elastic properties of the metallic material are **E = 70 GPa** and **ν = 0.33**.

The geometry of the panel has been reproduced in the Figure 22.

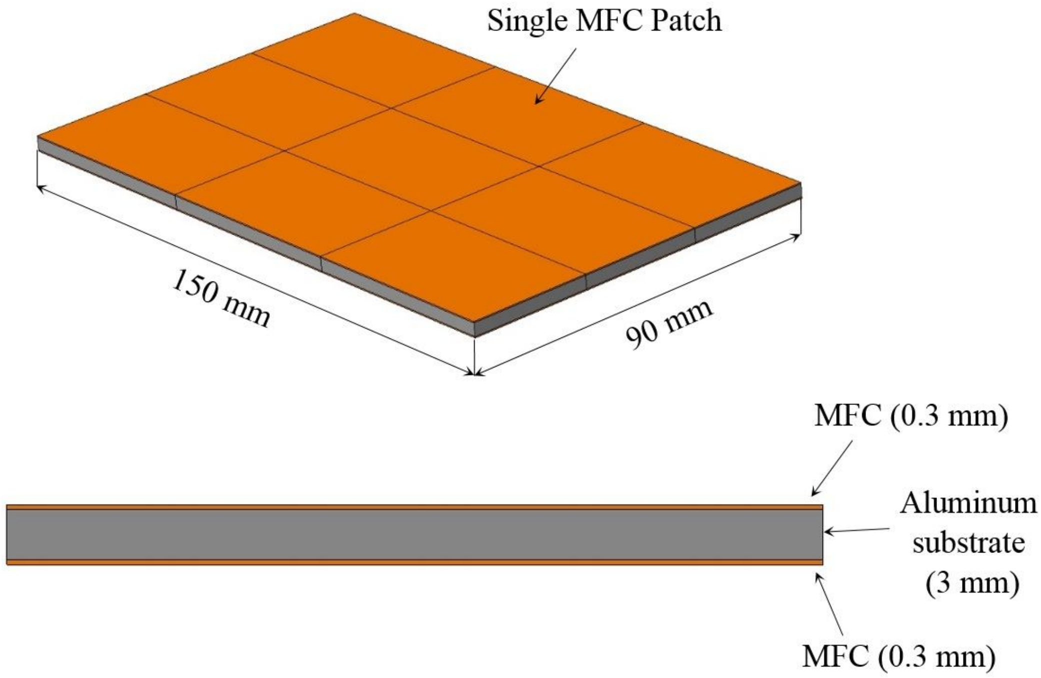

Figure 22: Geometry of the Specimen Type 1 (9 patches for each active layers)

The following lists summarizes the set of the analyses carried out in this case (overall voltage load applied to the piezo-layers is equal to 1000 V).

Constraint conditions (a): panel clamped along a short side maintaining free the other three sides. In this way bending and torsion deformation effects have been observed. In all the analyses the x axis coincides with the longitudinal axis of the panels while the z-axis lays in the thickness direction of the panels.

A.1.1: the active fibers in the piezo-layers are parallel to the x axis: 0 degrees orientation (bending).

A.1.2: the active fibers in the piezo-layers are oriented with angles of ±45 degrees with respect to x axis (upper layer +45 degrees – lower layer –45 degrees) (torsion).

A.1.3: 0 degrees orientation of the active fibers: simulation of the electrical failure of the first upper MFC strip (coupled bending-torsion).

A.1.4: ±45 degrees orientation of the active fibers: simulation of the electrical failure of the first upper MFC strip (coupled bending-torsion).

A.1.5: 0 degrees orientation of the active fibers: simulation of a combined structural and electrical loading condition (uniform downward pressure of 8500 Pa + Voltage effects). (modeling of electro-mechanical bending: the piezo-layers are activated to reduce or to change the mechanical load effects)

Constraint conditions (b): the panel has been constrained to deform freely in the x-y global reference plane (out of plane deformations not allowed - rigid motion not allowed). In this way pure shear deformation effects have been reproduced (neglecting at this first level of analysis the localized boundary effects).

A.1.6: the active fibers in the upper and in the lower piezo-layers are oriented with angles of +45 degrees (in this case the voltage loads tend to deform in the same manner both the upper and lower active layers) (modeling of pure shear).

A.1.7: the active fibers in the upper and in the lower piezo-layers are oriented with angles of +45 degrees: simulation of a combined structural and electrical loading condition (self equilibrated shear forces distribution along the sides of the panel equal to $5x10^6$ Pa + Voltage effects) (modeling of electro-mechanical pure shear deformation: the piezo-layers are activated to reduce or to change the mechanical load effects).

5.2 Hybrid specimens with aluminum substrate and embedded piezo-layers: Specimen Type 2

The second group of specimens analyzed are composed with a substrate of isotropic aluminum sheet together with embedded piezo-electric active layers. In this case the outer layers are made of aluminum thin sheet with a thickness of 0.125 mm. These metallic layers cover the piezo-electric active layers (0.3 mm thick) while the core is made of aluminum (2.75 mm thick).

The geometry of the panel has been reproduced in the Figure 23.

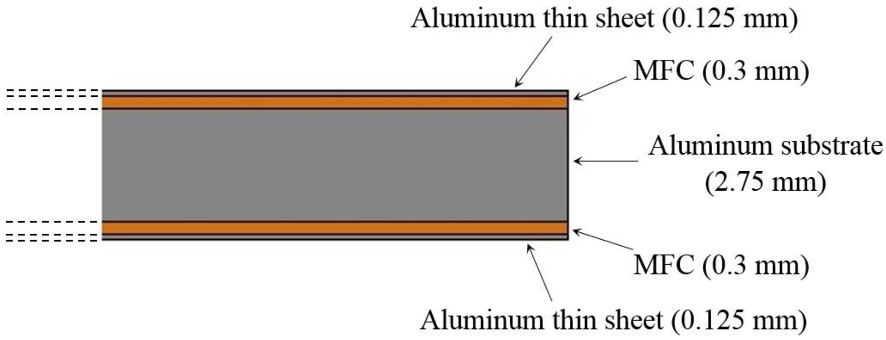

Figure 23: Geometry of the Specimen Type 2

Constraint conditions (a): panel clamped along a short side maintaining free the other three sides.

A.2.1: the active fibers in the piezo-layers are parallel to the x axis: 0 degrees orientation (bending).

A.2.2: the active fibers in the piezo-layers are oriented with angles of ±45 degrees with respect to x axis (upper layer +45 degrees – lower layer –45 degrees) (torsion).

A.2.3: 0 degrees orientation of the active fibers: simulation of the electrical failure of the first upper MFC strip (coupled bending-torsion).

A.2.4: ±45 degrees orientation of the active fibers: simulation of the electrical failure of the first upper MFC strip (coupled bending-torsion).

A.2.5: 0 degrees orientation of the active fibers: simulation of a combined structural and electrical loading condition (uniform downward pressure of 8000 Pa + Voltage effects). (modeling of electro-mechanical bending: the piezo-layers are activated to reduce or to change the mechanical load effects)

Constraint conditions (b): the panel has been constrained to deform freely in the x-y global reference plane (out of plane deformations not allowed - rigid motion not allowed).

A.2.6: the active fibers in the upper and in the lower piezo-layers are oriented with angles of +45 degrees (in this case the voltage loads tend to deform in the same manner both the upper and lower active layers) (modeling of pure shear)

A.2.7: the active fibers in the upper and in the lower piezo-layers are oriented with angles of +45 degrees: simulation of a combined structural and electrical loading condition (self equilibrated shear forces distribution along the sides of the panel equal to $5x10^6$ Pa + Voltage effects) (modeling of electro-mechanical pure shear deformation: the piezo-layers are activated to reduce or to change the mechanical load effects)

5.3 Hybrid specimens with carbon fibers substrate: Specimen Type 3

The third group of specimens analyzed are composed with a substrate of isotropic carbon fibers laminates together with piezo-electric active layers. The elastic properties of the carbon fibers laminae adopted in the analyses (material T300-934) are shown in the Table 5.1. The analyses refer to different plies stacking sequences as indicated in the table: all the sequence examined provide symmetrical lay-ups. All the orthotropic laminates are composed using 24 layers 0.125 mm thick.

The geometry of the panel has been reproduced in the Figure 24.

Sequence N.	0 degrees	+ 45 degrees	- 45 degrees	E11 [GPa]	E22 [GPa]	v12	v21	G12 [GPa]
1	24	0	0	148	9.66	0.3	0.02	4.55
2	16	4	4	105	18.3	0.613	0.107	14.2
3	12	6	6	83.2	23.7	0.713	0.203	21.4
4	8	8	8	61	25.7	0.752	0.36	27
5	0	12	12	16.4	16.4	0.801	0.801	38.2

Table 5.1: Elastic properties of the carbon fibers laminae in the Specimen Type 3

The following lists summarizes the set of the analyses carried out in this case (overall voltage load applied to the piezo-layers is equal to 1000 V).

Constraint conditions (a): panel clamped along a short side maintaining free the other three sides. In this way bending and torsion deformation effects have been observed.

The indexes used for the notations indicate: Type of specimen, Stacking Sequence Number, Type of analysis.

A.3.1.1: the active fibers in the piezo-layers are parallel to the x axis: 0 degrees orientation (bending).

A.3.1.2: the active fibers in the piezo-layers are oriented with angles of ±45 degrees with respect to x axis (upper layer +45 degrees – lower layer –45 degrees) (torsion).

A.3.1.3: 0 degrees orientation of the active fibers: simulation of the electrical failure of the first upper MFC strip (coupled bending-torsion).

A.3.1.4: ±45 degrees orientation of the active fibers: simulation of the electrical failure of the first upper MFC strip (coupled bending-torsion).

A.3.1.5: 0 degrees orientation of the active fibers: simulation of a combined structural and electrical loading condition (uniform downward pressure of 8500 Pa + Voltage effects). (modeling of electro-mechanical bending: the piezo-layers are activated to reduce or to change the mechanical load effects)

Constraint conditions (b): the panel has been constrained to deform freely in the x-y global reference plane (out of plane deformations not allowed - rigid motion not allowed).

A.3.1.6: the active fibers in the upper and in the lower piezo-layers are oriented with angles of +45 degrees (in this case the voltage loads tend to deform in the same manner both the upper and lower active layers) (modeling of pure shear)

A.3.1.7: the active fibers in the upper and in the lower piezo-layers are oriented with angles of +45 degrees: simulation of a combined structural and electrical loading condition (self equilibrated shear forces distribution along the sides of the panel equal to $5x10^6$ Pa + Voltage effects) (modeling of electro-mechanical pure shear deformation: the piezo-layers are activated to reduce or to change the mechanical load effects)

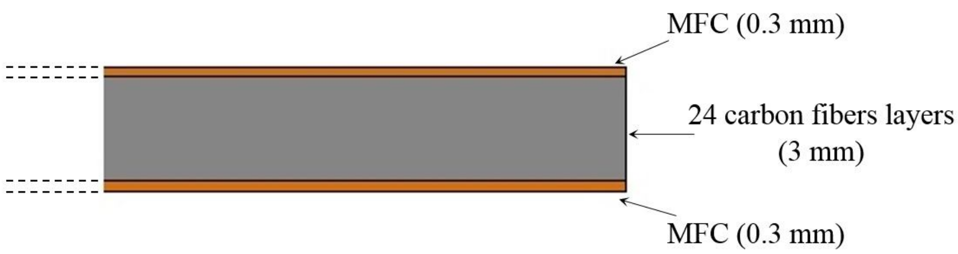

Figure 24: Geometry of the Specimen Type 3

All the carbon fibers stacking sequences indicated in the Table 5.1 have been examined according to the previous lists of analyses.

5.4 Hybrid specimens with carbon fibers substrate and embedded piezo-layers: Specimen Type 4

The fourth group of specimens analyzed are composed with a substrate of orthotropic carbon fibers laminate together with embedded piezo-electric active layers. In this case the outer layers are made of a single lamina of carbon fiber with a thickness of 0.125 mm: these layers cover the piezo-electric active layers (0.3 mm thick) while the core is made with the remaining laminae (2.75 mm thick).

The geometry of the panel has been reproduced in the Figure 25.

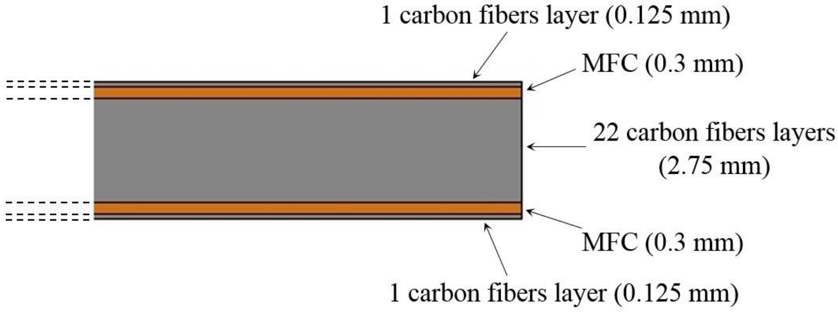

Figure 25: Geometry of the Specimen Type 4

For this specimen configuration have been carried out analyses similar to the specimen Type 3.

5.5 Summary of the numerical results

In the Table 5.2-a/g and 5.4-a/b are summarized the main results obtained with the preliminary numerical analyses carried out on hybrid specimens.

Analysis Id	Max Displacement **U-z [mm]** (bending)	Max Displacement **U-z [mm]** (torsion)	Max Rotation **Rot-x [deg]** (torsion)	Max axial deformation **με** (MFC)	Max shear stress **τ** and **σ_z** at the MFC interface **[MPa]**	Max Electrical Power **[W]**
A.1.1	2.50	/	/	733	11.33 / 5.02	1.71
A.1.2	/	0.77	0.98	611	14.69 / 7.76	1.65
A.1.3	2.05*	/	0.05	824	13.08 / 4.99	1.40
A.1.4	/	0.86*	0.26	637	14.76 / 7.34	1.36
A.1.5	0	/	/	731	11.37 / 7.09	1.53
A.1.6	/	/	/	529	15.81 / 1.94	1.62
A.1.7	/	/	/	400	15.28 / 1.82	1.54

Table 5.2-a: Numerical results – specimen Type 1 (Al substrate)

(*) Note: the data are referred to combined bending and torsion effects.

Analysis Id	Max Displacement **U-z [mm]** (bending)	Max Displacement **U-z [mm]** (torsion)	Max Rotation **Rot-x [deg]** (torsion)	Max axial deformation **με** (MFC)	Max shear stress **τ** and **σ_z** at the MFC interface **[MPa]**	Max Electrical Power **[W]**
A.2.1	2.17	/	/	435	6.70 / 5.16	1.68
A.2.2	/	0.67	0.86	471	9.81 / 7.35	1.64
A.2.3	1.81*	/	0.05	477	8.09 / 5.12	1.38
A.2.4	/	0.75*	0.23	564	9.84 / 6.99	1.35
A.2.5	0	/	/	434	6.77 / 6.83	1.53
A.2.6	/	/	/	335	11.29 / 0.85	1.62
A.2.7	/	/	/	221	15.28 / 1.82	1.54

Table 5.2-b: Numerical results – specimen Type 2 (Al substrate + embedded piezo)

Analysis Id	Max Displacement **U-z [mm]** (bending)	Max Displacement **U-z [mm]** (torsion)	Max Rotation **Rot-x [deg]** (torsion)	Max axial deformation **με** (MFC)	Max shear stress **τ** and **σ_z** at the MFC interface **[MPa]**	Max Electrical Power **[W]**
A.3.1.1	1.35	/	/	741	11.31 / 5.13	1.66
A.3.1.2	/	1.66	2.12	1493	10.41 / 9.67	1.79
A.3.1.3	0.35*	/	0.15	887	17.37 / 16.85	1.40
A.3.1.4	/	1.52*	1.84	1348	10.42 / 17.79	1.56
A.3.1.5	0.14	/	/	741	11.32 / 6.74	1.56
A.3.1.6	/	/	/	967	13.43/ 5.78	1.68
A.3.1.7	/	/	/	626	16.09 / 6.97	2.12

Table 5.2-c: Numerical results – specimens Type 3 (Carbon-fibers Substrate: Sequences: N. 1)

(*) Note: the data are referred to combined bending and torsion effects.

Analysis Id	Max Displacement **U-z [mm]** (bending)	Max Displacement **U-z [mm]** (torsion)	Max Rotation **Rot-x [deg]** (torsion)	Max axial deformation **με** (MFC)	Max shear stress **τ** and **σ_z** at the MFC interface **[MPa]**	Max Electrical Power **[W]**
A.3.2.1	1.78	/	/	703	11.78 / 4.85	1.68
A.3.2.2	/	1.09	1.37	932	15.39 / 8.73	1.71
A.3.2.3	0.35*	/	0.08	816	18.02 / 16.85	1.40
A.3.2.4	/	1.05*	1.20	928	15.36 / 17.50	1.49
A.3.2.5	0.09	/	/	702	11.77 / 6.80	1.55
A.3.2.6	/	/	/	704	18.05 / 8.10	1.59
A.3.2.7	/	/	/	515	17.81 / 7.96	2.21

Table 5.2-d: Numerical results – specimens Type 3 (Carbon-fibers Substrate: Sequences: N. 2)

Analysis Id	Max Displacement **U-z [mm]** (bending)	Max Displacement **U-z [mm]** (torsion)	Max Rotation **Rot-x [deg]** (torsion)	Max axial deformation **με** (MFC)	Max shear stress **τ** and **σ_z** at the MFC interface **[MPa]**	Max Electrical Power **[W]**
A.3.3.1	2.04	/	/	711	11.91 / 4.86	1.69
A.3.3.2	/	0.86	1.10	693	17.02 / 8.30	1.68
A.3.3.3	0.37*	/	0.06	791	18.31 / 16.85	1.40
A.3.3.4	/	0.88*	0.96	807	17.02 / 17.42	1.46
A.3.3.5	0.09	/	/	710	11.94 / 6.85	1.54
A.3.3.6	/	/	/	623	19.31 / 8.90	1.56
A.3.3.7	/	/	/	474	18.39 / 8.44	2.22

Table 5.2-e: Numerical results – specimens Type 3 (Carbon-fibers Substrate: Sequences: N. 3)

(*) Note: the data are referred to combined bending and torsion effects.

Analysis Id	Max Displacement **U-z [mm]** (bending)	Max Displacement **U-z [mm]** (torsion)	Max Rotation **Rot-x [deg]** (torsion)	Max axial deformation **με** (MFC)	Max shear stress **τ** and **σ_z** at the MFC interface **[MPa]**	Max Electrical Power **[W]**
A.3.4.1	2.48	/	/	754	11.92 / 8.49	1.71
A.3.4.2	/	0.75	0.95	646	17.75 / 12.37	1.66
A.3.4.3	0.42*	/	0.05	782	18.43 / 16.85	1.41
A.3.4.4	/	0.80*	0.82	742	17.72 / 17.30	1.45
A.3.4.5	0.50	/	/	1045	15.28 / 7.70	1.53
A.3.4.6	/	/	/	566	20.60 / 8.90	1.54
A.3.4.7	/	/	/	456	18.99 / 8.10	2.24

Table 5.2-f: Numerical results – specimens Type 3 (Carbon-fibers Substrate: Sequences: N. 4)

Analysis Id	Max Displacement **U-z [mm]** (bending)	Max Displacement **U-z [mm]** (torsion)	Max Rotation **Rot-x [deg]** (torsion)	Max axial deformation **με** (MFC)	Max shear stress **τ** and **σ_z** at the MFC interface **[MPa]**	Max Electrical Power **[W]**
A.3.5.1	4.44	/	/	1056	15.89 / 6.70	1.83
A.3.5.2	/	0.60	0.77	597	18.67 / 8.10	1.65
A.3.5.3	0.70*	/	0.04	919	18.13 / 16.92	1.47
A.3.5.4	/	0.82	0.53	676	18.59 / 17.30	1.44
A.3.5.5	0.11	/	/	751	12.01 / 7.00	1.54
A.3.5.6	/	/	/	587	19.77 / 9.50	1.55
A.3.5.7	/	/	/	457	18.55 / 8.89	2.23

Table 5.2-g: Numerical results – specimens Type 3 (Carbon-fibers Substrate: Sequences: N. 5)

(*) Note: the data are referred to combined bending and torsion effects.

Sequence N.	0 degrees	+ 45 degrees	- 45 degrees	E11 [GPa]	E22 [GPa]	ν12	ν21	G12 [GPa]
1 (core)	22	0	0	148	9.66	0.3	0.02	4.55
1 (external plies)	2	0	0	148	9.66	0.3	0.02	4.55
2 (core)	0	10	12	16.4	16.4	0.799	0.799	38
2 (external plies)	0	2	0	148**	9.66**	0.3**	0.02**	4.55**

Table 5.3: Elastic properties of the carbon fibers laminae in the Specimen Type 4 (Carbon-fibers Substrate + embedded piezo)

(**) Note: the data are referred to the single unidirectional ply.

Analysis Id	Max Displacement **U-z [mm]** (bending)	Max Displacement **U-z [mm]** (torsion)	Max Rotation **Rot-x [deg]** (torsion)	Max axial deformation **με** (MFC)	Max shear stress **τ** and **σ_z** at the MFC interface **[MPa]**	Max Electrical Power **[W]**
A.4.1.1	1.27	/	/	433	5.97 / 5.24	1.64
A.4.1.2	/	1.55	1.98	1370	6.32 / 9.14	1.78
A.4.1.3	1.05*	/	0.30	356	7.00 / 5.45	1.06
A.4.1.4	/	1.41*	1.71	1219	6.28 / 8.55	1.47
A.4.1.5	0.14	/	/	302	5.98 / 6.60	1.55
A.4.1.6				844	9.47 / 9.74	1.68
A.4.1.7				1198	9.51 / 10.46	1.69

Table 5.4-a: Numerical results – specimens Type 4 (Carbon-fibers Substrate: Sequences: N. 1)

(*) Note: the data are referred to combined bending and torsion effects.

Analysis Id	Max Displacement **U-z [mm]** (bending)	Max Displacement **U-z [mm]** (torsion)	Max Rotation **Rot-x [deg]** (torsion)	Max axial deformation **με** (MFC)	Max shear stress **τ** and **σ_z** at the MFC interface **[MPa]**	Max Electrical Power **[W]**
A.4.5.1	4.26	/	/	870	22.32 / 6.62	1.80
A.4.5.2	/	1.64	2.09	1171	5.93 / 9.18	1.76
A.4.5.3	2.79*	/	0.07	831	8.28 / 6.10	1.12
A.4.5.4	/	1.51*	1.80	1018	5.86 / 8.53	1.45
A.4.5.5	0.50*	/	/	862	7.38 / 7.92	1.51
A.4.5.6	/	/	/	776	9.12 / 9.90	1.65
A.4.5.7	/	/	/	1153	9.23 / 10.49	1.66

Table 5.4-b: Numerical results – specimens Type 4 (Carbon-fibers Substrate: Sequences: N. 5)

(*) Note: the data are referred to combined bending and torsion effects.

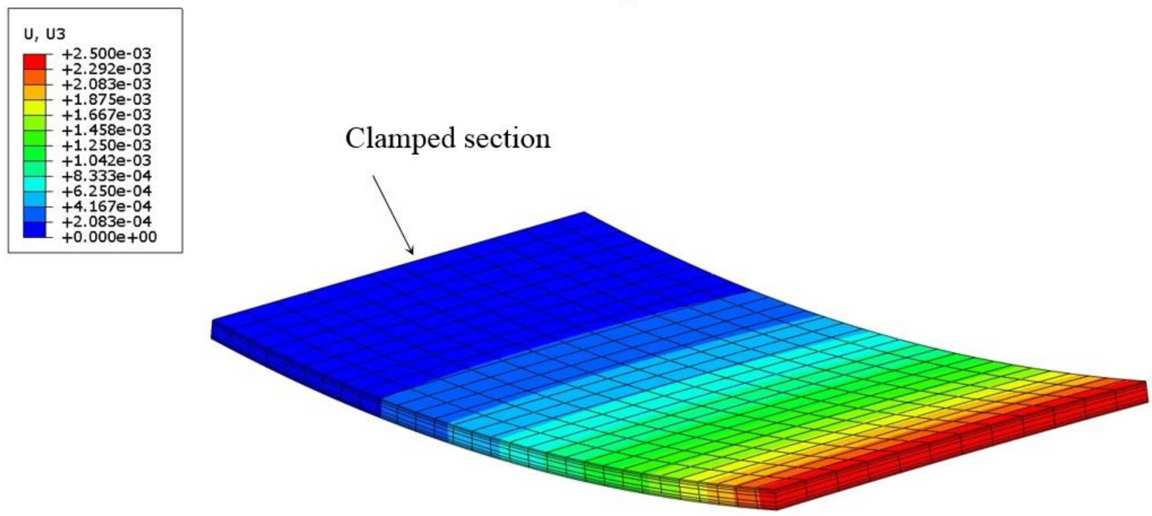

Figure 26: Deformed shape for the analysis A.1.1 – Bending (units: m).
Specimen Type 1: ΔV = 1000 V.
The fibers in the piezo-layers are parallel to the x axis (1 in Fig. 21): 0 degrees orientation.

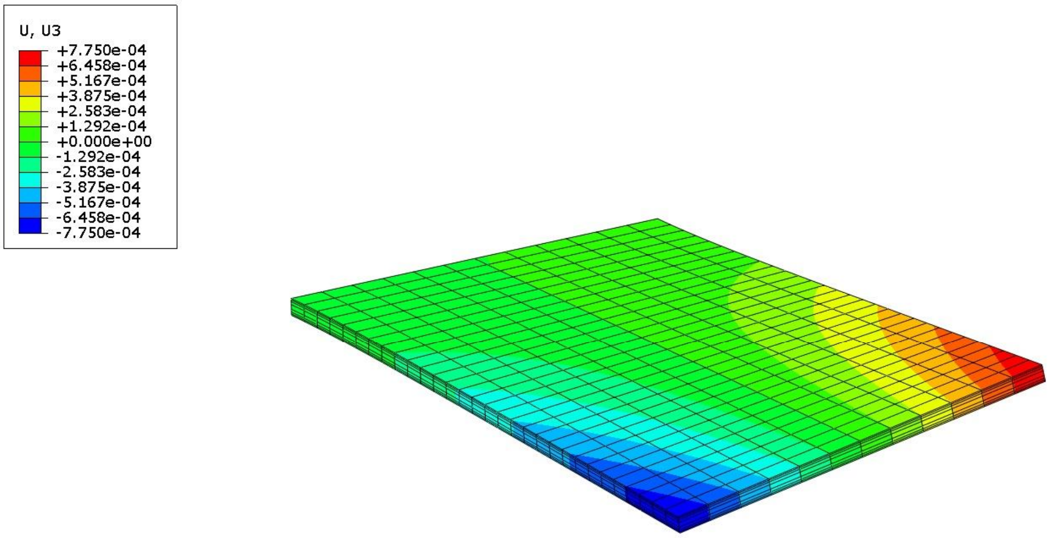

Figure 27: Deformed shape analysis A.1.2 – Torsion (units: m).
Specimen Type 1: ΔV = 1000 V.
The fibers in the piezo-layers are oriented with angles of ±45 degrees with respect to x axis.

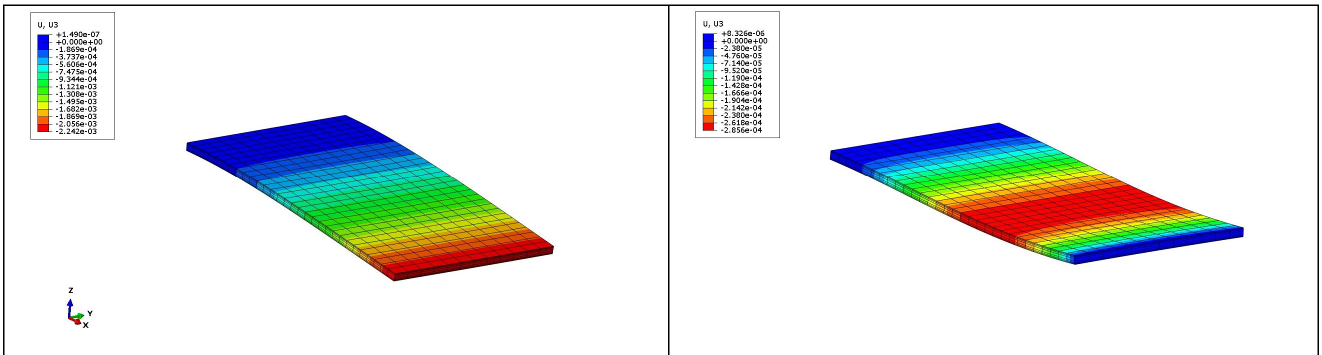

(a) Only Uniform Pressure Loads (8500 Pa)	(b) Combined Loads

Figure 28: Deformed shape analysis A.1.5 – Bending (units: m).
Specimen Type 1: ΔV = 1000 V.
Active fibers with 0 degrees orientation: effect of combined loads (pressure and voltage).

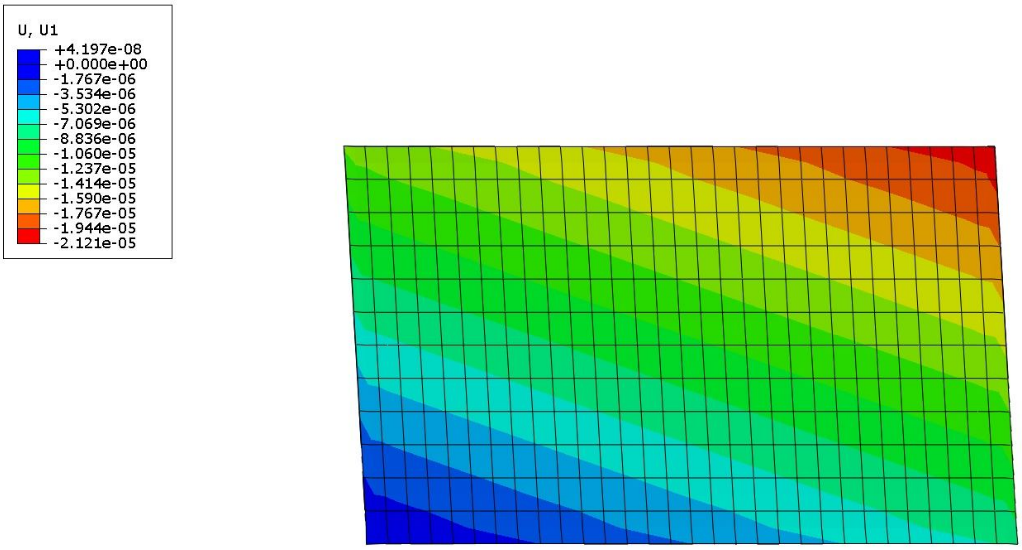

Figure 29: Deformed shape analysis A.1.6 – In-Plane Shear (units: m).
Specimen Type 1: ΔV = 1000 V.
The fibers in the piezo-layers are oriented with angles of +45 degrees with respect to x axis.

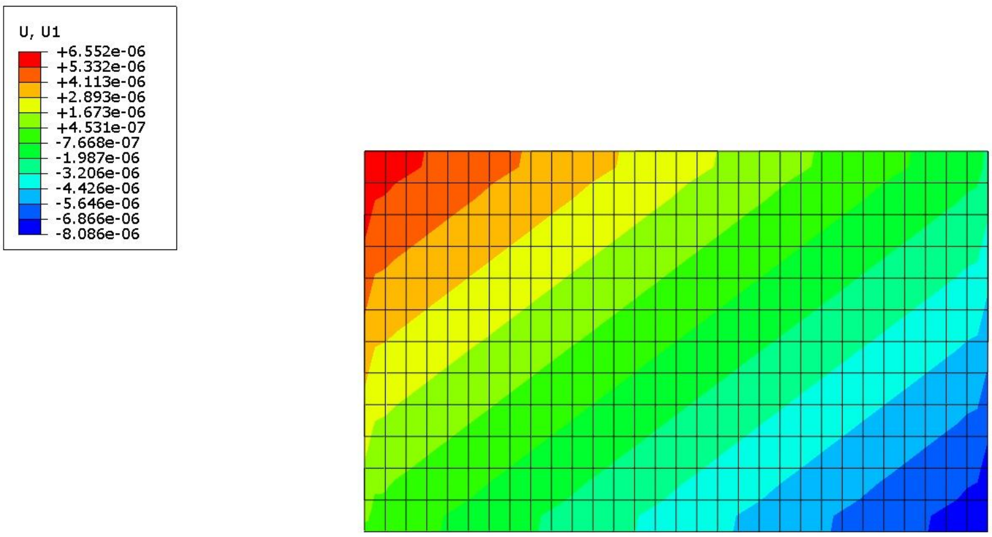

Figure 30: Deformed shape analysis A.1.7 – In-Plane Shear (units: m).
Specimen Type 1: ΔV = 1000 V.
Active fibers with +45 degrees orientation: effect of combined loads (shear and voltage).
(distributed shear load of $5x10^6$ Pa along the four sides of the panel)

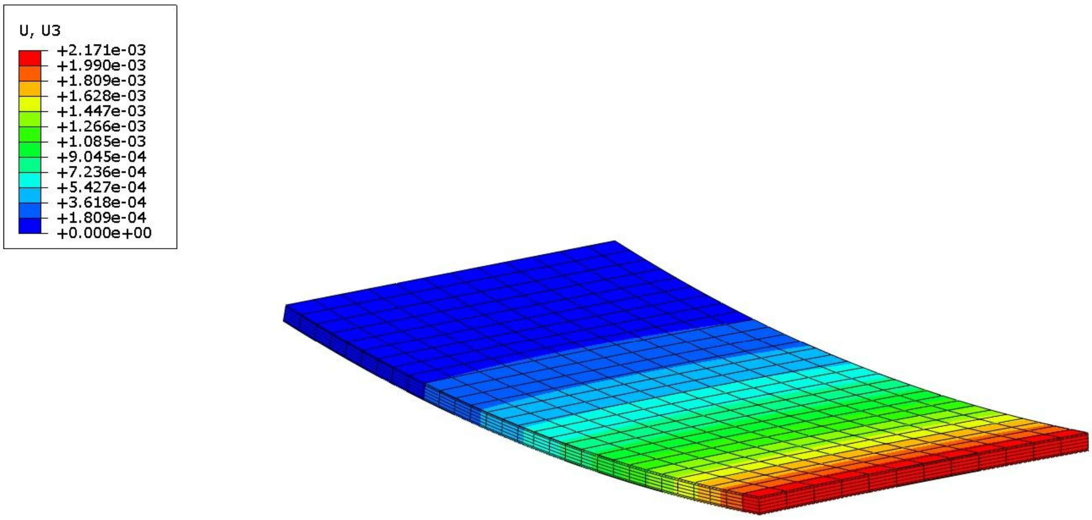

Figure 31: Deformed shape analysis A.2.1 – Bending (units: m).
Specimen Type 2: ΔV = 1000 V.
The fibers in the piezo-layers are parallel to the x axis (1 in Fig. 21): 0 degrees orientation.

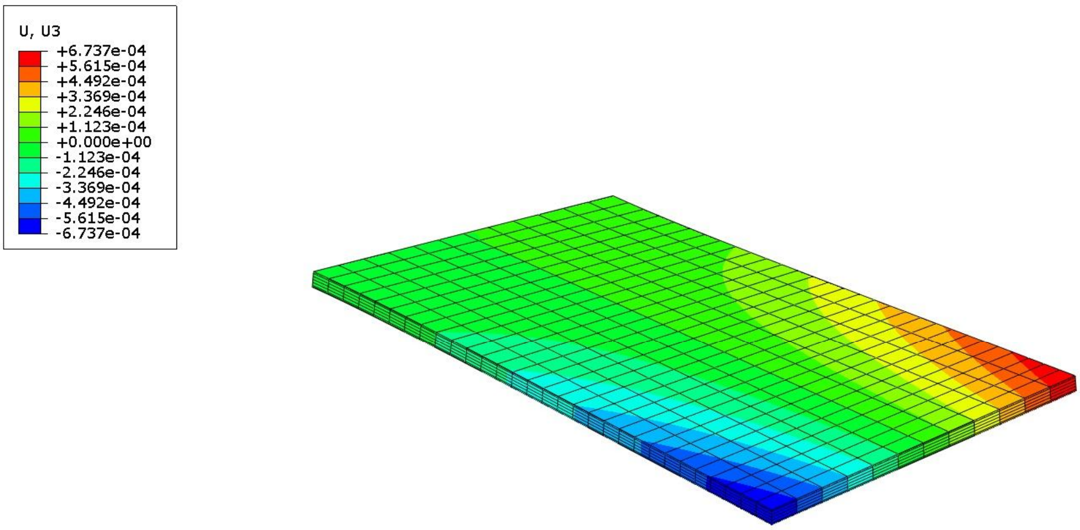

Figure 32: Deformed shape analysis A.2.2 – Torsion (units: m).
Specimen Type 2: ΔV = 1000 V.
The fibers in the piezo-layers are oriented with angles of ±45 degrees with respect to x axis.

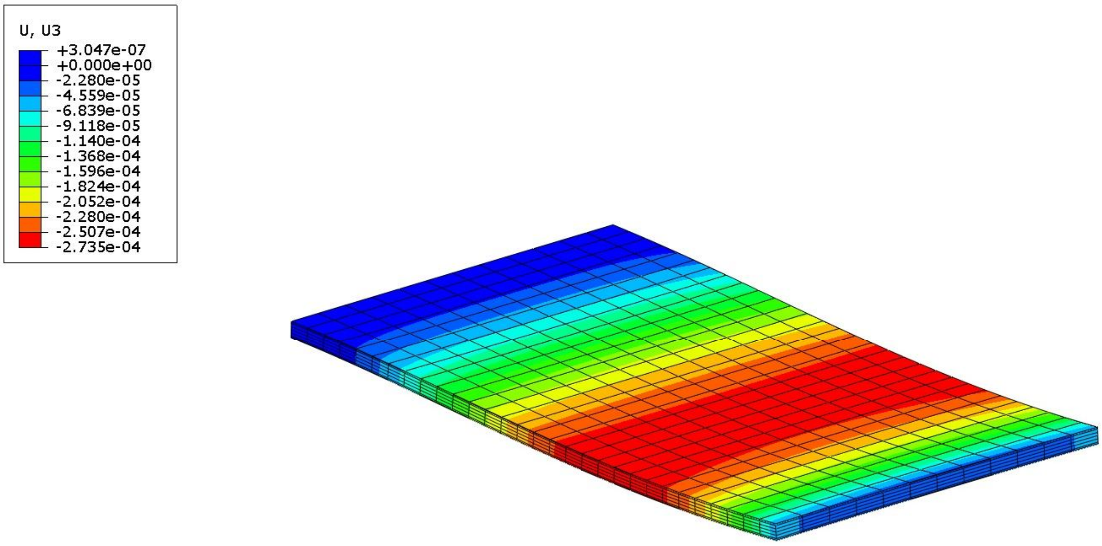

Figure 33: Deformed shape analysis A.2.5 – Bending (units: m).
Specimen Type 2: ΔV = 1000 V.
Active fibers with 0 degrees orientation: effect of combined loads (pressure and voltage).

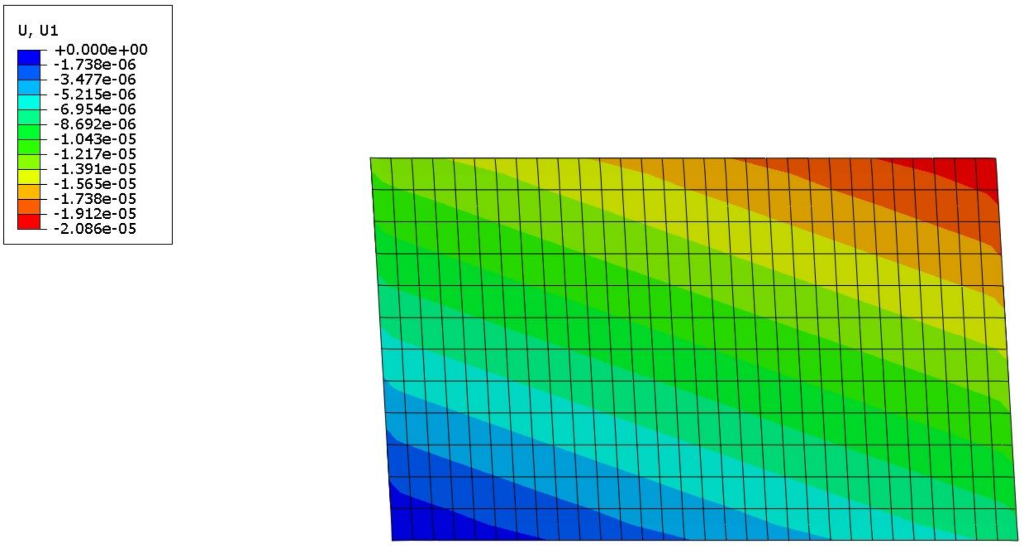

Figure 34: Deformed shape analysis A.2.6 – In-Plane Shear (units: m).
Specimen Type 2: ΔV = 1000 V.
The fibers in the piezo-layers are oriented with angles of +45 degrees with respect to x axis.

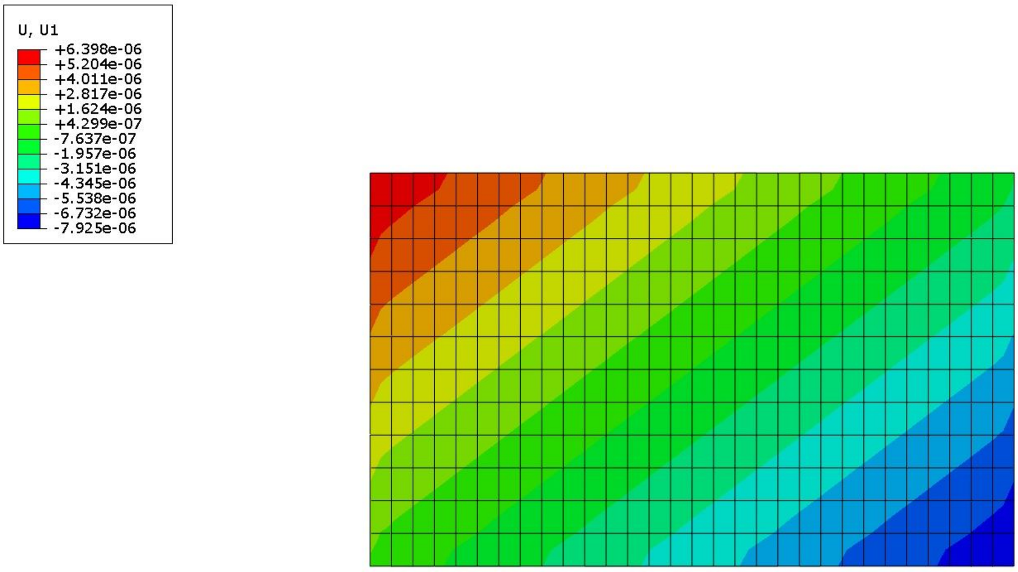

Figure 35: Deformed shape analysis A.2.7 – In-Plane Shear (units: m).
Specimen Type 2: ΔV = 1000 V.
Active fibers with +45 degrees orientation: effect of combined loads (shear and voltage).

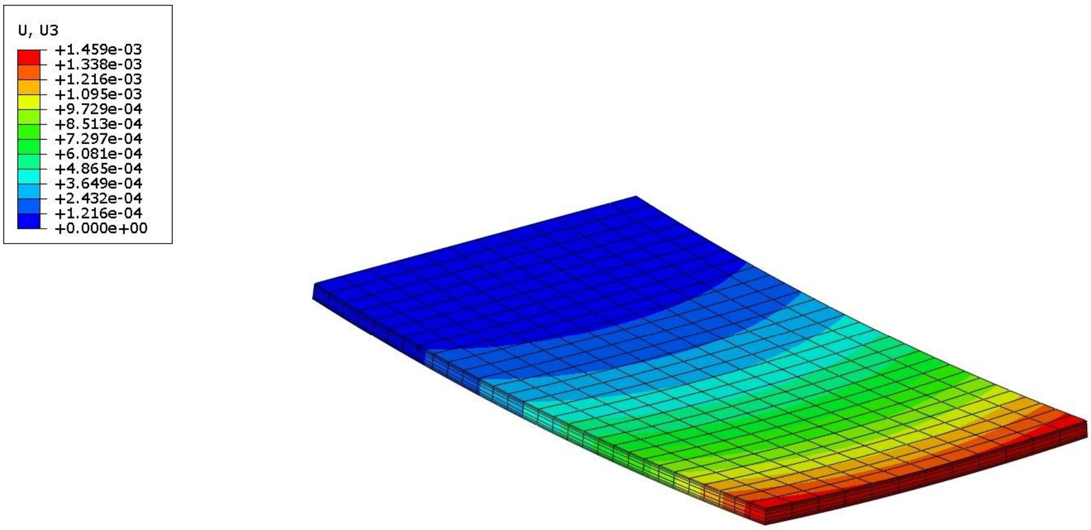

Figure 36: Deformed shape analysis A.3.1.1 – Bending (units: m).
Specimen Type 3 – Sequences N. 1: ΔV = 1000 V.
The fibers in the piezo-layers are parallel to the x axis (1 in Fig. 21): 0 degrees orientation.

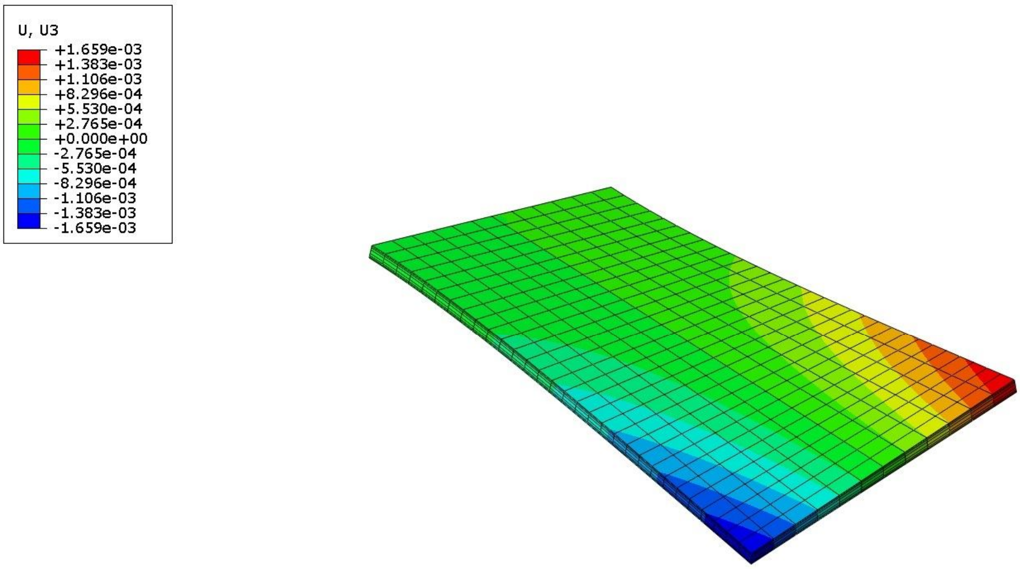

Figure 37: Deformed shape analysis A.3.1.2 – Torsion (units: m).
Specimen Type 3 – Sequences N. 1: ΔV = 1000 V.
The fibers in the piezo-layers are oriented with angles of ±45 degrees with respect to x axis.

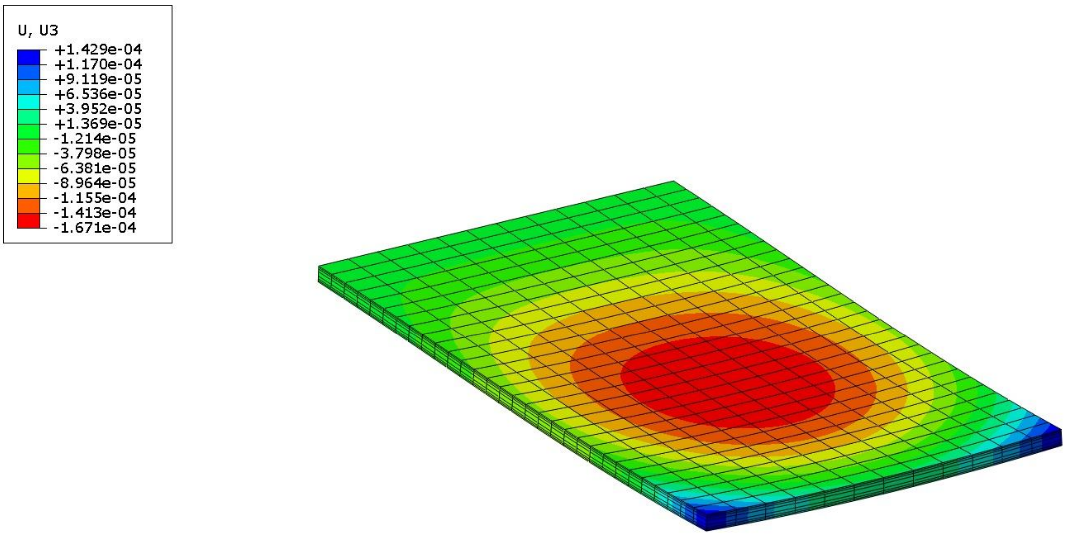

Figure 38: Deformed shape analysis A.3.1.5 – Bending (units: m).
Specimen Type 3 – Sequences N. 1: ΔV = 1000 V.
Active fibers with 0 degrees orientation: effect of combined loads (pressure and voltage).

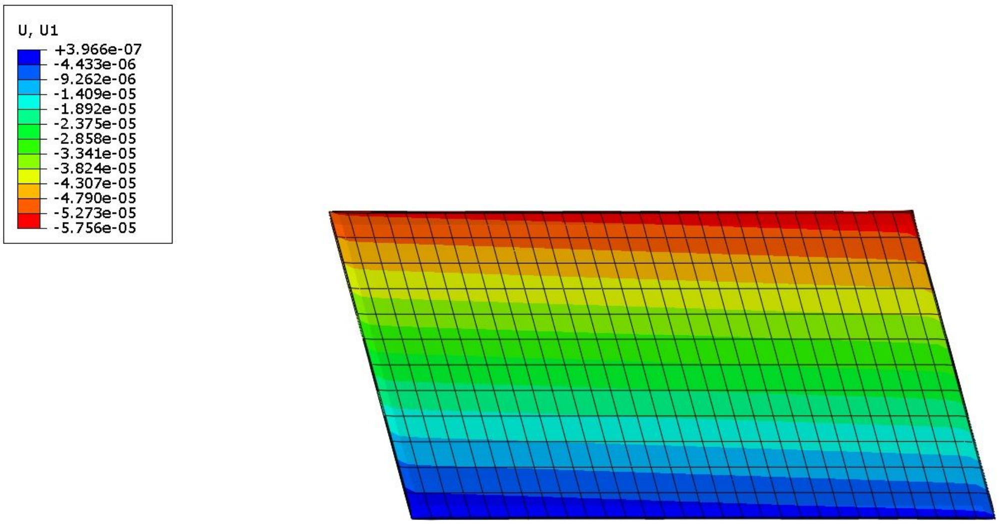

Figure 39: Deformed shape analysis A.3.1.6 – In-Plane Shear (units: m).
Specimen Type 3 – Sequences N. 1: ΔV = 1000 V.
The fibers in the piezo-layers are oriented with angles of +45 degrees with respect to x axis.

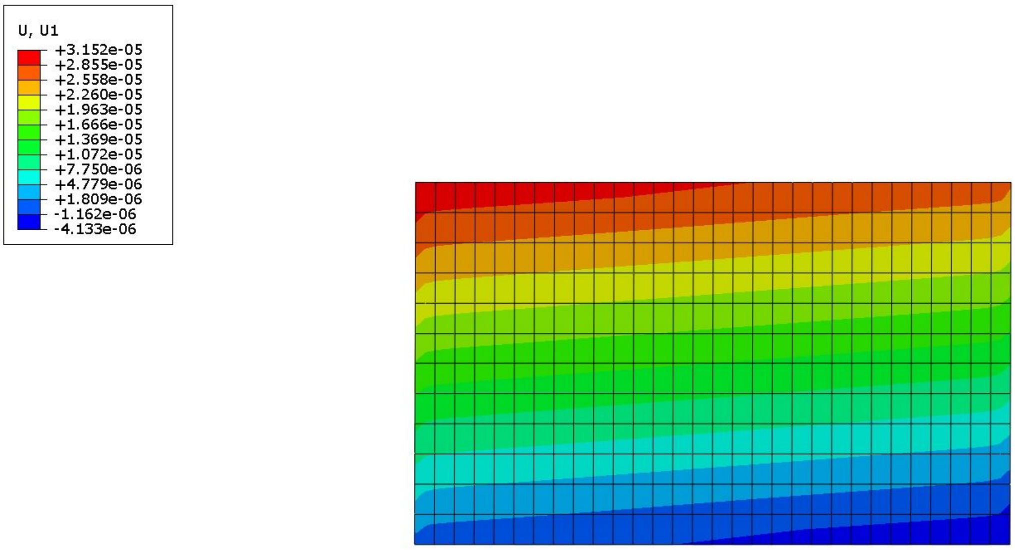

Figure 40: Deformed shape analysis A.3.1.7 – In-Plane Shear (units: m).
Specimen Type 3 – Sequences N. 1: ΔV = 1000 V.
Active fibers with +45 degrees orientation: effect of combined loads (shear and voltage).

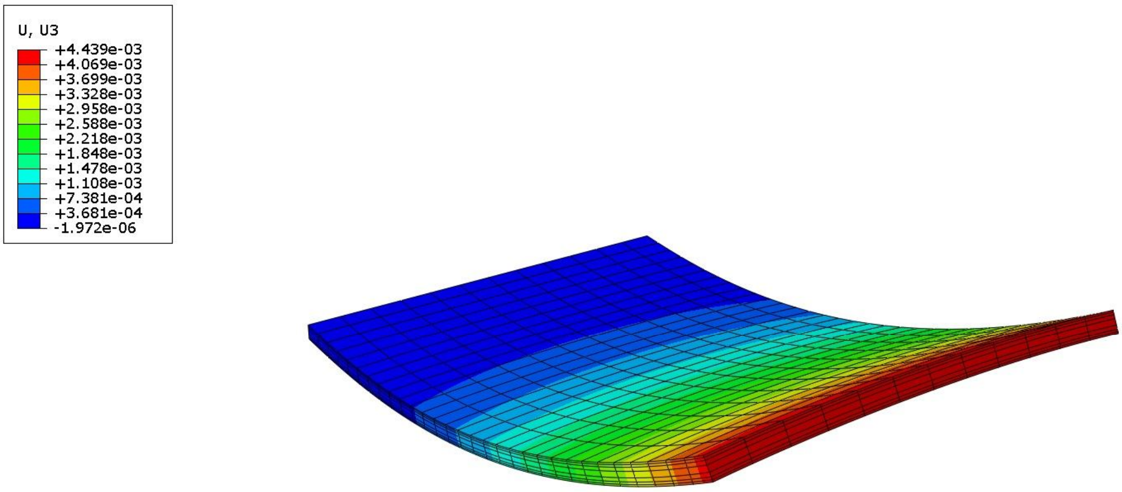

Figure 41: Deformed shape analysis A.3.5.1 – Bending (units: m).
Specimen Type 3 – Sequences N. 5: ΔV = 1000 V.
The fibers in the piezo-layers are parallel to the x axis (1 in Fig. 21): 0 degrees orientation.

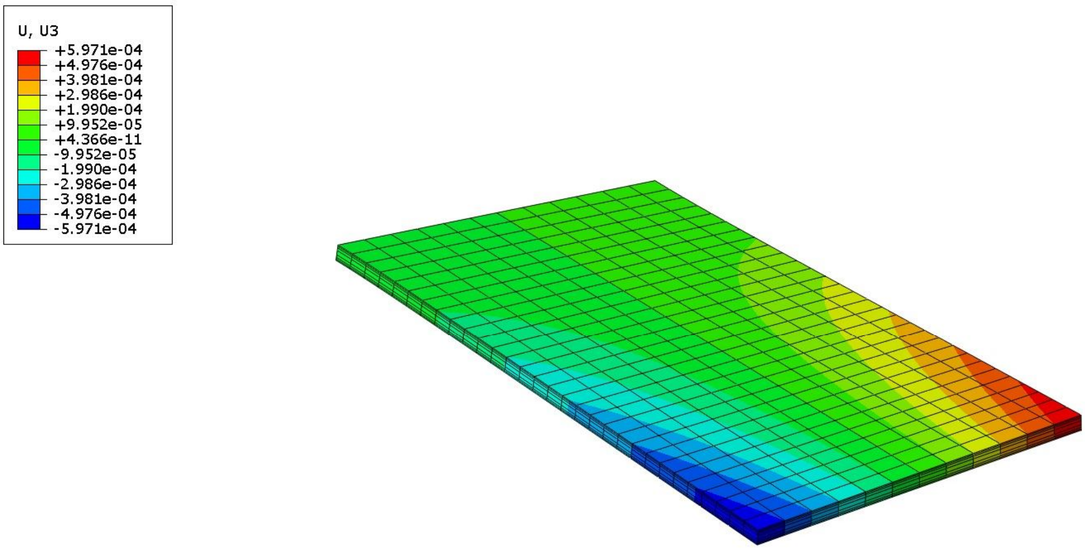

Figure 42: Deformed shape analysis A.3.5.2 – Torsion (units: m).
Specimen Type 3 – Sequences N. 5: ΔV = 1000 V.
The fibers in the piezo-layers are oriented with angles of ±45 degrees with respect to x axis.

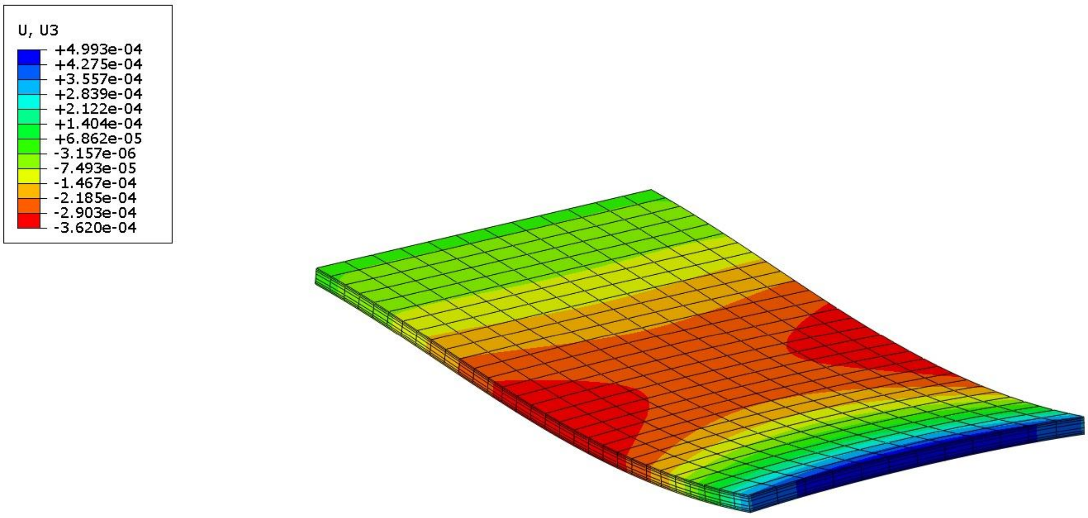

Figure 43: Deformed shape analysis A.3.5.5 – Bending (units: m).
Specimen Type 3 – Sequences N. 5: ΔV = 1000 V.
Active fibers with 0 degrees orientation: effect of combined loads (pressure and voltage).

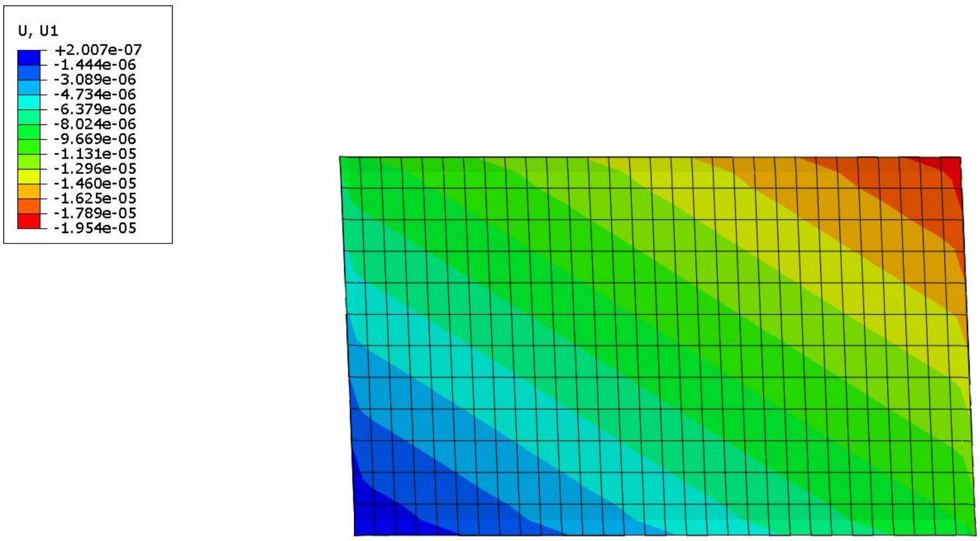

Figure 44: Deformed shape analysis A.3.5.6 – In-Plane Shear (units: m).
Specimen Type 3 – Sequences N. 5: ΔV = 1000 V.
The fibers in the piezo-layers are oriented with angles of +45 degrees with respect to x axis.

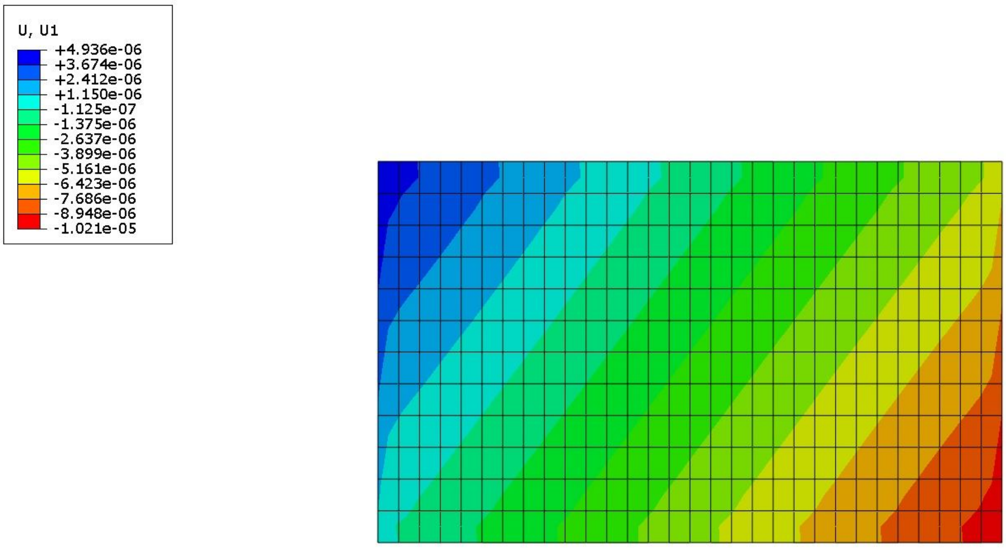

Figure 45: Deformed shape analysis A.3.5.7 – In-Plane Shear (units: m). Specimen Type 3 – Sequences N. 5: ΔV = 1000 V. Active fibers with +45 degrees orientation: effect of combined loads (shear and voltage).

5.6 Brief discussion of the results

The preliminary campaign of numerical analyses carried out within the FutureWings project shows that the application of the MFC technology to build specimens of hybrid material appears to be very promising.

In terms of displacements and rotations the results are very significant: this means that the required flexural-torsional deformed shapes of suitable wing box models of the FutureWings Unit will be obtained with similar technology.

More in particular, for the geometry examined (a plate with a width of 90 mm and a length of 150 mm, see Fig. 22) the maximum displacements at the tip section range between 0.1 mm and 4.5 mm and the angular rotations at the tip section range between 0 deg and 2 deg.

Pure shear deformations can be obtained controlling in a suitable way the active piezoelectric layers: this fact will be very important to control the torsion deformation of the wing box models of the FutureWings Unit.

In the Table 5.2 and 5.4 are shown the absolute values of the maximum axial deformations in the MFC fibers. These values agree with the allowable values of the piezoelectric material (compare the data of Figure 9-(a) with the $\mu\varepsilon$ data of Table 5.2 and Table 5.4).

The design of the FutureWings Unit will be based on a stiffness approach: that is the displacements of the wing box will be controlled to get the desired shape of the unit. From this point of view, the available technology provided by MFC elements appear to guarantee sufficient reliability to get the basic goals of the project adopting both the MFC P1 and/or the MFC P2 patches as shown in the Annex 1. The estimated electric power required by the specimens reaches fully acceptable values.

According to the present preliminary results, in the desing phase of the specimens will be taken into the correct account the real behaviors of the MFC P1 and MFC P2 patches.

5.7 References of Section 5

5.1 J. Riemenschneider et alii, *Overview of the common DLR/ONERA project "ACTIVE TWIST BLADE" (ATB)*, 30th European Rotorcraft Forum, 14th-16th September 2004, Marseilles, France

5.2 P. Masarati et alii, *Optimal design of an active twist 1:2.5 scale rotor blade*, 31th European Rotorcraft Forum, 13th-15th September 2005, Florence, Italy

5.3 M. Schulz, S. Opitz, J. Riemenschneider, "*A new concept to determine the mass distribution of an active twist rotor blade*", Deutsches Zentrum fur Luft- und Raumfahrt e.V. 2012

5.4 C. Niezrecki, D. Brei, S. Balakrishnan, and A. Moskalik, *"Piezoelectric Actuation: State of the Art"*, Department of Mechanical Engineering, University of Florida, Gainesville, FL; Department of Mechanical Engineering and Applied Mechanics, University of Michigan,Ann Arbor, MI, USA, 2001

5.5 D. Cadogan, T. Smith, F. Uhelsky, M. MacKusick, *"Morphing Inflatable Wing Development for Compact Package Unmanned Aerial Vehicles"*, American Institute of Aeronautics and Astronautics

5.6 M. Sitti, D. Campolo, J. Yan, R. S. Fearing, T. Su, D. Taylor, T. D. Sands, *"Development of PZT and PZN-PT Based Unimorph Actuators for Micromechanical Flapping Mechanisms"*, Proceedings of the 2001 IEEE International Conference on Robotics & Automation, Seoul, Korea, May 21-26, 2001

5.7 K. S. Ha, Y. Huang, Y. Nagata, A. Ming, *"Development of an Active Wing for Flight Machines Using Macro Fiber Composites"*, Proceedings of the 2006 IEEE International Conference on Mechatronics and Automation, Luoyang, China, June 25 - 28, 2006

6 Preliminary concept of the control system

With the introduction of novel active components as part of the flight steering and control system the design of the suitable control algorithm and hardware is essential. With respect to the fact that all piezoelectric materials are typically showing some hysteresis effects all open-loop control approaches will fail.

For this background the structure needs to be deformed using a closed-loop control system as shown in principle in Figure 46.

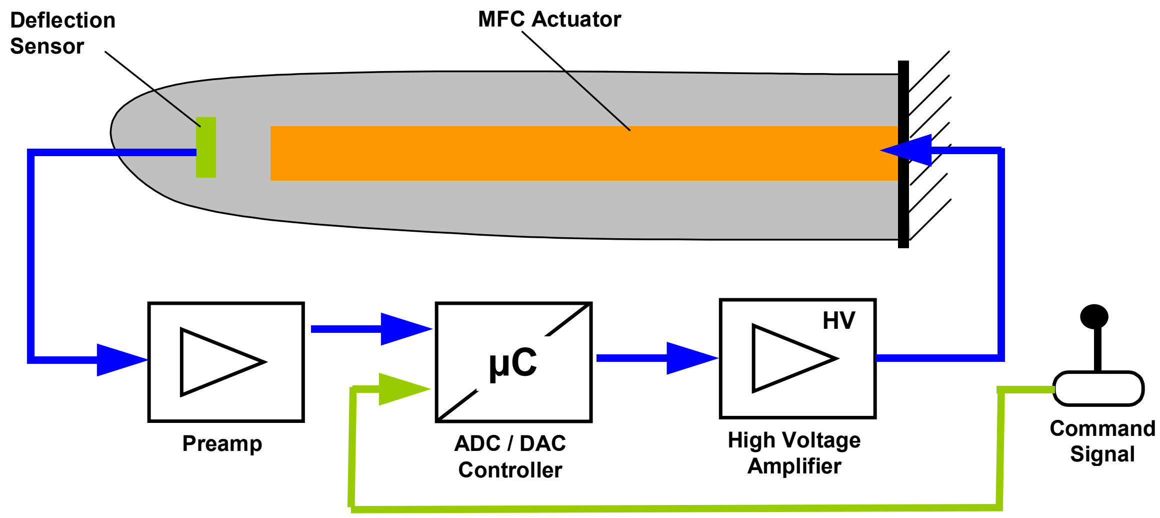

Figure 46: Principle of a closed-loop control system

Using command signal from the pilot the central controller unit generates a low voltage signal for the piezo actuators which is being amplified with the HV amp to a suitable high voltage level and applied to the MFC actuators. Due to the generated strain the wing is being twisted and the reached deformation will be detected using the also embedded deflection sensor. After a pre-amplification of this signal the controller unit will be able to compare the required command signal position with the real reached deformation and can adjust the MFC signal if needed.

Using such a closed-loop system will be necessary as due to the deformation of the wing the aerodynamic loads will vary so that there will always be an overlay of piezoelectric and aeroelastic deformation.

7 Overall References

Thunder Publication List

1. A. Hoyt Haight, L. Harrah, R. Allred,; S. Scarborough, D. Gleeson, and D. Cadogan, "Thermal Reversibility and Morphing of Light Cured Inflatable Composite Beams," *46th AIAA/ASME/ASCE/AHS/ASC Structures, Structural Dynamics and Materials Conference,* **AIAA-2005-1808**, Apr. 18-21, 2005, Austin TX.
2. Aimmanee, S., and Hyer, M. W., "Analysis of the Manufactured Shape of Rectangular THUNDER®-Type Actuators," *Smart Materials and Structures*, **13**, 1389–1406 (2004).
3. N. Pern and J. Jacob, "Comparison between Zero Mass Flux Flow Control Methods for Low Speed Airfoil Separation Control," *AIAA,* **2005-4884**, (2005).
4. Alexander, Paul W. and Diann Brei, "Piezoceramic Telescopic Actuator Quasi-Static Experimental Characterization," *Journal of Intelligent Material Systems and Structures*, **14**, 643–655 (2003).
5. Allison, S.G., Fox, R.L., Froggatt, M.E., Childers, B.A., "Novel piezoelectric actuators for tuning an optical fiber Bragg grating," *Optical Engineering*, **41**(10), 2448 – 2455 (2002).
6. Allison, S.G., Fox, R.L., Froggatt, M.E., Childers, B.A., "THUNDER piezoelectric actuators as a method of stretch-tuning an optical fiber grating," *Proc. SPIE*, Vol. **3991**, 74 - 83 (2000).
7. Andoh, Fukashi Gregory Washington, Hwan-Sik Yoon, and Vadim Utkin, "Efficient Shape Control of Distributed Reflectors with Discrete Piezoelectric Actuators," *Journal of Intelligent Material Systems and Structures*, **15**, 3 – 15 (2004).
8. Balakrishnan, S., and Niezrecki, C., "Investigation of THUNDER (TM) Actuators as Underwater Propulsors," *Journal of Intelligent Material Systems and Structures*, **13**, 193 – 207 (2002).
9. Ball, B.L., Smith, R.C. and Ounaies, Z., "A Dynamic Hysteresis Model for THUNDER® Transducers," *Proceedings of the SPIE Int. Soc Opt*., **5049**, 100 – 111 (2003).
10. Aydin Dogan; James Tressler; Robert E. Newnham, "Solid-State Ceramic Actuator Designs," *AIAA Journal-0001-1452*, **39** (7), 1354 - 1362 (2001).
11. Bechet, Antoine Yves H. Berthelot, and Christopher S. Lynch., "A Stress Gradient-enhanced Piezoelectric Actuator Composite (GEPAC) with Integrated Ultrasonic NDE Capability for Continuous Health Monitoring," *Journal of Intelligent Material Systems and Structures*, **16**, 85 – 93 (2005).
12. Bishop, R., and Mossi, K., "High displacement, high force piezoelectric actuator and sensor," *The Journal of the Acoustical Society of America*, **104(**3), 1828 (1998).
13. Bishop, R., Mossi, K., Swain, B., and Rose, N., Rugged, Robust, Reliable, "New Multi-Function, High-Sensitivity Sensor," *NASA Technology 2007 Conference*, Boston, MA.. (2007).
14. Bras, J. F., Johnson, M. E, and Fuller, C. R., "Active Control of Mechanical Impedance for Characterizing Actuator Performance," *138th ASA Meeting*, Norfolk, VA (1998).
15. Brei, Diann, Neal T. Berner, and Paul W. Alexander., "Modeling and Study of the Quasi-Static Behavior of Piezoceramic Telescopic Actuation Architectures," *Journal of Intelligent Material Systems and Structures*, **12,** 303 – 313 (2001).
16. Bryant, R. G., Mossi, K. M., Robbins, J. A., Batherl, B. F., "The Correlation of Electrical Properties of Prestressed Unimorphs as a Function of Mechanical Strain and Displacement," *Integrated Ferroelectrics*, **71**, 267 – 287 (2005).
17. Castro, N., "Numerical Modeling of Synthetic Jets in Quiescent Air with Moving Boundary Conditions," Master's thesis, Virginia Commonwealth University (2005).
18. Chung, Soon Wan and Kim, Seung Jo., "Investigation of actuating displacement performance of curved actuator by large-scale computation," *Smart Mater. Struct.,* **14**(4). 615 - 623 (2005).
19. Camargo, G; Ashford, G; Naco, E; Usher, T., "Experimental measurements and finite element models of High Displacement Piezoelectric Actuators," *Bulletin of the American Physical Society-Part 1.* Vol. **49**(1) K1, 223 (2004).
20. Capozzoli, M., Gopalakrishnan, J., Hogan, K., Massad, J., Tokarchik, T., Wilmarth, S., Banks, H., Mossi, K., and Smith, R., "Modeling Aspects Concerning THUNDER Actuators," *Proceedings of the SPIE Int. Soc. Opt.*, **3667**, 719 – 727 (1999).
21. Cheeseman, B. A.; Ruan, X. P.; Safari, A.; Danforth, S. C.; Chou, T. W., "Modeling and optimization of novel actuators produced by Solid Freeform Fabrication," *Materials Research Society Symposium Proceedings* **625** (Solid Freeform and Additive Fabrication), 159 -164 (2000).
22. Pavlos P. Vlachos, Martin J. Donnelly, Tavis L. Potter, Demetri P. Telionis and Norman W. Schaeffler, "Post-stall flow control of sharp edged-wings," *AIAA,* **1999-924**, (1999).
23. Choi, Sang H. Kyo D. Song, Glen C. King, Charles Woodall, Rectenna performances for smart membrane actuators," *Proc. SPIE*, Vol. **4700**, 213 - 221 (2002).
24. Chopra, Inderjit, "Review of state of art smart structures and integrated systems," *AIAA Journal*, **40**(11), 2145 - 2187 (2002).
25. Chung, Soon W. Seung J. Kim, "Optimal design of curved actuator through high-performance computing," *Proc. SPIE*, Vol. **5056**, 247 - 254 (2003).
26. Clark, William W. Randall Smith, Katherine Janes, John Winkler, Michael Mulcahy, "Development of a piezoelectrically actuated cell stretching device," *Proc. SPIE*, Vol. **3991**, 294 - 301 (2000).
27. Corsaro, Robert D., "Lightweight low-frequency woofer for active sound control in payload fairings," *Proc. SPIE,* Vol. **4332**, p. 254 - 258 (2001).
28. Cox, Adam Daniel Monopoli, Dragan Cveticanin, Michael Goldfarb and Ephrahim Garcia, "The Development of Elastodynamic Components for Piezoelectrically Actuated Flapping Micro-air Vehicles," *Journal of Intelligent Material Systems and Structures*, **13**, 611 – 615 (2002).
29. Dano, M. L. and Hyer, M. W., "Thermally-Induced Deformation Behavior of Unsymmetric Laminates," *International Journal of Solids and Structures*, **35**(17), 2102 – 2120 (1998).
30. Dogan, Aydin; Tressler, James; Newnham, Robert E., "Solid-state ceramic actuator designs," *AIAA Journal*, **39**(7), 1354 - 1362 (2001).
31. Doherty Kathleen M. and Mehrdad N. Ghasemi-Nejhad, "Performance of an Active Composite Strut for an Intelligent Composite Modified Stewart Platform for Thrust Vector Control," *Journal of Intelligent Material Systems and Structures*, **16**, 335 – 354 (2005).
32. Glenn Waterfield, "High Performance Pre-stressed Piezoelectric Bender Actuator for Digital Valves," *Ceramic Transactions,* **105**, 467 - 482 (2004).
33. Gao, J X and L Cheng, "Modelling of a high performance piezoelectric actuator assembly for active and passive vibration control," Smart Mater. Struct., **13**(2), 384 - 392 (2004).
34. Goo, Nam Seo Andi Haris, Hoon Cheol Park, and Kwang Joon Yoon, "Validation of a Laminated Beam Model of LIPCA Piezoelectric Actuators," *Journal of Intelligent Material Systems and Structures*, **16**, 189 – 195 (2005).
35. Goo, Nam Seo Cheol Kim, Young-Doo Kwon, and Kwang Joon Yoon, "Behaviors and Performance Evaluation of a Lightweight Piezo-Composite Curved Actuator," *Journal of Intelligent Material Systems and Structures*, **12**, 639 – 646 (2001).
36. Granger, R., Washington, G. N., and Kwak, S. K., "Modeling and Control of a Singly Curved Active Aperture Antenna Using Curved Piezoceramic Actuators," *J. of Intelligent Material Systems and Structures*, **11**(3), 225 – 233 (2000).
37. Granger, Richard Gregory Washington, and Seung-Keon Kwak, "Modeling and Control of a Singly Curved Active Aperture Antenna Using Curved Piezoceramic Actuators," *Journal of Intelligent Material Systems and Structures*, **11**, 225 – 233 (2000).
38. Green, C., Mossi, K., and Bryant, R., "Scavenging Energy From Piezoelectric Materials For Wireless Sensor Applications," *ASME: Proceedings of IMECE05* (2005).
39. Hodges, C.A., Mossi, K., and Scott, L., "Adhesive characterization in pre-stressed piezoelectric laminates," *Proceedings of the SPIE Int. Soc. Opt*., **5053**, 467 – 474 (2003).
40. Horner Garnet and Barmac Taleghani, "Single Axis Piezoceramic Gimbal," *Journal of Intelligent Material Systems and Structures*, **12**, 157 – 160 (2001).
41. Hyder, Christoph Garnett C. Horner, William W. Clark, "Linear traveling wave motor," *Proc. SPIE,* Vol. **3674**, 205 - 211 (1999).
42. Hyer, M.W., and A Jilani, "Predicting the Deformation Characteristics of Rectangular Unsymmetrically Laminated Piezoelectric Materials," *Smart Materials and Structures*, **7,** 784 – 791 (1998).
43. Hyer, Michael W. and Adel B. Jilani, "Manufactured Configurations of Piezoceramic Disk-Style Actuators," *Journal of Intelligent Material Systems and Structures*, **14**, 359 – 370 (2003).
44. Jayachandran, V., Meyer, N.E., Westervelt, M.A., and Sun, J.Q., "Piezoelectrically driven speakers for active interior noise suppression," *Applied Acoustics*, **57**, 263 – 277 (1999).
45. Jayachandran V, Patrick King, Nancy E Meyer, Florence J. Li, Maria Petrova, Melissa A. Westervelt, S. M. Hirsch and J. Q. Sun., "Real-time feed forward control of low-frequency interior noise using shallow spherical shell piezoceramic actuators," *Smart Mater. Struct*., **8**(5), 579 - 584 (1999).
46. Kahn, Manfred, Krause, D., and Chase, M., "Flaw Detection in d_{33} Mode Multilayer Ceramic Actuators Using Impedance-Frequency Scans," *Materials Evaluation*, **54**(6), 749 – 754 (1996).
47. Kugel, V.D., Chandran, S., and Cross, L.E., "Comparative analysis of piezoelectric bonding-mode actuators," *Proceedings of the SPIE Int. Soc Opt*., **3040**, 70 – 80 (1997).
48. Kymissis, J., C. Kendall, J. Paradiso, and N. Gershenfeld, "Parasitic Power Harvesting in Shoes," *Second IEEE International Conference on Wearable Computing*, (1998).
49. Lee, Sangki Byung C. Cho, Hoon C. Park, Nam S. Goo, and Kwang J. Yoon, "Piezoelectric Actuator–Sensor Analysis using a Three-Dimensional Assumed Strain Solid Element," *Journal of Intelligent Material Systems and Structures*, **15**, 329 – 338 (2004).
50. Lobontiu, Nicolae O. Goldfarb, Michael and Garcia, Ephrahim, "Elastodynamic analysis and design of an inchworm robotic insect," *Proc. SPIE,* Vol. **3668**, 724 - 735 (1999).
51. Mane, P., Mossi, K., Bryant, R., "Pressure Loading of Piezo-Composites Unimiorphs, *MRS,* November 2005, submitted.
52. Mane, P., Mossi, K., Bryant, R., "Synthetic jets with piezoelectric diaphragms," *Proceedings of the SPIE Int. Soc. Opt*., **5761**, 233 — 243 (2005).
53. Marouzé, J. P. and Cheng, L., "A feasibility study of active vibration isolation using THUNDER actuators, *Smart Mater. Struct*., **11**(6), 854 - 862 (2002).
54. Mouhli, M., "Analysis and Shape Modeling of Piezoelectric Actuators, Master's Thesis, Virginia Commonwealth University (2005).
55. Mossi, K. Bishop, R., Smith, R., Banks, H., "Evaluation Criteria for THUNDER Actuators," *Proceedings of the SPIE Int. Soc. Opt*., **3667**, 738 – 743 (1999).
56. Mossi, K., and Bishop, R.P., "Characterization of Different types of High Performance THUNDER Actuators," *Proceedings of the SPIE Int. Soc. Opt*., **3675**, 43 – 52 (1999).
57. Mossi, K., Bryant, R., "Piezoelectric Actuators for Synthetic Jet Applications," *Materials Research Society*, 407 – 412 (2003).
58. K. Mossi, R. Bryant, "Characterization of Piezoelectric Actuators for Flow Control Over a Wing," *Actuator 2004: 9th International Conf. on New Actuator*s, Paper **A5.2**, 181 (2004).
59. Mossi, K., Bryant, R., "Pre-stressed Circular Actuators," *Ceramic Transactions*, **150**, 445 – 454 (2004).
60. Mossi, K., Bryant, R., and Bishop, R., "THUNDER—A New Family of High Performance Piezoelectric Devices to Enable Advanced Automation, Drive, Sensor and Motion Systems," *Official Proceedings of the International AMD and C Conference* (1998).
61. Mossi, K., Bryant, R., Mane, P., "Piezoelectric Composites as Bender Actuators," *Integrated Ferroelectrics*, **71**, 221 – 232 (2005).
62. Mossi, K., Castro, N., Bryant, R., Mane, P., "Boundary Condition Effects on Piezo-Synthetic Jets," *Integrated Ferroelectrics*, **71**, 257 – 266 (2005).
63. Mossi, K., Costley, J., Ounaies, Z., Bryant R., "Piezoelectric behavior of pre-stressed curved actuators under load," *Proceedings of the SPIE Int. Soc Opt*., **5387**, 432 – 441 (2004).
64. Mossi, K., Green, C., Ounaies, Z., Hughes, E., "Harvesting Energy Using a Thin Unimorph Pre-Stressed Benders: Geometrical Effects," *Journal of International Materials Systems and Structures*, **16**, 249 – 261 (2005).
65. Mossi, K., Mane, P., Bryant, R., "Velocity Profiles for Synthetic Jets Using Piezoelectric Circular Actuators," *46th AIAA/ASME/ASCE/AHS/ASC Structures, Structural Dynamics and Materials Conference*, **AIAA 2005-2341**, April 18-21, 2005, Austin, Texas.
66. Mossi, K., Ounaies, Z., and Oakley, S., "Optimizing Energy Harvesting of a Composite Unimorph Pre-Stressed Bender", *American Society for Composites*, *Sixteenth Technical Conference*, September 9-12, 2001, Blacksburg, VA, USA,.
67. Mossi, K., Ounaies, Z., and Smith, R., "Pre-stressed curved actuators: characterization and modeling of their piezoelectric behavior," *Proceedings of SPIE Int. Soc. Opt*., **5053**, 423–435 (2003).
68. Mossi, K., Scott, L., "Sensor Measurements for Diagnostic Equipment," *First World Congress on Biomimetics and Artificial Muscles,* Dec 9-12, 2002, Albuquerque, NM, on CD-ROM.
69. Mossi, K., Scott, L., Haran, S., "Characterization of Loaded Pre-stressed Piezoelectric Actuators," *Proceedings of the SPIE Int. Soc. Opt*., **5053**, 453 – 459 (2003).
70. Mossi, K., Selby, G., Bryant, R., "Thin-Layer Composite Unimorph Ferroelectric Driver and Sensor Properties," *Materials Letters*, **35**, 39 – 49 (1998).
71. Mossi, K., Smith, B, Mouhli, M., and Bryant, R., "Characteristics of Carbon Reinforced Piezoelectric Composites," *Proc. of ICEST Conference*, Seoul, Korea (2005).
72. Mossi, K.; Ounaies, Z., "Piezoelectric actuators for sensor applications, Advanced Smart Materials and Smart Structures Technology," *1st International Workshop*, Jan. 12-14, 2004, Honolulu, HI, United States.
73. Mulling, J., Usher, T., Dessent, B., Palmer, J., Franzon, P., Grant, E., and Kingon, A., "Load characterization of high displacement piezoelectric actuators with various end conditions," *Sensors and Actuators A: Physical,* **94**(1-2), 19 – 24 (2001).

74. Munday, D., and Jacob J., "Active Control of Separation on a Wing with Conformal Chamber," *39th AIAA Aerospace Sciences Meeting and Exhibit*, January 8-11, Reno, NV (2001).
75. Niezrecki, C., Brei, D., Balakrishnan, S., and Moskalik A., "Piezoelectric Actuation: State of the Art," *The Shock and Vibration Digest*, Vol. **33**(4), 269 - 280 (2001).
76. Niezrecki, Christopher and Sivakumar Balakrishnan, "Power characterization of THUNDER actuators as underwater propulsors," *Proc. SPIE*, Vol. **4327**, p. 88 - 98 (2001).
77. Nothwang W. D., Cole, M. W., Schwartz, R. W., "Stressed-Biased Actuators: Fatigue And Lifetime," *Integrated Ferroelectrics*, Volume **71**, 249 - 255 (2005).
78. Nothwang, W. D., Cole, M. W., Schwartz, R. W., "Stressed-Biased Actuators: Lateral Stress And Loading Effects," *Integrated Ferroelectrics*, Volume **71**, 207 - 219 (2005).
79. Ounaies, Z., Mossi, K., Smith, R., and Berndt J., "Low-Field and High Field Characterization of Thunder Actuators," *Proceedings of the SPIE Int. Soc. Opt.*, **4333**, 399 – 407 (2001).
80. Park, Hoon C. Sangki Lee, Byung C. Cho, Kwang J. Yoon, Nam Seo Goo, "Three-dimensional assumed strain solid element for piezoelectric actuator/sensor analysis," *Proc. SPIE*, Vol. **4326**, p. 538 - 547, (2001).
81. Parker, M., "Ambient Energy Harvesting," The University of Queensland, Australia, B.S. Thesis in Electrical Engineering (2003).
82. Pinkerton, J. L., A. R. McGowan, R. W. Moses, R. C. Scott, and J. Heeg, "Controlled aeroelastic response and airfoil shaping using adaptive materials and integrated systems," *Proceedings of the SPIE Int. Soc. Opt.*, **2717**, 166 - 177 (1996).
83. Pinkerton, J. L., and R. W. Moses, "A feasibility study to control airfoil shape using THUNDER," *NASA TM 4767* (1997).
84. Prosser, W. H., Wu, M-C., Allison, S. G., DeHaven, S. L., and Ghoshal, A., "Structural Health Monitoring Sensor Development at NASA Langley Research Center," *Proceedings of the International Conference on Computational & Experimental Engineering and Sciences (ICCES '03)*, Corfu, Greece, Paper ID **149**, July 25-29, (2003).
85. Ramsay, M. J., and Clark, W. W., "Piezoelectric Energy Harvesting for Bio MEMS Applications," *SPIE 8th Annual International Symposium on NDE for Health Monitoring and Diagnostics*, March 4-8, (2001).
86. Rodgers, Jesse C., William W. Clark, Vipperman Jeffrey S., "Analysis and testing of a THUNDER piezoelectric actuator as a prime mover in a gas flow control valve," *Proc. SPIE*, Vol. **5764**, 290 - 301 (2005).
87. Schwartz, R. W., Cross, L. E. and Wang, Q.-M., Schwartz, R. E. and Narayanan, M., "Development of High Performance Stress-Biased Actuators through the Incorporation of Mechanical Pre-Loads," *Sensors Actuators,* Physical *A*, **101**(3), 322 – 331 (2002).
88. Schwartz, Robert W. Youngwoo Moon, "Domain configuration and switching contributions to the enhanced performance of rainbow actuators," *Proc. SPIE*, Vol. **4333**, 408 - 417 (2001).
89. Schwartz, R. W., Laoratanakul, P., Nothwang, W. D, Ballato, J., Moon, Y., and Jackson, A., "Understanding Mechanics and Stress Effects in Rainbow and Thunder Stress-Biased Actuators," *Proceedings of the SPIE Int. Soc. Opt.*, **3992**, 363 – 375 (2000).
90. Shakeri, C., Bordonaro, C. M., Noori, M. N., and Champagne, R., "Experimental Study of THUNDER: A New Generation of Piezoelectric Actuators," *Proc. of the SPIE Int. Soc. Opt.*, **3675**, 63 – 71 (1999).
91. Shenck, N. S., "A demonstration of useful electric energy generation from piezoceramics in a shoe," media.mit.edu, Master thesis (1999).
92. Sodano, H. A., Park, G; Inman, D. J., "Estimation of Electric Charge Output for Piezoelectric Energy Harvesting," *Strain,* Vol. **40**(2), 49 - 58 (2004).
93. Sodano, Henry A. Daniel J. Inman, and Gyuhae Park, "A Review of Power Harvesting from Vibration Using Piezoelectric Materials," *The Shock and Vibration Digest*, **36**, 197 – 205 (2004).
94. Song, Jun K. Gregory N. Washington, "Thunder actuator modeling and control with classical and fuzzy control algorithm," *Proc. SPIE,* Vol. **3668**, 866 - 877 (1999).
95. Suleman, A., and Venkayya, VB., "A Simple Finite Element Formulation for a Laminated Composite Plate with Piezoelectric Layers," *Journal of Intelligent Material Systems and Structures*, **6**, 776 – 782 (1995).
96. Smith, R., "Smart Materials Systems, Model Development. Frontiers in Applied Mathematics," SIAM publishers (2005).
97. Taleghani, B. K. and Campbell, J. F., "Non-Linear Finite Element Modeling of THUNDER Piezoelectric Actuators," *Proceedings of the SPIE Int. Soc. Opt.*, **3668**, 555 – 566 (1999)
98. Taleghani, Barmac K., "Validation of high displacement piezoelectric actuator finite element models," *Proc. SPIE.*, Vol. **4073**, 37 - 45 (2000).
99. Taylor, Chris J. Washington, Gregory N., "Comprehensive piezoceramic actuator review," *Proc. SPIE .*, Vol. **4701**, 443 - 454 (2002).
100. Tressler, James F.; Howarth, Thomas R., "Thin, low frequency, high displacement actuator panels," *Materials Research Innovations*, **2**(5), 270-277 (1999)
101. Uchino, K., J. Zheng, A. Joshi, Y. Chen, S. Yoshikawa, S. Hirose, S. Takahashi, and J.W.C. De Vries, "High power characterization of piezoelectric materials," *Journal of Electroceramics*, **2**(1), 33 - 40 (1998).
102. Usher, Timothy D. Alec Sim, Gevale Ashford, Gilbert Camargo, Adalia Cabanyog, Kenneth Ulibarri, Jr., "Modeling and applications of new piezoelectric actuator technologies," *Proc. SPIE*, Vol. **5383**, 31 - 38 (2004).
103. Washington, G. N., and Song, J. K., "Mechatronic Design and Control of Singly and Doubly Curved Composite Mesoscale actuator Systems," *IEEE/ASME Transaction on Mechatronic*, **5**(1) 49 – 57 (2000).
104. Wieman, R., Smith, R. C., Kackley, T., Ounaies, Z. and Bernd, J., "Displacement Models for THUNDER Actuators Having General Loads and Boundary Conditions," *Proceedings of the SPIE Int. Soc. Opt.*, **4326**, 253 – 263 (2001).
105. Wise, S. A., "Displacement Properties of RAINBOW and THUNDER piezoelectric actuators," *Sensors and Actuators, Physical A*, **69**(1), 33 – 38 (1998).
106. Yoon H. S., and Washington, G. N., "Modeling, Design, and Zero Gravity Testing of a Doubly Curved Aperture Antenna," *Journal of Intelligent Material Systems and Structures*, **10**(2), 141 – 148 (2000).
107. Yoon H. S., and Washington, G. N., "Analysis and Design of Doubly Curved Piezoelectric Strip-Actuated Aperture Antennas," *IEEE Transaction on Antennas and Propagation*, **48**, 755 – 763 (2000).
108. Yoon, K. J., Park, K. H., Park, H. C., Lee, S. K., and Goo, N. S., "Analytical design model for a piezo-composite unimorph actuator and its verification using lightweight piezo-composite curved actuators.," *Smart Materials and Structures*, **13**, 459 – 467 (2003).
109. Yoon, K.J., Shin, S., Park, H.C. and Goo, N.S., "Design and Manufacture of Lightweight Piezoceramic Curved Actuator", *Smart Materials and Structures*, Volume **11**, 163 – 168 (2002).
110. Yoon; Hwan-Sik, Washington, G.; Theunissen, W. H., "Analysis and design of doubly curved piezoelectric strip-actuated aperture antennas," *Antennas and Propagation,* IEEE Transactions, Volume **48**(5), 755 – 763 (2000).
111. Yoon, K. J., Chung, J. H., Goo, N. S., and Park, H. C., "Thermal Deformation and Residual Stress Analysis of Lightweight Piezo-composite Curved Actuator Device," *Proceedings of the SPIE Int. Soc. Opt.*, **4333**, 418 – 425 (2001).
112. Yoon, K. J., Park, K. H., Park, H. C., and Perraux, D., "Thermal Deformation Analysis of Curved Actuator LIPCA with Piezoceramic Layer and Fiber Composite Layers," *Composites Science and Technology*, **63**, 501 – 506 (2003).
113. Yoon, Kwang J. Sukjoon Shin, Jusik Kim, Hoon C. Park, Moon K. Kwak, "Development of lightweight THUNDER with fiber composite layers," *Proc. SPIE*, Vol. **3992**, 57 - 64, (2000).
114. Yung, Chung, Sheung, Siu Wing, Or, Helen, Lai, Wa Chan, Ping, Kong, Choy, Peter, Chou, Kee Liu, "Development of a piezoelectric induced-strain actuator with an innovative internal amplifying structure," *Proc. SPIE,* Vol. **5764**, 22 - 33 (2005).
115. Zhou, Xiaoqin Jinqiang Zhao, Gangbing Song, J. Alexis De Abreu-Garcia, "Preisach modeling of hysteresis and tracking control of a Thunder actuator system," *Proc. SPIE*, Vol. **5049**, 112 - 125 (2003).
116. See Also : http://www.faceinternational.com/

MFC Publication List

1. Jan-Sang Park, Ji-Hwan Kim, "Analytical development of single crystal Macro Fiber Composite actuators for active twist rotor blades," *Smart Mater. Struct.,* **14**(4),
2. Lloyd, J. M., Williams, R. B., Inman, D. J. and Wilkie, W. K., "An Analytical Model of the mechanical Properties of the Single-Crystal Macro-Fiber Composite Actuator," *Proceedings of SPIE Smart Structures and Materials Symposium*, March 14-18, 2004, San Diego, CA.
3. Marc R. Schultz, Michael W. Hyer A Morphing Concept based on Unsymmetric Composite Laminates and Piezoceramic MFC Actuators, *45th AIAA Structures, Structural Dynamics & Materials Conference,* **2004-1806***,* 19 - 22 (2004).
4. Ruggiero, Eric J., Gyuhae Park, Daniel J. Inman, and Jan Wright., "Multi-Input, Multi-Output Modal Testing Techniques for Gossamer Spacecraft," *Proceedings of 2002 ASME International Mechanical Engineering Congress and Exposition,* November 11-16, 2002, New Orleans, LA.
5. S. G. Allison, Q. A. Shams and R. L. Fox "Stretch Tuning Optical Fiber Bragg Gratings Using Macro-Fiber Composite (MFC) piezoelectric actuators," accepted for presentation at SPIE Optics East, Boston, MA October 23-26, 2005.
6. Schultz, M. R., Hyer, M. W., Williams, R. B., Wilkie, W. K., and Inman, D. J., "Use of Piezoelectric Actuators to Effect Snap-Through Behavior of Unsymmetric Composite Laminates," *Proceedings of the American Society for Composites 18th Technical Conference*, October 19-22, 2003, Gainesville, FL.
7. Sodano, H.A., Park, G., Inman, D. J., "An investigation into the performance of macro-fiber composites for sensing and structural vibration applications**,"** *Mechanical Systems and Signal Processing*, **18,** 683 – 697 (2004).
8. T. Tupper Hyde and Gregory Agnes," Adaptive Structures," *Aerospace America*, Dec. 2000.
9. W. K. Wilkie, R. G. Bryant, J. W. High, R. L. Fox, R. F. Hellbaum, A. Jalink, Jr., B. D. Little, P. H. Mirick, "Low-Cost Piezoceramic Actuator for Structural Control Applications", *Proceedings of the SPIE – Smart Structures and Materials: Industrial and Commercial Appl. of Smart Structures Tech.*, **3991**, 323 (2000).
10. W. Wilkie, W. Williams, J. High, D. Inman, "Recent Developments in NASA Piezocomposite Actuator Technology," *Actuator 2004: 9th International Conf. on New Actuator*s, Paper **A 4.9**, 160, (2004).
11. W. Wilkie, D. Inman and J. Lloyd, "Anisotropic Piezocomposite Actuator Incorporating Machined PMN-PT Single Crystal Fibers," *45th AIAA/ASME/ASCE/AHS/ASC Structures, Structural Dynamics and Materials Conference*, **AIAA-2004-1889**, Apr. 19-22, 2004, Palm Springs, California.
12. Williams, R. B., Inman, D. J. and Wilkie, W. K., "Nonlinear Actuation Properties of Macro Fiber Composite Actuators," *Proceedings of IMECE'03, 2003 ASME International Mechanical Engineering Congress & Exposition*, November 16-21, 2003, Washington, D. C.
13. Williams, R. B., Schultz, M. R., Hyer, M. W., Inman, D. J., and Wilkie, W. K. "Nonlinear Tensile and Shear Behavior of Macro Fiber Composite Actuators," *18th Annual Technical Conference American Society for Composites*, October 19-22, 2003, Gainesville, FL.
14. Williams, R. B., Grimsley, B. W., Inman, D. J. and Wilkie, W. K., "Manufacturing and Mechanics-Based Charactorization of Micro Fiber Composite Actuators," *Proceedings of 2002 ASME International Adaptive Structures and Material Systems Symposium*, Nov. 17-22, 2002, New Orleans, LA.
15. Williams, R. B., Austin, E. M. and Inman, D. J., "Limitations of Using Membrane Theory for Modeling PVDF Patches on Inflatable Structures," *Journal of Intelligent Material Systems and Structures*, Vol. **12**(1), 11 - 20 (2001).
16. Williams, R. B., Austin, E. M. and Inman, D. J., "Local Effects of Piezopolymer Patches on Inflatable Space-Based Structures," *Journal of Spacecraft and Rockets*, Vol. **39**(2), 299 - 305 (2002).
17. Williams, R. B., Inman, D. J. and Wilkie, W. K., "Manufacturing and Cure Kinetics Modeling for Macro Fiber Composite Actuators, *Journal of Reinforced Plastics and Composites*, Vol. **23**(16), 1741 – 1754 (2004).
18. Williams, R. B., Schultz, M. R., Hyer, M. W., Inman, D. J. and Wilkie, W. K., "Nonlinear Mechanical Behavior of Macro Fiber Composite Actuators," *Journal of Composite Materials*, Vol. **38**(10), 855 – 870 (2004).

19. Williams, R. B., Inman, D. J. and Wilkie, W. K., "Temperature-Dependent Coefficients of Thermal Expansion in Macro Fiber Composite Actuators," *Journal of Thermal Stresses*, Accepted for publication.
20. Williams, R. B., Inman, D. J. and Wilkie, W. K., "Nonlinear Response of The Macro Fiber Composite Actuator to Monotonically Increasing Excitation Voltages," *Journal of Intelligent Material Systems and Structures*, In Review.
21. Williams, R. B., Schultz, M. R., Hyer, M. W., Inman, D. J. and Wilkie, W. K., "Nonlinear Tensile and Shear Behavior of Macro Fiber Composite Actuators," *Proceedings of the American Society for Composites 18th Technical Conference*, October 19-22, 2003, Gainesville, FL.
22. Williams, R. B., Inman, D. J. and Wilkie, W. K., "Temperature-Dependent Coefficients of Thermal Expansion in Macro Fiber Composite Actuators," *Proceedings of the 5th International Congress on Thermal Stresses*, June 8-11, 2003, Blacksburg, VA.
23. Williams, R. B., Inman, D. J. and Wilkie, W. K., "Nonlinear Mechanical Behavior of Macro Fiber Composite Actuators," *Proceedings of the Sixth International Conference on Sandwich Structures*, March 31-April 2, 2003, Ft. Lauderdale, FL.
24. Williams, R. B., Grimsley, B. W., Inman, D. J. and Wilkie, W. K., "Manufacturing and Mechanics-Based Characterization of Macro Fiber Composite Actuators," *Proceedings of the 2002 ASME International Mechanical Engineering Congress & Exposition*, November 17-22, 2002, New Orleans, LA. R Bryant NASA LaRC (200
25. Williams, R. B., Park, G., Inman, D. J. and Wilkie, W. K., "An Overview of Composite Actuators with Piezoceramic Fibers," *Proceedings of IMAC-XX: Conference on Structural Dynamics*, February 4-7, 2002, Los Angeles, CA.
26. Williams, R. B., Austin, E. M. and Inman, D. J., "Local Effects of PVDF Patches on Inflatable Space-Based Structures," *Proceedings of the 42nd AIAA/ASME/ASCE/ AHS/ASC Structures, Structural Dynamics, and Materials Conference and Exhibit,* April 16-19, 2001, Seattle, WA.

General Website Reference List

1. www.smart-material.com
2. www.advancedcerametrics.com
3. www.mide.com
4. http://www.physikinstrumente.com/en/products/piezo/piezo_actuator_selection.php#bend
5. http://www.fibraplex.com/news.htm
6. http://www.zonatech.com

General Website Reference List

1. DESCRIPTION OF NEW INFLATABLE/RIGIDIZABLE HEXAPOD STRUCTURE TESTBED FOR SHAPE AND VIBRATION CONTROL O. Adetona , L.H. Keel, Tennessee State University L.G. Horta, Structural Dynamic Branch, NASA Langley Research Center D.P. Cadogan, G.H. Sapna, S.E. Scarborough, ILC Dover, Inc. AIAA-2002-1451
2. F-16 Ventral Fin Buffet Alleviation Using Piezoelectric Actuators Joseph S. Browning, Richard G. Cobb, Robert A. Canfield and Sean K. Miller Air Force Institute of Technology, Wright-Patterson AFB, Oh, 45433
3. Correcting Thermal Deformations in a Meter-Scale Reflector System using Piezocomposite Actuators S Case Bradford, Catherine M. Ohara, Gregory S. Agnes, W. Keats Wilkie Jet Propulsion Lab and NASA Langley Research Center, Sept. 2011
4. Aerodynamic and Electromechanical Design, Modeling and Implementation of Piezocomposite Airfoils Onur Bilgen Dissertation submitted Department of Mechanical Engineering, Virginia Tech, Blacksburg, Virginia
5. Nonlinear Tensile and Shear Behavior of Macro Fiber Composite Actuator R. Brett Williams, Marc R. Schultz, Michael W. Hyer, Daniel J. Inman and W. Keats Wilkie Department of Mechanical Engineering, Virginia Tech, Blacksburg, Virginia
6. MINIATURE PIEZO COMPOSITE BIMORPH ACTUATOR FOR ELEVATED TEMPERATURE OPERATION Charles W. Seeley, Eladio Delgado, Dirk Bellamay, General Electric Jan Kunzmann, Smart Material Corp Proceedings of IMECE 2007, ASME 2007 International Mechanical Engineering Congress & Exposition November 11-16, 2007, Seattle, Washington, USA
7. A Morphing Concept Based on Unsymmetric Composite Laminates and Piezoceramic MFC Actuators Marc R. Schultz NASA Langley Research Center, Hampton, VA, 23681-2199 Michael W. Hyer Virginia Polytechnic Institute and State University, Blacksburg, VA, 24061
8. NEXT GENERATION ACTIVE BUFFET SUPPRESSION SYSTEM Robert W. Moses et al, NASA Langley Research Center, Virginia AIAA 2000
9. Nonlinear Tensile and Shear Behavior of Macro Fiber Composite Actuators R. Brett Williams, Marc R. Schultz, Michael W. Hyer, Daniel J. Inman, Virginia Polytechnic Institute and State University Blacksburg, VA 24061, USA W. Keats Wilkie NASA Langley Research Center, Hampton, VA 23681, USA
10. RECENT DEVELOPMENTS IN NASA PIEZOCOMPOSITE ACTUATOR TECHNOLOGY W. Wilkie U.S. Army Research Laboratory, Hampton, VA, USA D. Inman Virginia Polytechnic and State University, Blacksburg, Virginia, USA J. High NASA Langley Research Center, Hampton, Virginia, USA R. Williams NASA Jet Propulsion Laboratory, Pasadena, California, USA
11. Reliability Investigation of piezoelectric Macro Fibre Composite (MFC) Actuators Authors: Dr. J. Nuffer*, Fraunhofer LBF, Germany Dr. A. Schönecker, B. Brückner, Fraunhofer IKTS, Germany D. Kohlrautz, ERAS GmbH, Germany Dr. P. Michelis, IMMG, Greece O. Adarraga, Inasmet Tecnalia, Spain Dr. K. Wolf, TU Darmstadt, Germany August 2003
12. Reliability Testing of NASA Piezocomposite Actuators W. Wilkie, J. High, J. Bockman U.S. Army Research Laboratory and NASA Langley Research Center, Hampton, Virginia, USA
13. TEMPERATURE –DEPENDENT COEFFICIENTS OF THERMAL EXPANSION FOR MACRO FIBER COMPOSITE ACTUATORS R. Brett Williams, Daniel J. Inman, and W. Keats Wilkie Department of Mechanical Engineering, CIMSS, Virginia Tech Structural Dynamics Branch, NASA Langley Research Center
14. Morphing Inflatable Wing Development for Compact Package Unmanned Aerial Vehicles David Cadogan, Tim Smith et al, ILC Dover, Frederica, DE 19946 AIAA 2004-1807 SDM Adaptive Structures Forum

Annexes

Sources:

MFC (Annex 1)	**Smart Material GmbH**
QuickPack (Annex 2)	**Midé**
DuraAct (Annex 3)	**PiCeramic GmbH**
AFC/PFC (Annex 4)	**Advanced Cerametrics, Inc.**

Annex 1

MACRO FIBER COMPOSITE - MFC

Actuator, Sensor, Energy Harvester
Energy Harvesting Systems
Piezo Powering and Instrumentation
Engineering Services

www.smart-material.com

SMART MATERIAL

What is a Macro Fiber Composite (MFC)?

MFC benefits

- Flexible and durable
- Increased strain actuator efficiency
- Directional actuation / sensing
- Damage tolerant
- Available as elongator (d_{33} mode) and contractor (d_{31} mode)
- Conforms to surfaces
- Readily embeddable
- Environmentally sealed package
- Demonstrated performance
- Different piezo ceramic materials available

Schematic structure of the MFC

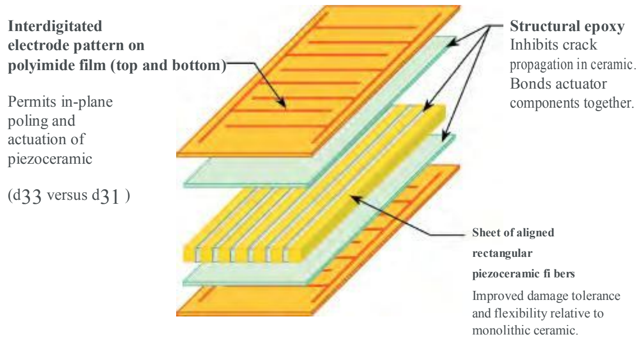

The Macro Fiber Composite (MFC) is the leading low-profile actuator and sensor offering high performance, durability and flexibility in a cost – competitive device.

The MFC was invented by NASA in 1996. Smart Material started commercializing the MFC as the licensed manufacturer and distributor of the patented invention* worldwide in 2002. Since then, the MFC has been continuously improved and customized to fit the customers' specific needs and to meet the requirements for new applications. Today more than 25 standard inventory sizes are available.

The MFC consists of rectangular piezo ceramic rods sandwiched between layers of adhesive, electrodes and polyimide film. The electrodes are attached to the film in an interdigitated pattern which tranfers the applied voltage directly to and from the ribbon shaped rods. This assembly enables in-plane poling, actua-tion and sensing in a sealed and durable, ready to use package. As a thin, surface conformable sheet it can be applied (normally bonded) to various types of structures or embedded in a composite structure. If voltage is applied it will bend or distort materials, counteract vibrations or generate vibrations. If no voltage is applied it can work as a very sensitive strain gauge, sensing deformations, noise and vibrations. The MFC is also an excellent device to harvest energy from vibrations.

The novel, pliable and conformable features of the MFC also allow for structural health monitoring applications, morphing and stiffening of structures, lambda wave generati-on and as a large area ultrasound 2–2 composi-te generator.

The MFC is available in d33 and d31 operational mode, a unique feature of the Macro Fiber Composite. The P1 type MFCs, including the F1 and S1 types are utilizing the d33 effect for actuation and will elongate up to 2000ppm if operated at the maximum voltage rate of -500V to +1500V. The P1 type MFCs are also very sensitive strain sensors. The P2, P3 type MFCs are utilizing the d31 effect for actuation and will contract up to 750ppm if operated at the maximum voltage rate of -60V to +360V. The P2 and P3 type MFCs are mostly used for energy harvesting and as strain sensors.

MFC P1 Type (d_{33} effect)

Elongator
- powerful actuator
- sensitive sensor

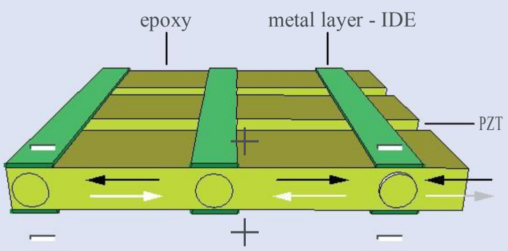

MFC P2 Type (d_{31} effect)

Contractor
- Low Impedance sensor
- energy generator

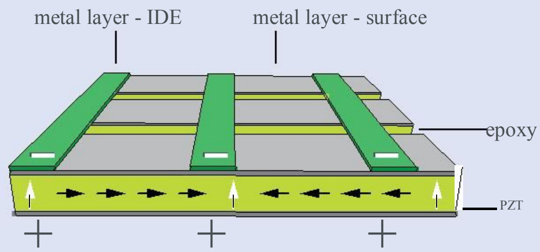

*protected under U.S. patent number 6,629,341, PCT/US00/18025; EP 1230689

General technical information for the MFC

High−field (|E| > 1kV/mm), biased−voltage−operation piezoelectric constants:

d33	4.6E + 02 pC/N	4.6E + 02 pm/V
d31**	-2.1E + 02 pC/N	-2.1E + 02 pm/V

Low-field (|E| < 1kV/mm), unbiased-operation piezoelectric constants:

d33*	4.0E + 02 pC/N	4.0E + 02 pm/V
d31**	-1.7E + 02 pC/N	-1.7E + 02 pm/V
Free-strain* per volt (low−field — high−field) for d33 MFC (P1)	~ 0.75 − 0.9 ppm/V	0.75 − 0.9 ppm/V
Free-strain* per volt (low−field — high−field) for d31 MFC (P2)	~ 1.1 − 1.3 ppm/V	~ 1.1 − 1.3 ppm/V
Free-strain hysteresis*	~ 0.2	~ 0.2
DC poling voltage, Vpol for d33 MFC (P1)	+1500 V	+1500 V
DC poling voltage, Vpol for d31 MFC (P2)	+450 V	+450 V
Poled capacitance @ 1kHz, room temp, Cpol for d33 MFC (P1)	~ 0.42 nF/cm²	~ 2.7 nF/in²
Poled capacitance @ 1kHz, room temp, Cpol for d31 MFC (P2)	~ 4.6 nF/cm²	~ 29 nF/in²

Orthotropic Linear Elastic Properties (constant electric field):

Tensile modulus, E1*	30.336 GPa	4.4E + 06 psi
Tensile modulus, E1**	15.857 GPa	2.3E + 06 psi
Poisson’s ratio, v12	0.31	0.31
Poisson’s ratio, v21	0.16	0.16
Shear modulus, G12 (rules-of-mixture estimate)	5.515 GPa	8.0E + 05 psi

Operational Parameters:

Maximum operational positive voltage, Vmax for d33 MFC (P1)	+1500 V	+1500 V
Maximum operational positive voltage, Vmax for d31 MFC (P2)	+360 V	+360 V
Maximum operational negative voltage, Vmin for d33 MFC (P1)	-500 V	-500 V
Maximum operational negative voltage, Vmin for d31 MFC (P2)	-60 V	-60 V
Linear − elastic tensile strain limit	1000 ppm	1000 ppm
Maximum operational tensile strain	< 4500 ppm	< 4500 ppm
Peak work-energy density	1000 in − lb/in3	~1000 in − lb/in3
Maximum operating temperature − Standard Version	< 80°C	< 176°F
Maximum operating temperature − HT Version	< 130°C	< 266 °F
Operational lifetime (@ 1kVp−p)	> 10E + 09 cycles	> 10E + 09 cycles
Operational lifetime (@ 2kVp−p, 500VDC)	> 10E + 07 cycles	> 10E + 07 cycles
Operational bandwidth as actuator, high electric field	0Hz to 10 kHz	0Hz to 10 kHz
Operational bandwidth as actuator, low electric field	0Hz to 750kHz	0Hz to 750kHz
active Area Density	5.44 g/cm³	5.44 g/cm³
Thickness for all MFC Types	approx 0.3mm	approx. 12 mil

* Rod direction
** Electrode direction

Work modes

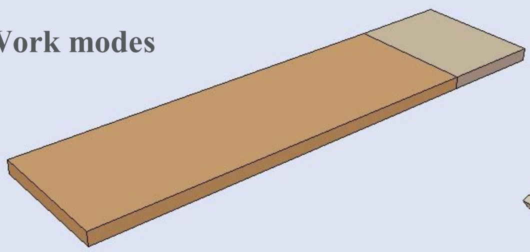

expansion

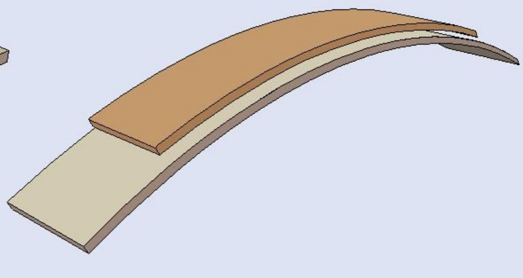

bending

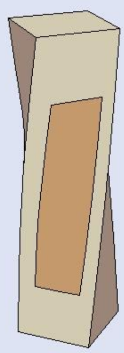

torsion

MFC Types specifications

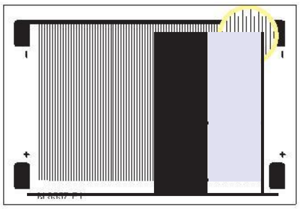

d33 Actuators with expanding motion P1

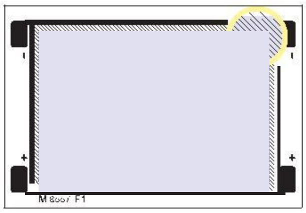

d33 Actuators with twisting motion F1

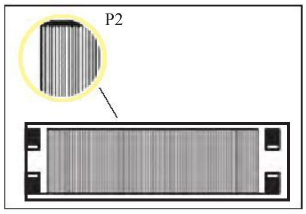

d31 Actuators with contracting motion P2

MFC P1 / F1 Types (d33 effect actuators)

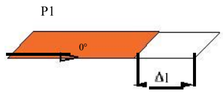

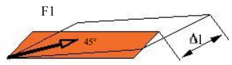

model	active length	active width	overall length	overall width	Capacitance	free strain	blocking force
	mm	mm	mm	mm	nF	ppm	N
P1−Types (0° fiber orientation)							
M-2503-P1	25	3	46	10	0.25	1050	28
M-2807-P1	28	7	40	18	0.33	1380	87
M-2814-P1	28	14	38	20	0.61	1550	195
M-4010-P1	40	10	54	22	1.00	1400	126
M-4312-P1	43	12	60	21	1.83	1500	162
M-8503-P1	85	3	110	14	0.68	1050	28
M-8507-P1	85	7	101	13	1.53	1380	87
M-8528-P1	85	28	112	40	5.70	1800	454
M-8557-P1	85	57	103	64	9.30	1800	923
M-14003-P1	140	3	160	10	1.45	1050	28
F1−Types (45° fiber orientation)							
M-8528-F1	85	28	112	43	6.30	1350	485 calc.
M-8557-F1	85	57	112	75	12.70	1750	945 calc.
M-14028-F1	140	28	175	40	8.00	1350	485 calc.
M-43015-F1	430	15	460	23	10.7	1280	253 calc.

MFC P2 / P3 Types (d31 effect actuators)

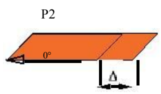

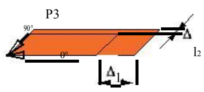

model	active length	active width	overall length	overall width	Capacitance	free strain	blocking force
	mm	mm	mm	mm	nF	ppm	N
P2−Types (anisotropic)							
M-2807-P2	28	7	42	14	12.4	-650	-40
M-2814-P2	28	14	37	18	25.7	-700	-85
M-5628-P2	56	28	70	34	113.0	-820	-205
M-8503-P2	85	3	113	8	12.3	-480	-13
M-8507-P2	85	7	108	11	38.4	-670	-42
M-8528-P2	85	28	105	34	172.0	-820	-205
M-8557-P2	85	57	105	61	402	-840	-430
M-8585-P2	85	85	105	90	605	-842	-650
P3−Types (orthotropic)							
M-2814-P3	28	14	36	16	29.5	-750	-110
M-5628-P3	56	28	70	34	121.7	-900	-265

Special MFC actuators & arrays

The Star MFC

Customized layouts and arrays

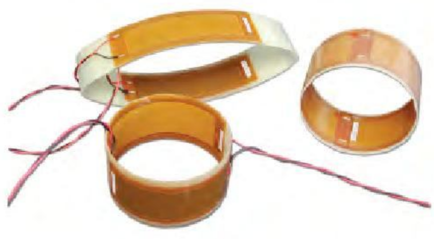

Advanced actuator elements

triangular MFC for strain adaptation

sensor/actuator arrays for closed loop control

customized contact pads

In addition to manufacturing MFCs in a wide variety of standard sizes for our customers, we are also offering many specialized MFC layouts to meet our customers' needs for specialized applica-tions.

These include for example the Star MFC, for pumps and synthetic jets, the S1 and S2 type MFCs, which consist of sensor and actuator elements for a closed loop control, as well as several other MFC arrays.

The MFC technology is highly adapta-ble to specific application needs. Custom designed layouts based on your own ideas and requirements have a typical lead time of 5 weeks.

Engineering and Prototyping Services

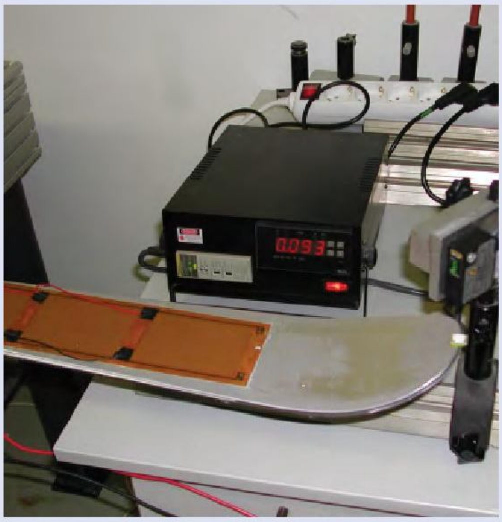

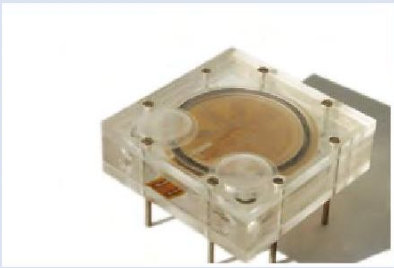

Due to our long - term experience in designing piezoelectric transducers and a well - equipped laboratory, we are able to help our customers along the whole development process so that their ideas come true.

- Analytical calculation and FEA on sensor & actuator systems
- Numerical design and simulation for ultrasonic transducers
- Prototyping and mechanical/ acoustical tests

High Voltage Amplifier and Pulser

SMART Power Amp PA05039 (made by TREK)

Smart Power Amp HVA 1500/50-4

SMART PowerSonic 280-PW

The design of the custom amplifier is based on the renowned Trek amplifier technology. With an output voltage of -500V to +1500V and a maximal output current of 50mA the PA05039 is designed to drive several P1 or F1 type (d_{33} effect) MFC's.

This multi−cannel amplifier series, with up to 4 independent channels, was designed for precise control of single MFC actuators and MFC actuator arrays .
These amplifiers are ideal power sources for both the P1/F1 and P2/P3 MFC's. An additional audio input allows the customer to apply signals easily from their notebook’s soundcard.

To enable customers to perform their own tests on low frequency ultrasonic transducers this µC controlled power pulser was developed. The pulses have a voltage of +/- 280V with a frequency up to 100 KHz.
Typical parameters like frequency, pulse number, refresh rate, uni−/bipolar mode and shut down time can be programmed via the RS 232 serial interface.

Data Acquisition Systems and Energy Harvesting

SMART Charge

SMART Logger

SMART Energy Harvester Development Kit

The MFC is capable of sensing strain based on the reverse piezo effect. Compared to a resistive strain gauge the MFC generates much higher output levels. This special preamplifier was developed to make strain measurements down to the static state possible. In contrast to typical channel amplifiers, no significant drift can be observed with this outstanding module.

Equipped with 4 independent input channels (high impedance voltage preamps) this module can be used to monitor dynamic events on the flight measured with MFC sensors from milliseconds up to some hours. All parameters for the SMART Logger can be programmed via USB.
A software allows to display the input signals and save the data as CSV−file.

Generating energy form environmental vibrations is one of the current challenges for engineers. This development kit consists of a simple on−desk shaker with suitable power amp unit, several MFC generator structures and 3 electronic modules with different measurements circuits.
It enables scientists from mechanical engineering and electronics to study causal relations between mechanical input parameters and electrical outputs.

MFC related Questions

Q: **Which adhesives are you recommending to bond MFCs to a structure?**

A: *We recommend two component adhesives like 3M's DP 460 Epoxy or Loctite's E120 HP Epoxy. Best results are obtained if the adhesive is cured at 50°− 60°C for 2 hours and the MFC is pressed against the structure with a fixture during curing.*

Q: **I want to use the MFC as a strain sensor but it seems I can not get any reading?**

A: *Make sure you have attached the MFC to a structure that is actually inducing a strain into the patch, i.e. stretching or compressing the fibers.*

Q: **What is the max force that an MFC can produce?**

A: *The MFC will expand at 1800 ppm over the length of the actuator (free strain). The blocking force is about 4kN/cm² for the active cross section of the MFC.*

Q: **Is the MFC porous or non−porous?**

A: *The MFC is non-porous due to its environmentally sealed packaging.*

Q: **What type of force does a standard MFC generate, including displacement?**

A: *The M8557P1 is generates about 900N blocking force and ~150µm displacement (free strain).*

Q: **What is the typical density of an MFC?**

A: *Typical areal density is 0.16g/cm² or volume density of 5.44 g/cm³*

Q: **What is the mechanical efficiency of an MFC, meaning electrical energy transformed into mechanical energy?**

A: *This question requires a little more in depth analysis:*

a) *In general a PZT 5A1 material used in the MFC has an effective coupling coefficient (k_{33}) of about 0.69. That is its first order electrical − to − mechanical energy conversion efficiency. k_{33} is a measure of efficiency, but not the actual efficiency*

b) *k_{33}^2 is the ratio of stored mechanical energy to input electrical energy (= 0.48), but this is not the same as output work energy efficiency, since one can not actually use all of the stored energy to do useful work.*

c) *Max. output work energy efficiency (under optimum loading condition) for the MFC will work out to about 0.16, so max 16% of input electrical energy can be converted into useful output work with an MFC.*

d) *Max. output − work energy efficiency is not the same as output − work to consumed electrical energy efficiency! Most (may be 97 − 99%, depending on dielectric loss of the package) of the electrical energy not converted to work is actually stored electrostatically, i.e., like in a capacitor. You can recover that energy, in principal, with a clever drive electronic design.*

Q: **How tight a radius of curvature can you bend the MFC before cracking? For example the standard size 3.4" x 2.2" MFC M8557P1.**

A: *Max. mechanical tensile strain the ceramics can endure is approx. 2500 ppm before fracturing. The package is still functional, although elastic properties will change. For 7− mil ceramic, this works out to a minimum curvature diameter of the actuator of about 3.5 inches (curled in fiber direction) and 3 inches curled perpendicular to the fiber direction.*

Smart Material Corporation
1990 Main Street, Suite 750
Sarasota, FL 34236 • U.S.A.
Tel: +1 (941) 870 3337 Fax: +1
(941) 847 0788
E-Mail: sarasota@smart-material.com
http://www.smart-material.com

Smart Material GmbH
Löbtauer Strasse 69
D - 01159 Dresden • Germany
Tel: +49 (0)351 4977 145
Fax: +49 (0)351 4977 146
E-Mail: dresden@smart-material.com
http://www.smart-material.com
Distributor Japan
TREK Japan K.K.
Sumitomo Aobadai Hills 10F
4-7-7 Aobadai, Meguro-Ku,
Tokyo, 153-0042 • Japan
Tel: +81 (3) 3460-9800
Fax: +81 (3) 3460-9801
E-Mail: smart-trek@trekj.com
http://www.trekj.com

SMART MATERIAL

SMART DOC# CPRO-V2.0en-0311

QuickPack®

PACKAGED PIEZOELECTRIC ACTUATORS AND SENSORS

FEATURES

- Dual functionality: piezoelectric actuator & sensor
- Robust Polyimide Packaging
- Quick Connect/Disconnect Connector
- Hermetically Sealed for Use in Harsh Environments
- Low Profile & highly flexible
- Available in Different Sizes to Suit Application
- Extra-Flexible Packs available for application to curved surfaces (pipes, etc.)

APPLICATIONS

- Vibration & strain sensing
- Passive vibration/strain detection
- Precise actuation
- Electronics cooling

DESCRIPTION

Midé's QuickPack product line takes advantage of a patented packaging process known as the " Piezo Protection Advantage". It allows the normally brittle piezoelectric ceramic to be encapsulated in protective polyimide layers. These protective layers drastically increases the actuator's robustness, and usefulness in real world applications.

The packaging process electrically isolates the piezoelectric ceramic, and allows the device to be used in otherwise adverse environmental conditions including submerged applications.

In addition to the standard QuickPack Products, Midé offers custom piezoelectric device design solutions. If a custom size is required please contact Midé Technology Corporation. Email: service@mide.com.

TYPICAL APPLICATIONS

SIMPLE SENSOR

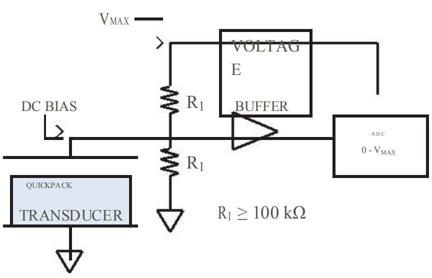

ADVANCED SENSOR

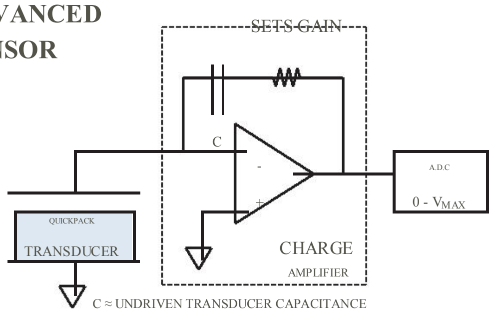

ACTUATOR

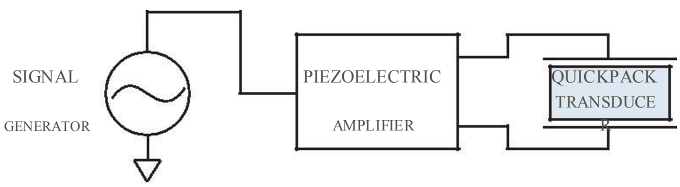

PRODUCT DIMENSIONS

NOTE:

1. All dimensions are in inches
2. Connector thickness = 0.100”

Product	Thick. (in)	Cap. (nF)*
QP10N	0.015	55
QP10W	0.015	85
QP10Ni	0.015	1.2
QP16N	0.010	125
PA16N	0.013	95
QP20N	0.030	100
QP20W	0.030	145
QP21B	0.030	125
QP22B	0.030	20
P. FAN	0.030	23

*Capacitance values are approximate and will vary from product to product.

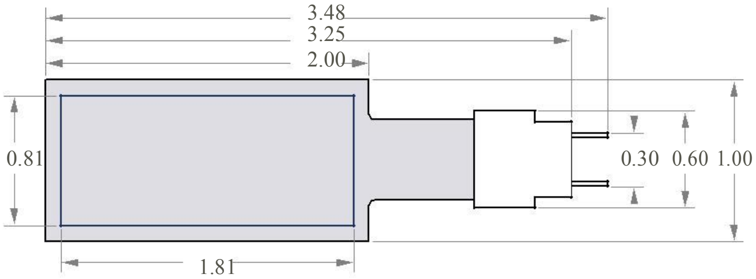

QP10N
QP16N

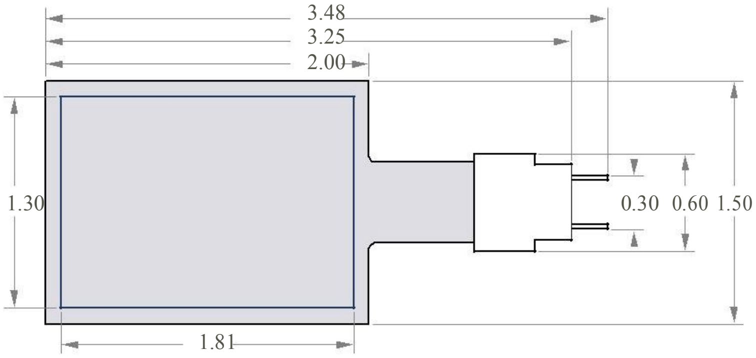

QP10W

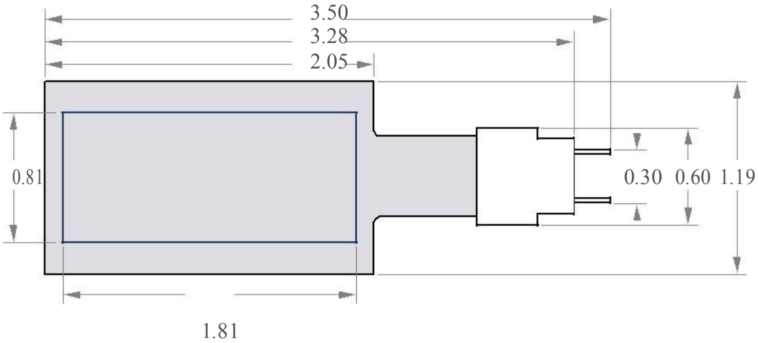

QP10Ni
PA16
N

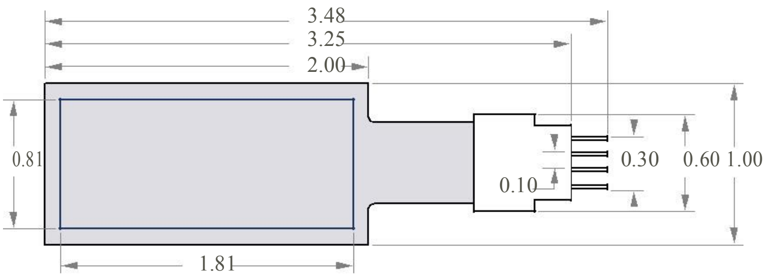

QP20N

PRODUCT DIMENSIONS

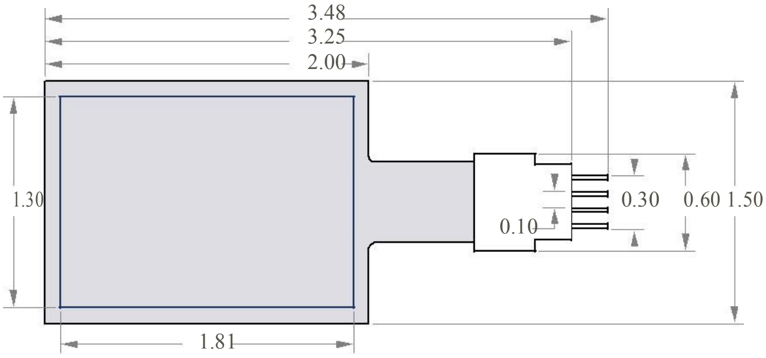

QP20W

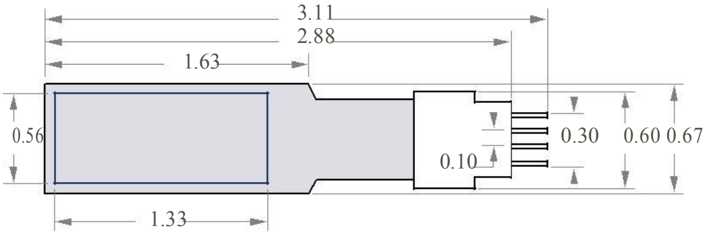

QP21B

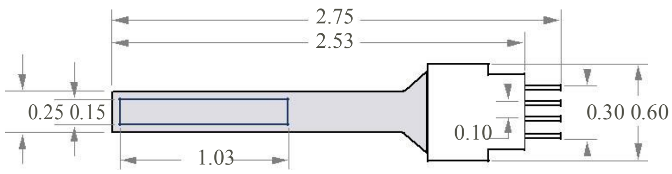

QP22B

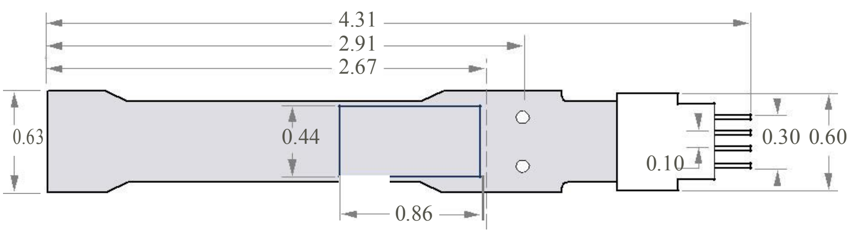

PIEZO FAN

FUNCTIONAL DIAGRAMS & COMPATIBLE CABLES

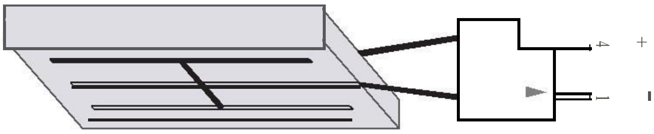

Cable:
CB-014

QP10N
QP10W
QP16N

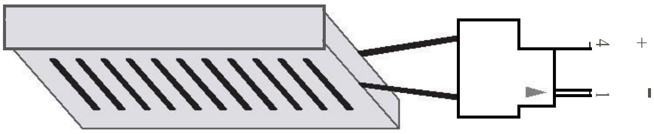

Cable:
CB-014

QP10Ni

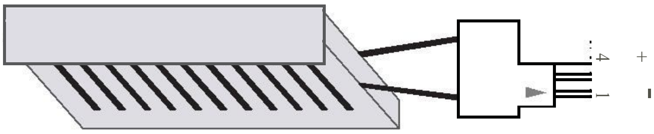

Cable:
CB-014

PA16N

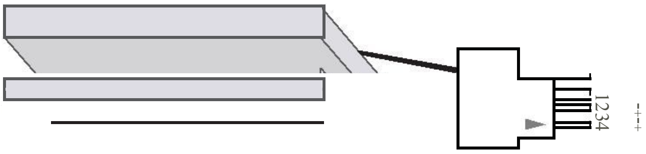

Cable:
CB-013

QP20N
QP20W

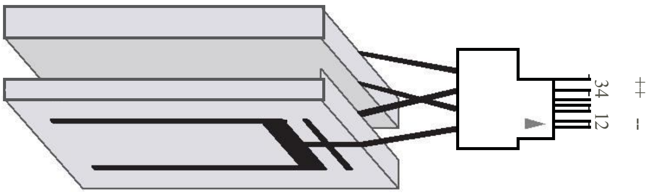

Cable:
CB-016

QP21B

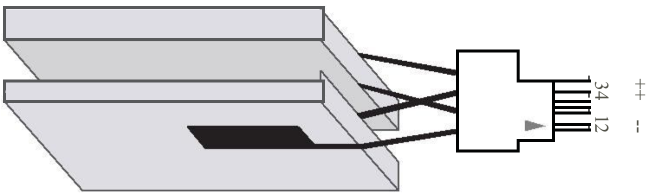

Cable:
CB-016

QP22B

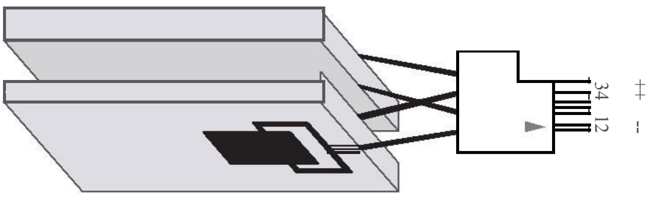

Cable:
CB-016

PIEZO FAN*

* Designed to work directly off line power

ABSOLUTE MAXIMUM RATINGS

Operating Temperature Range	-40 to 90 C
Operating Temperature Range (Without Connector)	-40 to 150 C
Storage Temperature Range	-60 to 90 C
Storage Temperature Range (Without Connector)	-60 to 150 C
Lead Temperatures (Soldering, 10 sec)	300 C
Piezo Strain, max	800 micro-strain

OPERATION

Piezoelectric ceramic is capable of providing a very precise signal in response to very small amounts of imposed strain. The same effect is true in reverse; a finely controlled input signal can produce an efficient response in the material when the device is used as an actuator.

Midé's QuickPack transducers are designed to provide precise and repeatable actuation or strain induced measurement in challenging operating environments. Midé's QuickPack transducers are suited for use in harsh environments commonly found in industrial applications. The QuickPack transducer is not, however, ideally suited to a specific application. Instead, Midé has developed a range of QuickPack products intended to provide a good starting point for your actuation or sensing needs. In order to maximize the cost effectiveness of implementing piezoelectric technology into your application, it may be necessary to investigate a custom design suited to your specific application. The standard QuickPack designs have been tailored to provide a sample of the many possibilities that exist when using piezoelectric transducers

Most QuickPack Transducers operate on the indirect piezoelectric 3-1 effect. The piezoceramic used in these packs is poled through the thickness, and expands and contracts in plane, perpendicular to the applied field. Through the use of a specially designed inter-digitized circuit, the QP10ni is able to take advantage of the stronger direct piezoelectric 3-3 effect. Instead of being polarized through the thickness, the piezoceramic is polarized along the length. This method causes the beam to behave like a stack instead of a bender. This causes the device to be much more sensitive to strain in the longitudinal direction than in the transverse direction.

A critical aspect to consider when using any type of strain dependent device is the bond layer thickness between the device and the surface where the transducer is installed. To maximize the transducer's capability to experience the equivalent strain as the surface it is mounted to, the bond layer thickness must be minimized. Midé offers a special epoxy which is capable of adhering QuickPack transducers to a variety of surfaces while ensuring an extremely thin bond layer.

OPERATION CONTINUED

Midé's QuickPack Piezoelectric Transducers can be used in a number of configurations depending on the intended application. Two of the most commonly used configurations for QuickPack Transducers are the bonded configuration and the cantilever configuration. The difference between these two types of configurations and examples of when this configuration would be appropriate are detailed below:

Bonded Configuration:

A QuickPack Transducer can be mounted directly to a surface. Such a configuration is referred to as a bonded configuration. A bonded QuickPack Transducer can be applied to a flat surface, a surface with non-uniform flatness, and even some curved surfaces. Single layer QuickPack Transducers are best suited for this type of operation.

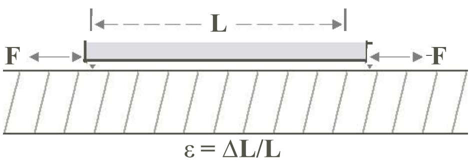

The bonded configuration is an excellent choice for sensing or creating vibrations in a relatively stiff structure. Transducers in this configuration can be used to monitor vibrations caused by an outside source, or by vibrations created in the structure by another QuickPack Transducer operating as an actuator.

Cantilever Configuration:

A QuickPack Transducer can be mounted with only part of the package secured in a clamp, and some part of the piezoelectric element suspended outside of the clamp. This configuration is referred to as a cantilever configuration. To use a QuickPack Transducer as a cantilevered transducer, the clamp can be positioned anywhere on the pack as long as the piezoceramic element is partially clamped. However, to obtain the best response, as little of the piezoelectric element should be clamped as possible. Midé prescribes a clamp line of 0.200" from the edge of the piezoelectric element to provide enough area to properly clamp one end of the piezoceramic. Bimorph QuickPack Transducers are best suited for cantilever operation because having the active element (piezoceramic) oriented some distance away from the neutral axis allows the transducer to achieve much greater tip displacement than a single layer transducer would.

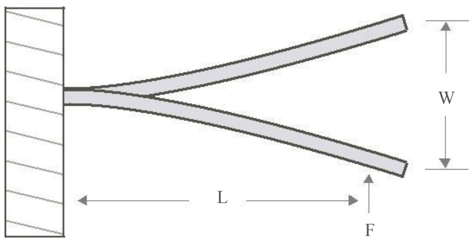

The cantilever configuration is typically employed when using a QuickPack Transducer as an actuator, although it could also be effective in using a QuickPack Transducer to sense low frequency vibrations or fluid or gaseous flow. Relatively high displacements are possible using this configuration. A prime example of a QuickPack Transducer used in a cantilever configuration is the Piezoelectric Fan.

QP10N TYPICAL PERFORMANCE POWER CHARACTERISTICS

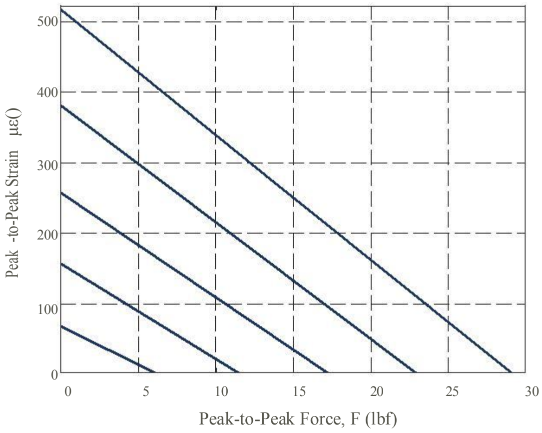

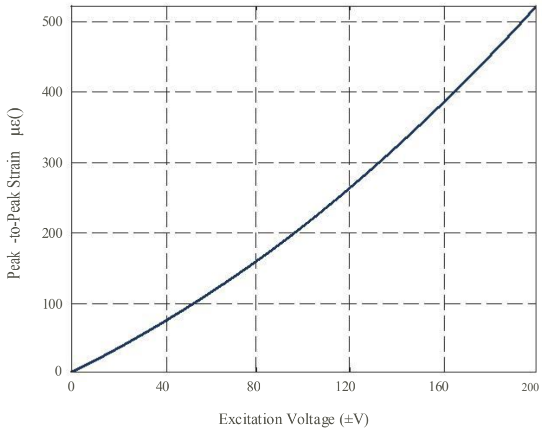

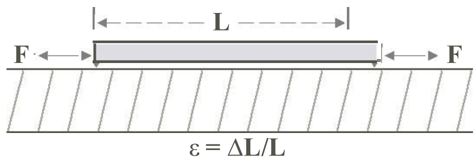

QP10W TYPICAL PERFORMANCE POWER CHARACTERISTICS

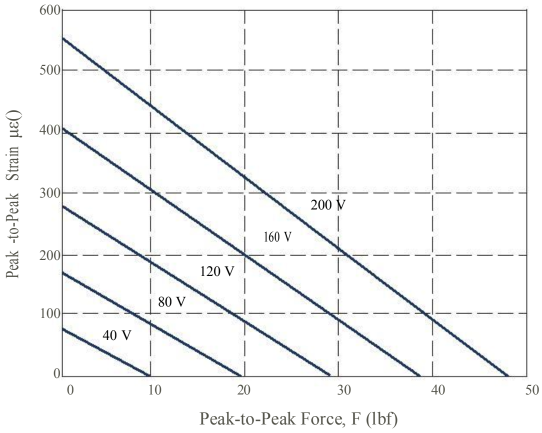

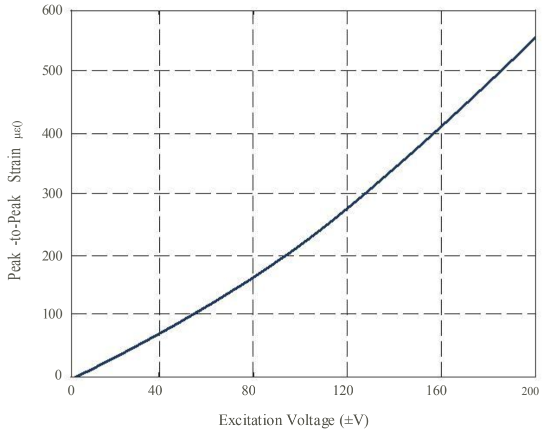

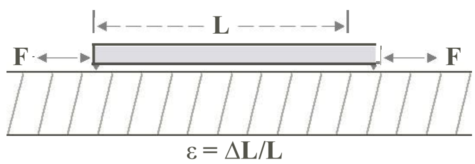

QP10Ni TYPICAL PERFORMANCE POWER CHARACTERISTICS

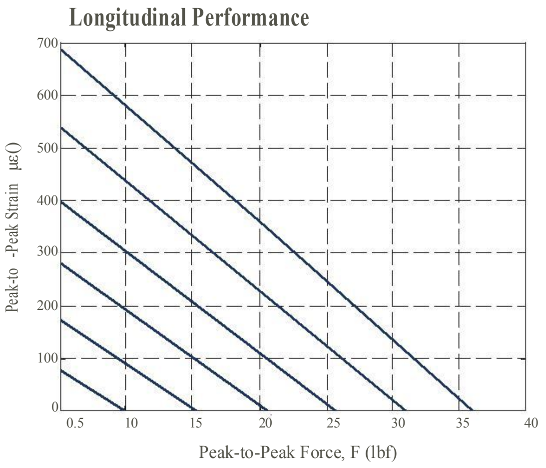

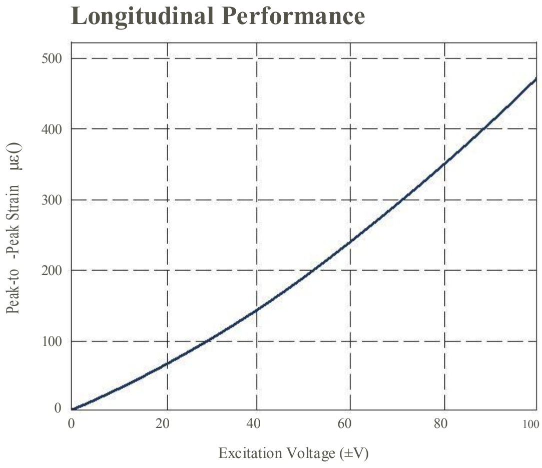

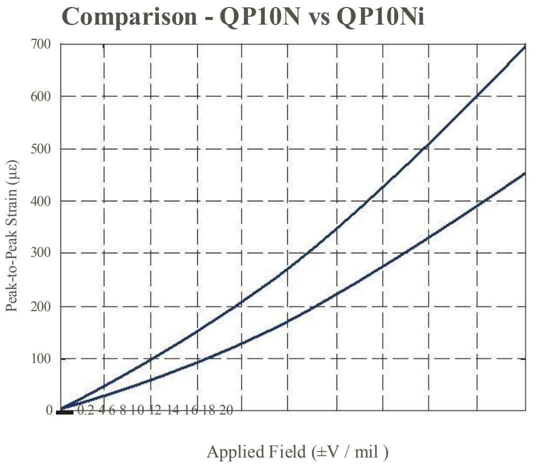

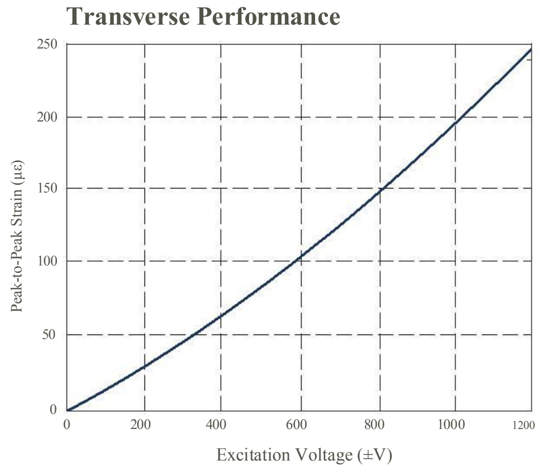

Note: The QuickPack IDE has different properties in the longitudinal and traverse directions. In the longitudinal direction, the actuator takes advantage of the d33 effect, while transverse direction is excited by the less efficient d31 effect. Strains in the longitudinal and transverse directions are out of phase with each other, i.e., when the length increases, the width decreases, and vice versa. Because it is directional. the QuickPack IDE actuator must be oriented properly in order to achieve desired performance.

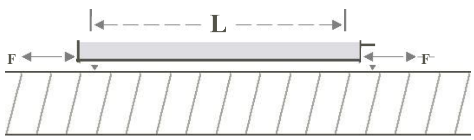

$\varepsilon = \Delta L/L$

QP16N TYPICAL PERFORMANCE POWER CHARACTERISTICS

Tuned to 110 Hz | 0 gram Tip Mass

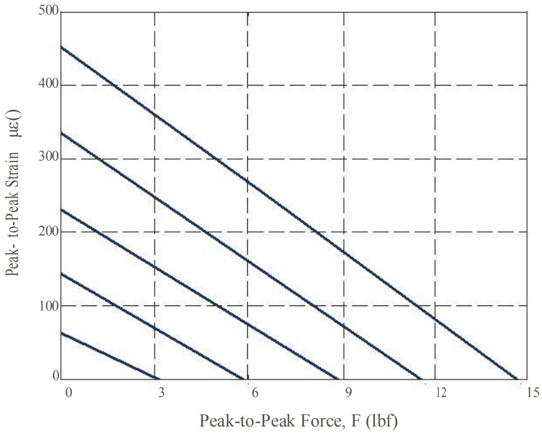

Tuned to 110 Hz | 0 gram Tip Mass

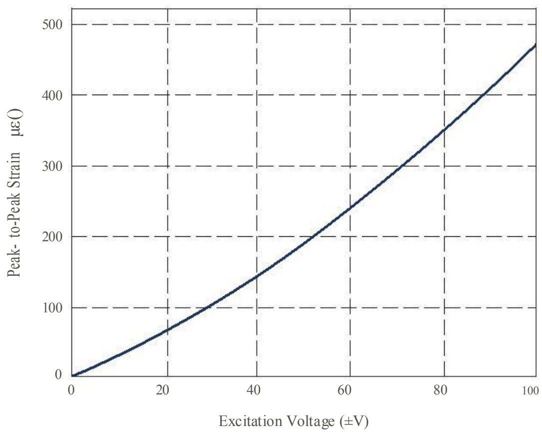

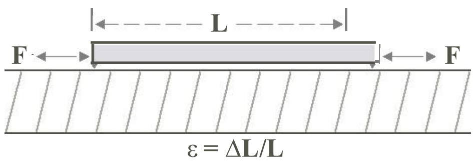

PA16N TYPICAL PERFORMANCE POWER CHARACTERISTICS

NOTE: PowerAct enables directional, conformable actuation. The PowerAct takes advantage of a unique process to improve the flexibility of the otherwise inflexible piezoceramic. In addition, an interdigital electrode geometry enhances electromechanical coupling via the primary or direct piezoelectric effect resulting in greater performance and directional behavior.

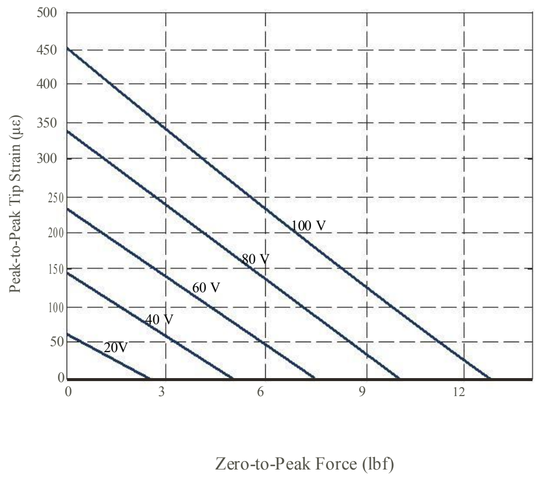

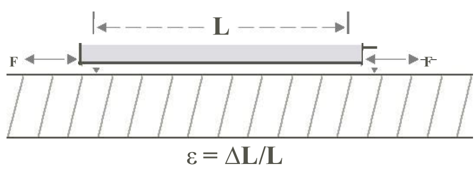

QP20N TYPICAL PERFORMANCE POWER CHARACTERISTICS

BONDED CONFIGURATION

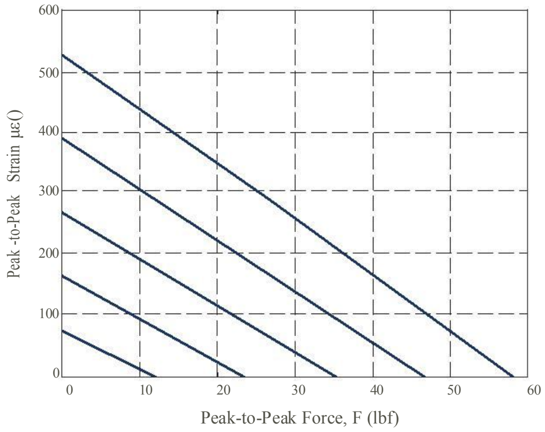

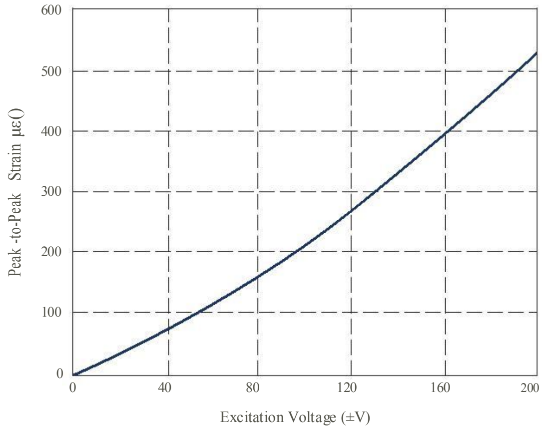

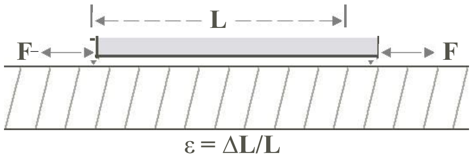

CANTILEVER CONFIGURATION

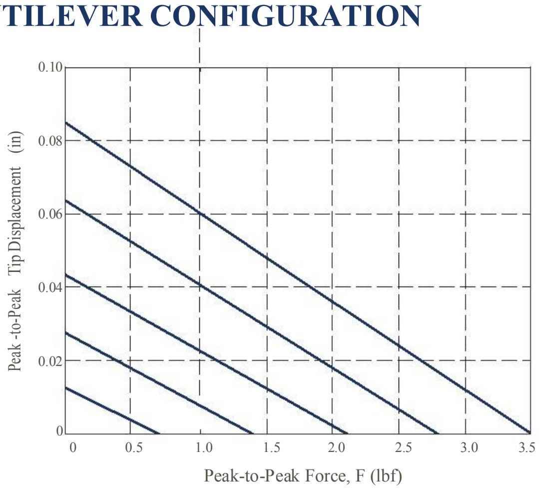

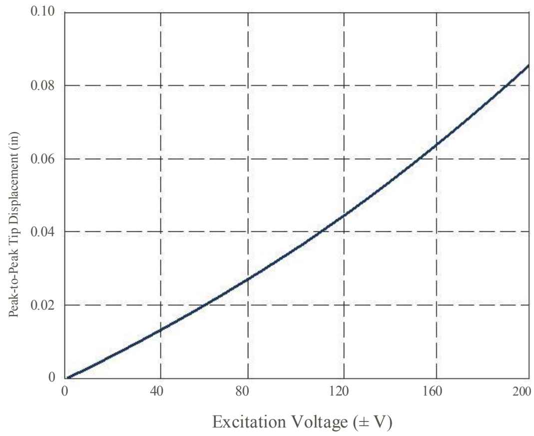

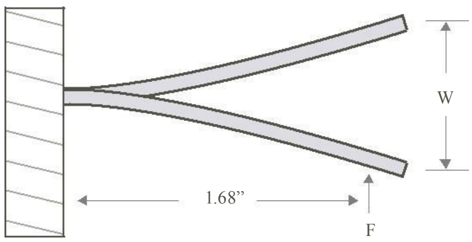

QP20W TYPICAL PERFORMANCE POWER CHARACTERISTICS

BONDED CONFIGURATION

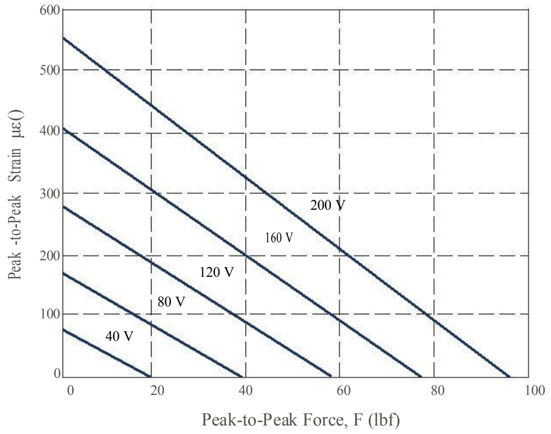

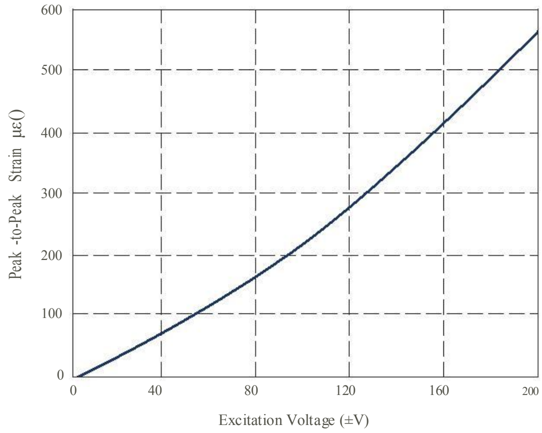

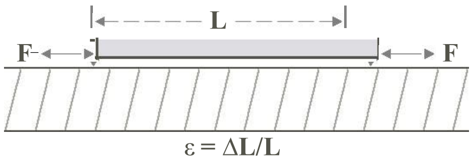

CANTILEVER CONFIGURATION

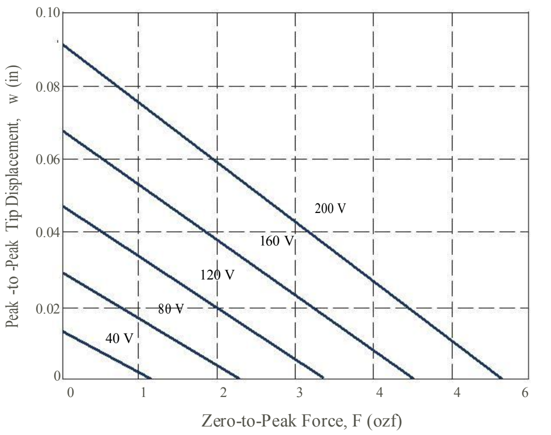

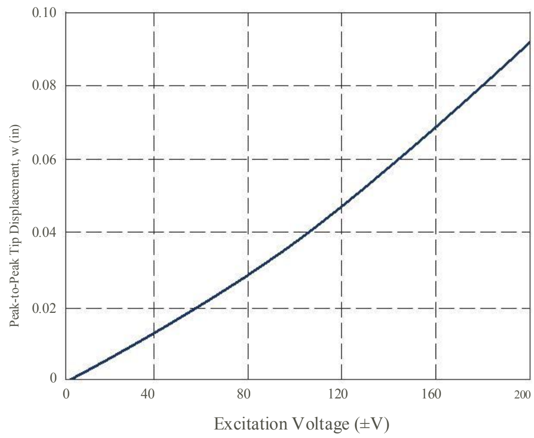

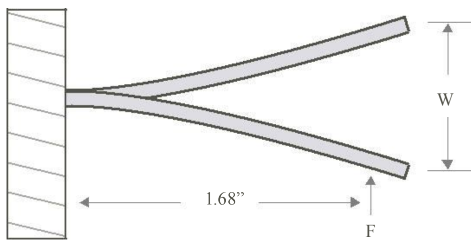

QP21B TYPICAL PERFORMANCE POWER CHARACTERISTICS

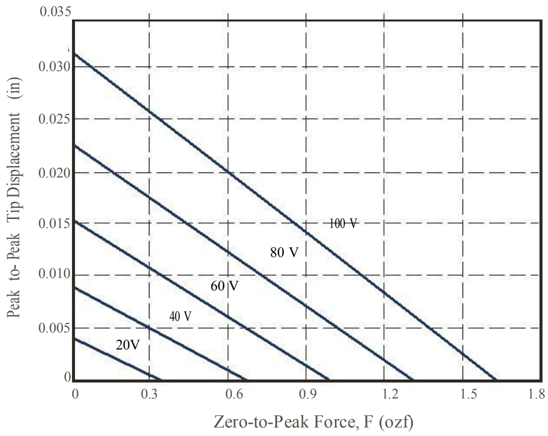

Frequency Response at ± 100 Volts

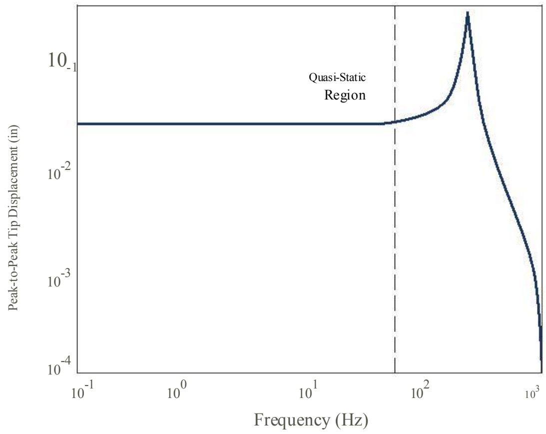

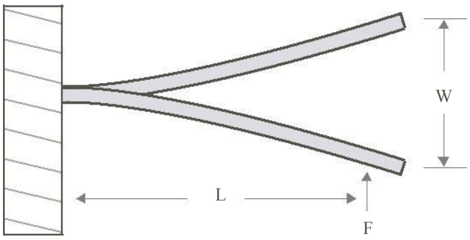

Product	L (in)
QP21B	1.00
QP22B	0.75

QP22B TYPICAL PERFORMANCE POWER CHARACTERISTICS

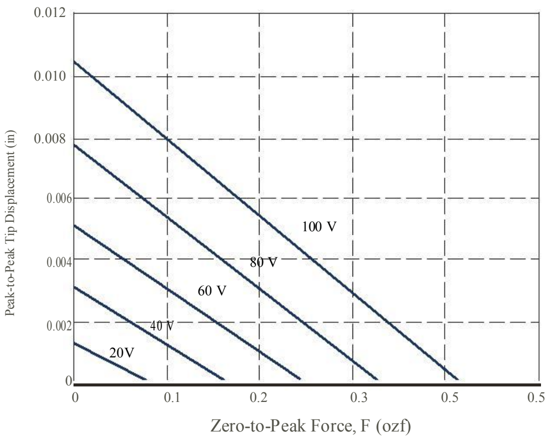

Frequency Response at+/- 100 Volts

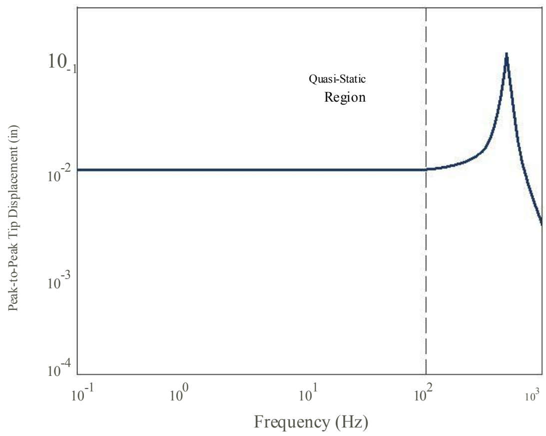

PIEZO FAN TYPICAL PERFORMANCE POWER CHARACTERISTICS

Drive Conditions	W(in)
120V / 60Hz	1.0
220V / 50Hz	1.5

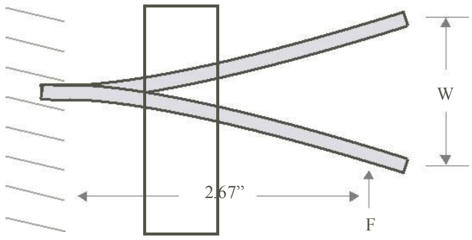

Annex 3

DuraAct Power Flächenwandler

H o c h e f f i z i e n t u n d r o b u s t

P-878

Einsatz als Aktor, Sensor oder Energieerzeuger

Niedrige Spannungen bis 120 V

Kompakte Bauweise

Individuelle Lösungen

Flächenwandler

Funktionalität als Aktor- und Sensorkomponente. Nominale Betriebsspannung von -20 bis 120 V. Mögliche Energieerzeugung für autarke Systeme bis in den Milli-wattbereich. Applizierbar auch auf gekrümmten Flächen.

DuraAct Power nutzt in Längsrichtung den hocheffizien-ten d_{33}-Effekt.

Robuster, kostengünstiger Aufbau

Laminierte Struktur aus PICMA® Multilayer-Piezoelement, Elektroden und Polymermaterialien. Herstellung durch blasenfreies Injektionsverfahren. Die Polymerummantelung dient gleichzeitig als elektrische Isolierung und als mecha-nische Vorspannung, sodass der DuraAct biegsam ist.

Kundenspezifische DuraAct Flächenwandler

Flexible Wahl der Größe

Variable Gestaltung der elektrischen Anschlüsse

Kombinierte Aktor-/Sensor-Applikationen, auch mit mehreren aktiven Lagen

Feldanordnungen (Array)

Einsatzgebiete

Industrie und Forschung. Applizierbar auch auf ge-krümmten Flächen, oder zur Integration in Strukturen. Für adaptive Systeme, Energy Harvesting, Strukturüber-wachung (Structural Health Monitoring)

Min. axiale Dehnung	1200	µm/m
Rel. axiale Dehnung	10	µm/V
Min. laterale Kontraktion	250	µm/m
Rel. laterale Kontraktion	1,2	µm/V
Blockierkraft	44	N
Abmessungen	27 mm × 9,5 mm × 0,5 mm	
Min. Biegeradius	24	mm
Aktives Element	15 mm × 5,4 mm	
Elektrische Kapazität	150	nF

Elektrische Kapazität: Toleranz ±20 %, gemessen bei 1 V_{pp}, 1 kHz, RT.
Piezokeramik: PIC 252.
Standardanschlüsse: Lötpunkte.
Betriebsspannungsbereich: -20 bis 120 V.
Betriebstemperaturbereich: -20 bis 150 °C.

Sonderausführungen und andere Spezifikationen auf Anfrage.

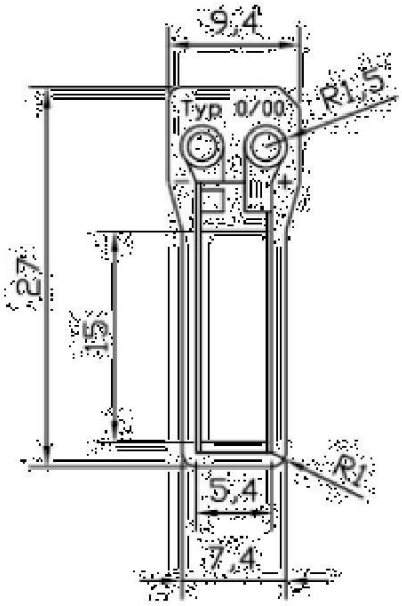

P-878.A1, Abmessungen in mm

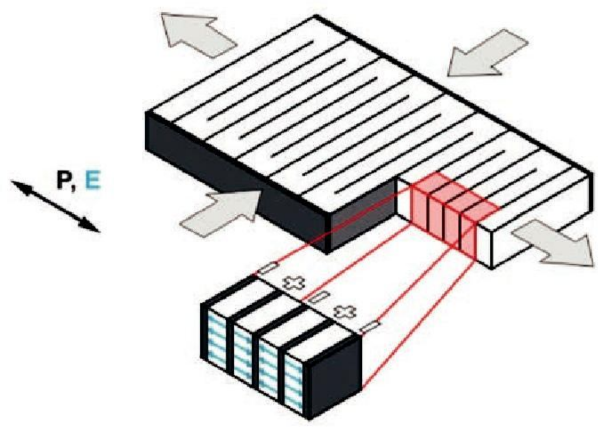

Die DuraAct Power Multilayer-Flächenwandler nutzen den Longitudinal- oder d_{33}-Effekt, bei dem die Auslenkung parallel zum elektrischen Feld E und der Polarisationsrichtung P des Piezoaktors erfolgt. Die piezoelektrischen Ladungskoeffizienten d_{33} für die longitudinale Auslenkung sind deutlich höher als die d_{31} für die transversale Auslenkung, die vollkeramische Wandler nutzen. (Quelle: Wierach, DLR)

Annex 4

Piezoelectric Fiber Composite (PFC)

PFC-W14's Engineering Properties

Property	Value
Dimensions [mm]	132×14×0.3
Piezoelectric Charge Coefficient, d_{33} @1kV [pC/N]	550
Electromechanical Coupling Factor, k_{33}	0.67
Young's Modulus, Y_{33} [10^{10} N/m^2]	2.44
Elastic Compliance, s^E_{33} [10^{-12} m^2/N]	41.0
Yield (Tensile) Strength [MPa]	157.3
Blocking Force, F @ 1 kV [N]	1.0

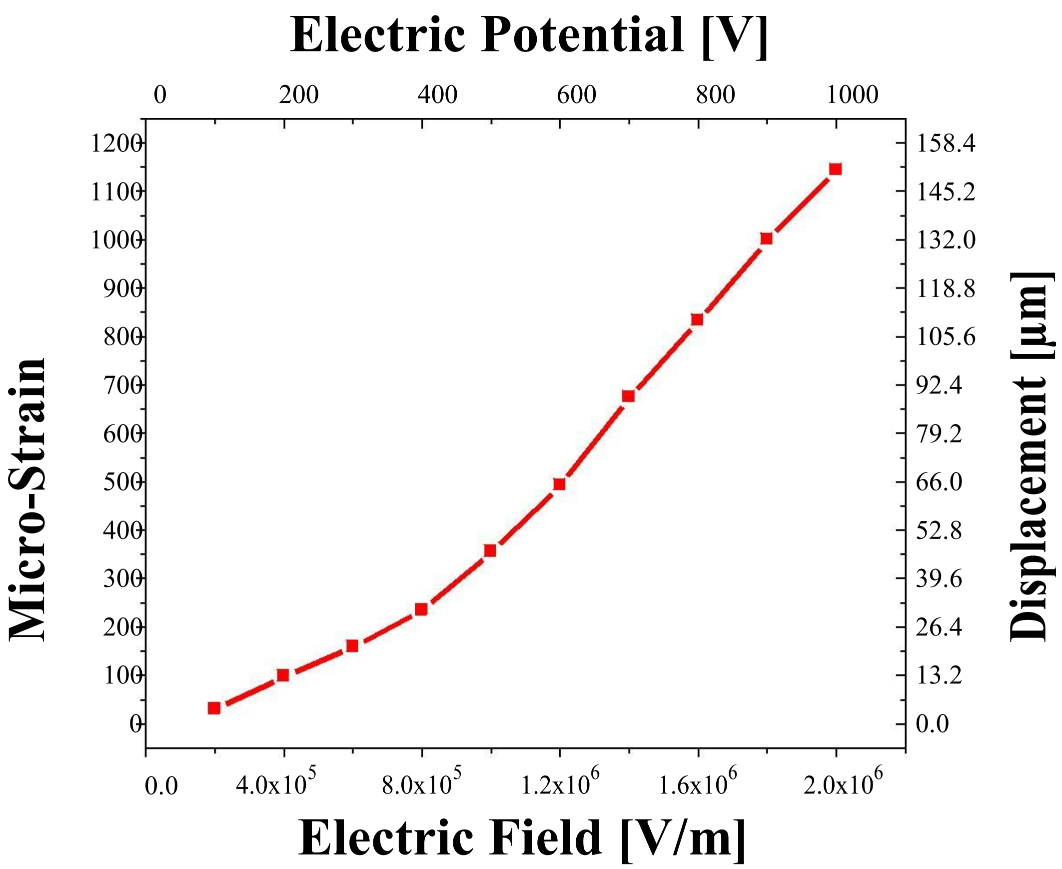

Annex 5: Bonding Techniques

"Bonding" is the best fixing process. The main material used in the process of bonding is epoxy glue, it creates strong and flexible joints, fatigue phenomena are absent and its work temperature reaches 150° C.
PZT layers can be bonded on metal surfaces using a thin stratus of **epoxy glue** (**M-Bond 610**[1]) cured for 24 hours at room temperature. Between sides of PZT and metal surfaces conductive **epoxy glue** (**CW2400**[2]) is putted in. The elements are circuited by **solded wires** (**MSF-003-NI**[3]). The result is shown in the Figure A.5.1 [A.1].
Alternatively insulant **epoxy resin** (**Eccobond 15LV**[4]) mixed with a **catalyst** (**Catalyst 15 LV**[5]) can be used. The resin-catalyst ratio is 3:1. After the application the glue is cured in oven for three hours at 65° C [A.2].

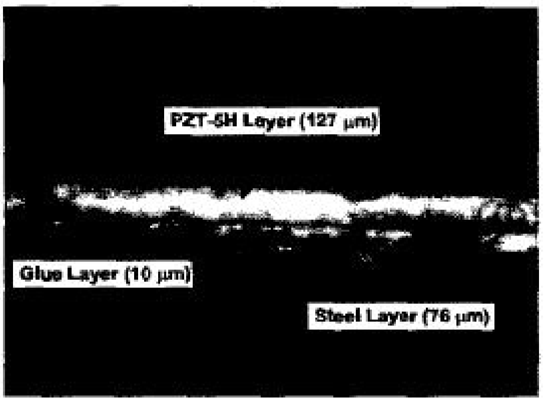

Figure A.5.1: Glued section [A.1].

Another kind of glue is **acrylate-based liquid**. In this case after the glue application a glass plate, Figure A.5.2, is pressed on the structure in order to come out the excessive glue. The process ends with polymerization of adhesive for half an hour at temperature of 85°C (see Figure A.5.3) [A.3].

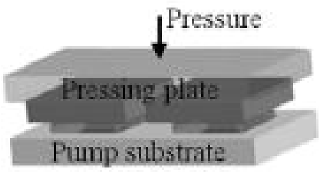

Figure A.5.2: Glass plate [A.3].

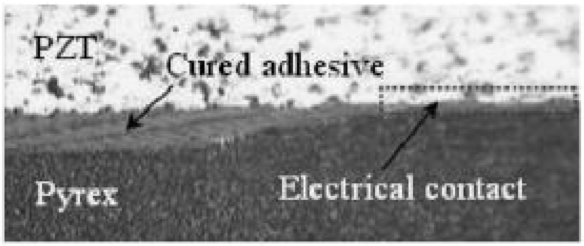

Figure A.5.3: Glued section [A.3].

---

[1] http://www.vishaypg.com/docs/11013/bond610.pdf
[2] http://www.all-spec.com/downloads/circuitworks/CW2400_040609s.pdf
[3] http://www.piezo.com/catalog8.pdf%20files/Cat8.58.pdf
[4] (rif. al 45 LV) http://hybris.cms.henkel.com/henkel/msdspdf?country=US&language=EN&matnr=1188168
[5] https://tds.us.henkel.com//NA/UT/HNAUTTDS.nsf/web/DFF5BD21DB3078C0852575D6006B4E9F/
$File/ECCOBOND%2045-CAT%2015-EN.pdf

References of Annex 5

A.1 M. Sitti, D. Campolo, J. Yan, R. S. Fearing, T. Su, D. Taylor, T. D. Sands, *"Development of PZT and PZN-PT Based Unimorph Actuators for Micromechanical Flapping Mechanisms"*, Proceedings of the 2001 IEEE International Conference on Robotics & Automation, Seoul, Korea, May 21-26, 2001

A.2 P. Ngernchuklin, A. Safari, *"Dome Bilayer Piezoelectric/Electrostrictive (PIE) Composite Flextensional Actuator"*, Department of Materials Science and Engineering Rutgers University, Piscataway, New Jersey, USA

A.3 J. Fang, K. Wang,K. F. Böhringer, *"Self-Assembly of PZT Actuators for Micropumps With High Process Repeatability"*, Journal Of Microelectromechanical Systems, Vol. 15, No. 4, August 2006